ASSESSMENT OF DEFORESTATION AND LAND COVER CHANGE IMPACTS ON FLOOD PEAK DISCHARGE IN MADURU OYA BASIN, SRI LANKA

Abdul Wahed Nab

(208358U)

Degree of Master of Science

Department of Civil Engineering

University of Moratuwa
Sri Lanka

February 2022

ASSESSMENT OF DEFORESTATION AND LAND COVER CHANGE IMPACTS ON FLOOD PEAK DISCHARGE IN MADURU OYA BASIN, SRI LANKA

Abdul Wahed Nab

(208358U)

Supervised by

Mr A. H. R. Ratnasooriya

Thesis submitted in partial fulfillment of the requirements for the degree
Master of Science in Civil Engineering

UNESCO Madanjeet Singh Centre for
South Asia Water Management (UMCSAWM)
Department of Civil Engineering

University of Moratuwa
Sri Lanka

February 2022

DECLARATION OF THE CANDIDATE AND SUPERVISOR

"I declare that this is my own work and this thesis does not incorporate without acknowledgement any material previously submitted for a Degree or Diploma in any other University or institute of higher learning and to the best of my knowledge and belief it does not contain any material previously published or written by another person except where the acknowledgement is made in the text".

Also, I hereby grant to University of Moratuwa the non-exclusive right to reproduce and distribute my thesis, in whole or in part in print, electronic or other medium. I retain the right to use this content in whole or part in future works (such as articles or books).

UOM Verified Signature

\- --- 03-Feb-2022

Abdul Wahed Nab Date

The above candidate has carried out research for the Master's thesis under my supervision

UOM Verified Signature

03-Feb-2022

Mr A. H. R. Ratnasooriya Date

ABSTRACT

Assessment of Deforestation and Land Cover Change Impacts on Flood Peak Discharge in Maduru Oya Basin, Sri Lanka

Population growth raises demand and competition for water resources and food stocks while it changes the landuse types by anthropogenic activities to adopt applicable measures for supplying water for domestic, agricultural, and industrial purposes. These changes alter the hydrological response of the river basins and can impose the communities to severe environmental risks like floods and landslides. Therefore, understanding of landuse change is crucial to study river basins' behavior and take mitigatory measures. The study presented here quantifies and analyzes the historical deforestation and landuse/landcover (LULC) change impacts on flood peak discharge of the Maduru Oya river basin, Sri Lanka using Hydrologic Engineering Centre-Hydrologic Modeling System (HEC-HMS) and remote sensing techniques. The Landsat Multispectral Scanner (MSS), Thematic Mapper (TM), and Operational Land Imager-thermal Infrared Sensor (OLI-TIRS) images are acquired in 1976, 1994, 2009, 2021 and classified using maximum likelihood algorithm of supervised classification.

The analysis of LULC change revealed that LU change was faster and in high magnitude from 1976 to 1994 compared to the remaining period to 2021. The LULC change quantification by analyzing each scenario revealed a 24.9% deforestation while a 2.2%, 9.8%, 8.4%, and 4.5% increase in homestead/garden, paddy, scrubland, and water body between 1976 to 1994, respectively. The deforestation further continued to a rate of 4.1% and a 2.0% decrease in water bodies was also found in 2009 while homestead/garden, paddy, and scrubland continued to increase by 3.5%, 1.4%, and 1.5% compared to 1994 landuse scenario, respectively. In contrast, the 2021 landuse scenario indicated a 7.6% decrease in scrubland while 3.6%, 0.5%, 1.5%, and 1.8% increase in forests, homestead/garden, paddy, and water bodies. The classified images were subjected to accuracy assessment. The overall accuracy of 82%, 84%, 88%, and 91% are found for 1976, 1994, 2009, and 2021 LU scenarios while having kappa coefficients of 0.78, 0.80, 0.85, and 0.89 for respective years. The Normalized Difference Vegetation Index (NDVI) assessment of scenarios corresponds to the landuse classified images.

An event-based HEC-HMS model is used to simulate the flood events in the Welikanda catchment of the Maduru Oya river basin. The model is calibrated and validated using the 1976 landuse and then the subsequent landuses are applied to study LU change impact on flood peak discharge. For model performance evaluation, the Nash-Sutcliffe, RMSE Observations Standard Deviation Ratio (RSR) Percent Bias (PBIAS), and the Coefficient of determination (R^2) were exploited. The average NSE, RSR, PBIAS, and R^2 values of 0.92, 0.25, 17.60, and 0.94 achieved in calibration and 0.73, 0.50, -3.03, and 0.78 are found in the validation which all can be rated very good performance except for PBIAS as satisfactory in calibration and NSE as good in the validation. The land cover change resulted in an increase (22.3%) in flood peak from 842 m^3/s in 1976 to 1,030 m^3/s in 2021. As a result of the landcover changes, the volume is also increased (42.3%) from 178.16 MCM in 1976 to 253.52 MCM in 2021. This study provides useful information for land and water managers, forests conservation units, and hydrologist to understand the LULC change impacts on floods and paves the way for broad LU and hydrological studies in Sri Lanka which are rarely conducted. The same approach can be applied in different parts of Sri Lanka which are exposed to severe LU changes.

Keywords: Data Scarcity, Forests, HEC-HMS, Hydrological Modeling, Satellite Observations, Water Cycle

DEDICATION

I would like to dedicate this study to my first teachers - my father and mother, in whom the existence gets a meaning, who have always stood up like the mountains against the challenges of life and have supported their children. When they were hardly surviving, they bought books and pens for their children to read, write and learn. It is with them that I feel big like the sky to spread the shade of kindness, smile, and supporting others. I owe them whatever I have in my life.

I also would like to dedicate this study to my family members, my brothers, and sisters who never spared to give me a hand when I was facing difficult times in my life.

I would like to honor the memory of my beloved late professor Ibrahim Najaf and my bachelor's degree supervisor Dr. Mohammad Hadi Asadi who have shaped my engineering life and dedicate this work to them.

Lastly, I would like to dedicate this work to my sweet homeland - Afghanistan in which I have grown up and do not know when to see it again, and Sri Lanka - my second homeland, the country that I have lived a life in so far.

ACKNOWLEDGEMENT

I would like to express my sincere gratitude to my supervisor Mr. Harsha Ratnasooriya for his persistent guidance, support, and continuous encouragement which enabled me to accomplish this study. My deep gratitude is extended to Dr. Janaka Bamunawala who instructed, guided, and provided me with his unsparing comments and assistance to shape this study.

I would like to honor and thank Prof. Lalith Rajapakse for his fruitful instructions, selfless cooperation, and invaluable guidance throughout this MSc. program. His unassuming approach to research and science is a source of inspiration. My deepest thanks go to Prof. Sohan Wijesekera for his lessons and unending inspirations. His vision, sincerity, and motivation have deeply inspired me throughout his lectures.

I wish to acknowledge the help provided by the panel members to accomplish this project, especially I would like to show my deep appreciation to Dr. Nimal Wijayaratna which helped me to figure out my research issues and obtain the required datasets. Taking the opportunity, I appreciate the Irrigation and Meteorological departments of Sri Lanka for providing the required datasets.

I would like to offer my sincere gratitude to the late Sri Madanjeet Singh for founding South Asia Foundation (SAF) and offering scholarships through UNESCO Madanjeet Singh Center for South Asia Water Management (UMCSAWM). The efforts by the SAF chapter of Afghanistan are highly appreciated which paved the way for obtaining the scholarship and processing of the documents.

I wish to acknowledge and thank the help provided by the technical and support staff in the UMCSAWM center especially Mr. Wajira Kumarasingh, Ms. Vinu Kalanika, and Ms. Janani Nisansala who patiently coordinated and cooperated throughout the course. I am fortunate to have been a student of the 6th intake and met my wonderful batchmates. I am indebted to all their cooperation during this MSc. course and project.

Nobody has been more important in persuading me to carry out my research successfully rather than my family and my beloved one that have always filled up my heart with their love, motivation, and inspiration.

TABLE OF CONTENTS

LIST OF FIGURES

LIST OF TABLES

LIST OF ABBREVIATIONS

AMP	Accelerated Mahaweli Program
ANN	Artificial Neural Networks
C3S	Copernicus Climate Change Service
CN	Curve Number
DEM	Digital Elevation Model
DS	Direct Sampling
ECMWF	European Centre for Medium-Range Weather Forecasts
EDA	Exploratory Data Analysis
EDASM	European Digital Archive of Soil Maps
ERA 40	40-yr European Centre for Medium-Range Weather Forecasts Re-analysis
ERA5	Fifth Generation of Atmospheric Reanalysis of the Global Climate
ERA-Interim	ERA-Interim Represents a Third Generation Reanalysis
ET	Evapotranspiration
ETM+	Enhanced Thematic Mapper Plus
FAO	Food and Agriculture Organization
FFPO	Fauna and Flora Protection Ordinance
GFDS	Global Flood Detection System
GIS	Geographical Information System
GSFC	Goddard Space Flight Center
HEC-HMS	Hydrologic Engineering Center - Hydrologic Modeling System
HRES	High-Resolution Forecast
LULC	Landuse/Landcover

MDP	Mahaweli Development Program
MERRA	Modern Era Retrospective-Analysis for Research and Applications
MI	Multiple Imputation
MLC	Maximum Likelihood Classifier
MLP	Multilayer Perceptron
MNN	Multivariate Nearest-Neighbor
MNP	Maduru Oya National Park
MSL	Mean Sea Level
MSS	Multispectral Scanner
NASA	National Aeronautics and Space Administration.
NCEP	National Centers for Environmental Prediction
NDVI	Normalized Difference Vegetation Index
NIR	Near-Infrared Reflactance
NSE	Nash-Sutcliffe Simulation Efficiency
OLI	Operational Land Imager
PBIAS	Percentage Bias
PRF	Peak Rate Factor
R^2	Coefficient of Determination
RED	Red Reflectance
REGEM	Regularized Expectation–Maximization Algorithm
RSR	Root Mean Square Error Observations Standard Deviation Ratio
SCS	Soil Conservation Service
SOM	Self-organizing Map
SRTM	Shuttle Radar Topography Mission

Tc	Time of Concentration
TM	Thematic Mapper
UH	Unit Hydrograph
UN-REDD	United Nations-Reducing Emissions from Deforestation aAnd Degradation
USACE	United States Army Corps of Engineers
USGS	United States Geological Survey

CHAPTER 1

1 INTRODUCTION

River basins have played an important role in maintaining human populations and other types of life since the dawn of civilization. A look back at history reveals the close link between a society's stability, economic and social progress, and the availability and reliability of water (Jaspers, 2003). River basins are continually susceptible to environmental, economic, social, and cultural pressures, i.e., the so-called 'driving forces' of land use and land cover (LULC) change, due to their dynamic characteristics (Verburg et al., 2008).

For a long time, ecosystems and hydrological cycles' interactivity have been one of the most important subjects in hydrology and ecosystem studies. Forests, specifically, are shown to control water cycles at different scales (Sun et al., 2005), and their appropriate management is regarded to be capable of reducing the impact of severe hydrological events like floods and droughts (Calder & Aylward, 2006). The hydrologic processes of catchments can be affected by LULC and climate change, resulting in variations in flash flood frequency (Kaspersen et al., 2017). For instance, Changes in LULC, caused by numerous anthropogenic activities, alter the dynamics of the catchment and exacerbate rapid hydrological responses, resulting in disastrous floods in low-lying regions (Douinot et al., 2016).

According to Hlásny et al. (2015), a review of some studies suggests that hydrological reactions to deforestation are highly inconsistent and most of the time complicated, but the obvious finding is that deforestation rises annual flow whereas the reforestation reduces it. Deforestation, on the other hand, raises flood peaks and volumes (Andréassian, 2004), whilst catchments with dense forest cover have higher infiltration, which reduces watershed runoff (T. Zhang et al., 2014).

Since natural disasters such as flooding can be caused by changes in forest and landuse policy (Lim et al., 2019), and LULC has the potential to have a significant impact on

floods due to human disturbance of natural landscapes (Rogger et al., 2017), an assessment of deforestation and LULC impacts on flood peaks is required to estimate changes in flood magnitude and volume.

To study the LULC change, there is a need for reliable data sources. The satellite images which are available on a local scale and provided by countries in high resolution or open-source available images with lower resolution are being widely used in LULC studies by different researchers (Kennedy et al., 2015; Rawat et al., 2013; Vermote et al., 2016; T. Zhang et al., 2014; Zope et al., 2016).

Satellite images of moderate-resolution are being used to map the LULC on a regional scale (Alberti et al., 2004). The NASA Earth observation data program Landsat Multispectral Scanner (MSS), Thematic Mapper (TM), and Enhanced Thematic Mapper Plus (ETM+) are among the widely used data sources in LULC investigations, giving a virtually continuous record of worldwide land cover since 1972, focusing mostly on forest and agricultural regions (Cohen & Goward, 2004).

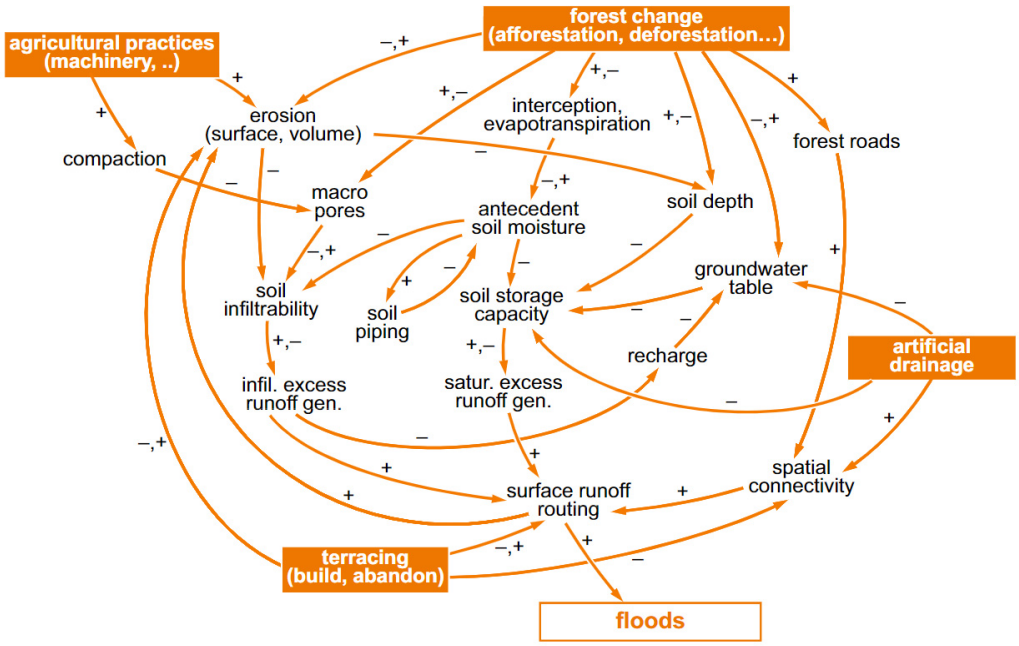

Figure 1-1: Schematic of process interactions in landuse change effects on floods (Rogger et al., 2017)

Figure 1-1, represents interactions in landuse change impacts on floods at catchment scale. The plus and minus signs show whether a rise in one variable causes another to rise or decline. The mechanisms depicted here are part of a larger framework that includes environmental and social factors (Rogger et al., 2017).

1.1 Problem Identification

Although forests clearing began with civilization (~10,000 years ago), the clearing rate had evolved since the 1900s when the area of cropland doubled (Houghton, 1994). Additionally, population growth with the rapid urbanization since the industrial revolution has caused changes and damages in ecosystem characteristics and services (Cao et al., 2018). Besides, forest clearing for producing woods and cultivation can accelerate the movement of sediments into river systems, resulting in higher sediment production than natural levels (Meade & Trimble, 1974; Reusser et al., 2015).

Sri Lanka's forest cover was believed to be 70% of the entire land area at the beginning of the nineteenth century. Since then, the forest area has gradually reduced (De Zoysa, 2001). A review of the forest cover over time suggests that the total forest cover of Sri Lanka amounts approximately to 1.95 million ha, representing 29.7% of the total land area of 6.56 million ha (Wijethunga, 2019).

The United Nations collaborative program on Reducing Emissions from Deforestation and Forest Degradation report indicates that by 1992, forest cover was restricted to a limited area in the wet zone of Sri Lanka while larger extents of dry and intermediate zones were still under forest cover (UN-REDD, 2015). The report also presents the results of GIS analysis based on forest cover maps prepared in 1992 and 2010. According to results, deforestation has taken place at a rate of 7,147 ha/year during this period, with most of the changes occurring in dry zone districts. The most significant forest cover change (in absolute terms) was recorded in Anuradhapura district (2,293 ha/year), followed by Moneragala (1,554 ha/year), Hambantota (1,255 ha/year), Ampara (1,018 ha/year), and Puttlam (982 ha/year).

The above studies and characteristics show that deforestation and changes in land cover are rapidly rising in the dry zone of Sri Lanka. As a result of deforestation and land cover changes, the infiltration rate reduces, and it may cause excessive floods and

sedimentation flows into the river and reservoirs. The situation gets even worse with the climate change impacts. Therefore, assessing deforestation and land cover change impacts on flood peak discharge is necessary to prevent the impending crisis.

In this regard, many researchers have used hydrological modeling techniques to project/assess the variability of overland/river flow due to landuse change at regional and local scales (Calder & Aylward, 2006).

Using satellite images as alternate sources for LULC studies paves the way to assess the disturbances in land cover and the subsequent impacts on riverflow or floods. There are hardly such assessments undertaken in Sri Lanka to investigate the effects of LULC on river flow. Since there is a significant landuse change in Sri Lanka, especially in the dry zone, it is vital to conduct such studies.

1.2 Problem Statement

Deforestation and landuse change have widely happened in the dry zone of Sri Lanka due to anthropogenic activities and development projects like the Mahaweli Development Program (MDP), which have subsequently aggravated the hydrological response of the river basins. Maduru Oya river basin, located in the dry zone, has also experienced deforestation and landuse changes due to human disturbances, and development schemes like Accelerated Mahaweli Program (AMP) which have caused adverse impacts in its hydrological behavior and an increase in the flood peak discharge and magnitude. There is no detailed study of deforestation and LULC change impacts on flood peaks conducted in the Maduru Oya basin so far. Therefore, this study will address the existing gap by quantifying deforestation and historical landuse change and investigating their impacts on flood peak discharge of the Maduru Oya basin using satellite observations and hydrological modeling.

1.3 Objectives

1.3.1 Main objective

The main objective of this study is to investigate the effect of deforestation and land cover changes on flood peak discharge of the Maduru Oya basin.

1.3.2 Specific objectives

The specific objectives of this study will be:

- **a)** To quantify the changes in land use and land cover during 1976-2020.
- **b)** To investigate the temporal evolution of flood peak discharge with historical land cover changes using a suitable hydrological model.
- **c)** To analyze the temporal trends of the basin's peak discharge and vegetation index.
- **d)** To verify the application of satellite observations for LULC change impact studies on flood peak discharge in the region.
- **e)** To derive conclusions and recommendations for proper land, water, and forest management in the basin.

1.4 Project Area

Maduru Oya with a length of ~135 km is one of the major river systems in Sri Lanka. The Maduru Oya has a drainage area of ~1,541 km^2 and emerges from Mahiyangana in the Badulla district. There are four administrative districts (Badulla, Polonnaruwa, Ampara and Batticaloa) and eight Divisional Secretariat divisions (Mahiyanganaya, Dimbulagala, Dehiaththakandiya, Padiyathalawa and Mahaoya, Welikanda, KoralaiPattu and KoralaiPattu West) which intersects with the Maduru Oya basin.

Maduru Oya basin with an average annual rainfall of ~1650 mm is located in the dry zone of Sri Lanka. The basin climate is tropical, with the northeast (December to February) and southwest (May to September) monsoons influencing the region. The northeast monsoon (Maha) is responsible for the majority of the yearly rainfall and runoff while due to the orographic impact of Sri Lanka's Central Highlands, the

southwest monsoon (Yala) is often dry (ACRES, 1980). Convective or cyclonic storms can provide rain during the intermonsoon period. When compared to larger swings in precipitation and streamflow, temperature fluctuations are often modest.

The majority of the Maduru Oya basin is less than 100 meters above sea level, while the highest point is less than 900 meters (Withanage et al., 2018). The watershed's main components are the Maduru Oya reservoir, river, and Maduru Oya national park. The inland areas are attractive for travelers who want to see the animals, while the seaside areas, particularly Pasikudah and Kayankerni, are popular among both locals and foreigners.

The Maduru Oya Reservoir is an irrigation reservoir with a hydroelectric installation providing secondary power to the national grid. The construction of the Maduru Oya reservoir commenced in 1979 under Accelerated Mahaweli Program (AMP) and was completed in 1986. The Maduru Oya program was launched to provide irrigation water to the Mahaweli System B area and to make it easier for 35,000 agricultural households to reside.

The Fauna and Flora Protection Ordinance (FFPO) of Sri Lanka established Maduru Oya National Park (MNP) in 1983 (Gazette No. 270/9) as an important component of the Mahaweli Protected Area Complex to provide a natural habitat for many local flora and fauna, especially for wildlife displaced by reservoir construction and hydropower development.

The Maduru Oya project is the biggest project which is implemented in the study area and has changed its land-use and land cover pattern. The dam site is located ~75 km upstream of the river mouth, about ~20 km south of Welikanda, and the catchment area is ~454 km^2. The Maduru Oya reservoir has a storage capacity of 596,000,000 m^3. A 543 m long earth-fill dam forms the Maduru Oya reservoir. The spillway length is 150 m, and the full supply level is at 96 m MSL, while the crest level of the dam is at 103.4 m MSL. The study area is shown in Figure 1-2.

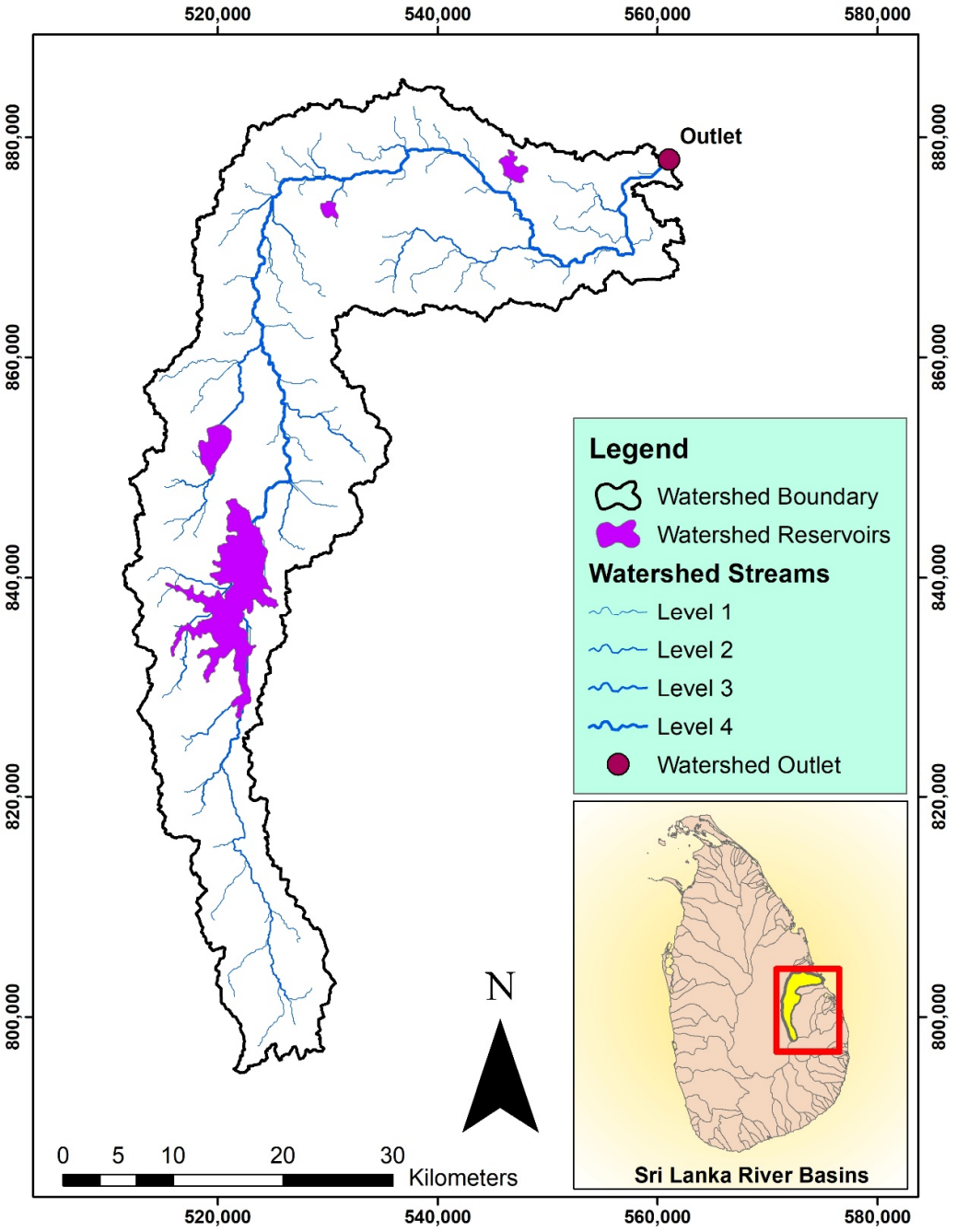

Figure 1-2: Study area (Maduru Oya basin)

1.5 Significance of the Study

The study of deforestation and reforestation has become more important due to climate changes, anthropogenic activities, and industrial development concerns. Previous and contemporary studies show deforestation at non-arid river catchments is always accompanied by an increase in flood peak discharge. This situation will exacerbate due to climate change impacts. Satellite images pave the way to study historical deforestation and its impacts on increasing peak discharge. In addition, it gives the possibility to predict future scenarios and take precautions steps.

The effect of deforestation on runoff has been estimated by Danáčová et al. (2020) using digital maps and hydrometeorological data from 1990-2018. The present influence of climate change and river basin deforestation on expected changes in design floods in the next decades was also assessed using a regional climate scenario during 2070–2100.

Although many studies are conducted to assess the causes of floods in Sri Lanka, deforestation and landuse change impacts are hardly considered. When the Maduru Oya River basin is considered, no research is undertaken using satellite observations and hydrological modeling. Hence, this study will fill this substantial knowledge gap by assessing the variation of peak flows due to LULC change in the Maduru Oya River Basin via developing and applying a satellite image-supported hydrological model.

The finding of this study will give a comprehensive knowledge of historical deforestation and land cover changes for land managers and forests conservation units in the Maduru Oya basin. Moreover, it will provide useful information for different stakeholders like water engineers, government agencies, and watershed managers about the watershed's behavior toward LULC change and the temporal evolution of peak discharge and flood magnitude over the period of 1976 – 2021. In addition, this study is one of the recent studies conducted to investigate LULC change impacts on flood peak discharge in Sri Lanka and will pave the way for broader practices in different climatic zones of the country using an event-based or continuous modeling approach.

CHAPTER 2

2 LITERATURE REVIEW

2.1 Landuse and Landcover Change Impacts on Flood Characteristics with a Focus on Deforestation

Sustainable and successful river basin water management necessitates a comprehensive knowledge of the various influencing factors that affect watershed characteristics. The hydrological response of a watershed to rainfall is intertwined with landuse and landcover (LULC). Landuse/landcover conversions have a significant impact on land deterioration, erosion, and water security (Vogels et al., 2017).

A change in LULC can alter watershed characteristics and cause a change in peak flood discharge or magnitude relevant to the LU type changes. For example, in the Delaware River Basin in the United States, Woltemade et al. (2020) investigated the influence of changing climate and landcover on flood magnitudes and discovered that landcover changes might increase the peak flood discharge by up to 10% in four of the five watersheds evaluated. Furthermore, they discovered that as the watersheds become more urbanized, peak discharge is expected to increase further.

Examination of the impact of LULC changes on peak discharge of a watershed in the Midwestern USA using the HEC-HMS model evaluated by Nash-Sutcliffe Efficiency showed good performance (Hu & Shrestha, 2020). Furthermore, their study results showed a 125-175% increase in peak discharge followed by an increase of the impervious surfaces of ~12%. Hussein et al. (2020) inspected the effect of landuse and landcover change on flooding risk along the UAE's eastern coast. They categorized various landuse categories using aerial imagery and found that the classified maps had an overall accuracy of 73 % to 78%, with Kappa coefficient values ranging from 68% to 71%. They discovered that classification values ranging from 61% to 80% might be in good agreement with real LULC.

A study of forest cover losses impact on surface runoff on 37 watersheds in east Africa revealed that deforestation causes an increase in annual discharges and surface runoff (Guzha et al., 2017). Another research conducted by Sandamali & Welikanna (2018) assessed deforestation and reforestation on Wilpattu National Park by satellite images. Their results show that there is an annual reforestation rate of 0.17% inside the park, whereas an annual deforestation rate of -0.29% is found outside its boundary using satellite images from 1977 to 2015.

Sri Lanka's dry zone covers 59% of the country's total land area, making it the country's most densely forested region. The findings of multi-decadal forest-cover dynamics research in Sri Lanka's dry zone from 1992 to 2019 found that the area had experienced significant forest loss totaling 250,000 hectares over the preceding 27 years which represents 8% of the country's net forest cover change (Ranagalage et al., 2020). They also found that the above-mentioned forest loss was high from 2010 to 2019.

Although there are sufficient studies of deforestation in the dry zone of Sri Lanka, to date, scientific studies concerning deforestation's impact on watershed hydrology are lacking. As per literature, deforestation combined with hydrological studies of river basins is widely used in different parts of the world to determine the impact of LULC change on flood peak discharge. Therefore, this study aims to merge this knowledge gap concerning the study of deforestation and watershed hydrology in the dry zone of Sri Lanka by developing a suitable hydrological model that simulates catchment responses under varied LULC conditions over the last four decades.

2.2 Runoff Variations due to Climate Change

Climate-change-driven changes in precipitation (reflected as runoff elasticity) and LULC change both influence runoff in river catchments. The precipitation elasticity of runoff, described as "the percentage variation in the mean annual runoff for a given percentage variation in mean annual precipitation", has long been used as a quick way to estimate runoff sensitivity to precipitation changes (Tang et al., 2019).

Precipitation elasticity of runoff considers both increase and decrease in runoff due to several climatic parameters change like temperature, precipitation, actual

evapotranspiration, sunshine duration, relative humidity, and wind speed. Huang et al. (2020) found that climate change causes runoff to increase by an average of 518% while anthropogenic activities make it decrease by an average of 418% during 1984 - 2004 in the Dongting lake in China. The authors discuss that according to Budyko-based methods, the fall of runoff caused by anthropogenic disturbances accounts for an average of 91% in 2005-2019, whereas the fall of runoff driven by climate change stands for 7% to 12%. Anthropogenic disturbances were shown to be the primary cause of runoff change throughout this period.

Fan et al. (2017) studied the differences in the climate elasticity of runoff across Chinas' Poyang Lake Basin. They employed the water-energy balance equation based on the Budyko framework to analyze temporal and geographical variations in the climate elasticity of runoff, revealing the impact of the catchment features' parameter and change on climate elasticity and runoff projection.

The impacts of geography on the contributors to streamflow variability are more important than the effects of geography on ET variability, according to an examination of variables impacting intra-annual variability of evapotranspiration and streamflow under various climatic situations (D. Zhang et al., 2016). The effects of vegetation on the contributors to ET variability, on the other hand, are greater than those of streamflow fluctuation.

2.3 Usage of HEC-HMS in LULC Studies

The HEC-HMS model is a physically-based and conceptually semi-distributed model for simulating precipitation-runoff processes in various geographic locations, ranging from big river basin water supply and flood hydrology to minor urban and natural watershed runoffs (Tassew et al., 2019).

The impact of LULC and urbanization on flooding in the Oshiwara River Basin in Mumbai, India, was studied by Zope et al. (2016) using the HEC-HMS model. Their findings demonstrate that for changes in landuse conditions, lower return period events resulted in the greatest change in volume and peak discharge compared to higher return period. Hydrological impacts of LULC change and detention basins on urban flood hazards were studied by Zope et al. (2017) in the Poisar River basin, Mumbai, India

using HEC-HMS. Their findings reveal that the addition of detention ponds inside the basin reduced peak flow by ~10% and ~34% for the 2-year and 200-year return period events, respectively.

Koneti et al. (2018) conducted hydrological modeling to assess the effects of LULC change on runoff dynamics in the Godavari River Basin. They observed that the HEC-HMS model is more consistent with rainfall-runoff simulation and performs better since it considers all of the variables that impact the process. In the Upper OumErRabia Basin (Morocco), a comparison of the event-based and continuous-process HEC-HMS model approaches reveals that both modes are highly predictable by HEC-HMS (Msaddek et al., 2020).

A literature survey of LULC studies in 37 watersheds reveals that HEC-HMS is widely used to study LULC change impact on catchment hydrology in East Africa (Guzha et al., 2017). The findings reveal that as forest cover declines, peak discharge rises, while afforestation lowers peak discharge and lowers low flows.

The literature shows that the HEC-HMS model successfully produces reliable results in LULC change impacts on the flood regime, magnitude, and peak discharge studies. Moreover, it is a simple model and provides reliable outputs with limitedly available data. Therefore, it is selected as the most suitable hydrological model in this study.

2.4 Literature on Hydrological Data Checking

Hydrological datasets should be checked before processing to assure their consistency and ability to produce reliable results. Historical paper chart records, state-of-the-art automated rain gauges, and the radar, which is desirable due to its high spatial resolution, are all possible data sources (Schilling, 1991). The duration of rainfall and streamflow data, as well as the qualities and number of gauging stations, are determined by each study objective. A rainfall-runoff model output is largely dependent on the input data. Before any further exploitation, any doubtful or incorrect data must be recognized and, if possible, replaced with valid data (Mourad, 2018).

2.4.1 Rainfall data checking and gap filling

Missing hydrometeorological data may be filled using a variety of approaches ranging from simple regression analysis to advanced statistical analysis. The method developed by Johann et al. (1998) demonstrated that using multiple regression analysis and weighted average models, it is possible to compute acceptable rainfall indicators for long-term modeling of sewage systems in urban hydrology. The method presented should only be applied if dense rain gauge networks are available.

Kalteh and Hjorth (2009) discussed imputations of missing values using self-organizing maps (SOM), multilayer perceptron (MLP), multivariate nearest-neighbor (MNN), regularized expectation-maximization algorithm (REGEM), and multiple imputations (MI) in the context of a precipitation–runoff process database in northern Iran to construct a serially complete database for analyses such as runoff prediction.

The program HEC4 created by the US Corps of Engineers is used to estimate monthly precipitation using linear regression and multiple linear regression algorithms. The results demonstrate that using multiple linear regression for monthly rainfall estimation reduces the Standard Deviation and Root Mean Squared Error by 36% as compared to using linear regression (Villazon & Willems, 2010).

Nkuna and Odiyo (2011) conducted a study to fill missing rainfall data in the Luvuvhu River Catchment. In this study, the authors have used artificial neural networks (ANNs) to estimate missing rainfall data. The results of this study show that ANNs can be used to estimate missing rainfall data in the study area.

The arithmetic averaging approach, multiple linear regression method, and non-linear iterative partial least squares algorithm perform well enough in estimating missing data in precipitation research (Sattari et al., 2017).

Dubey and Hardaha (2019) used the annual rainfall data of eight districts of the state Madhya Pradesh, India between 1901 to 2011 for estimating missing annual rainfall data. To detect missing rainfall records in the collected data, several existing standard models, such as arithmetic mean, normal ratio, inverse distance weighting, multiple linear regression, and innovative approaches, such as artificial neural network (ANN), were utilized and evaluated. The findings reveal that the multiple linear regression

model performs better than the other conventional models, but the ANN technique is best for predicting missing yearly rainfall data.

2.4.2 Streamflow Data Checking and Gap Filling

Numerous hydrological experiments, such as streamflow trend analysis, flood and drought analysis, and hydrological response variable estimations and projections, require gap-filling streamflow data (Zhang & Post, 2018). However, most hydrological studies lack a quantitative assessment of the gap-filled data accuracy. When assessing yearly trends for 217 ungauged catchments across Australia, Zhang & Post (2018) found that gap-filled streamflow data acquired using calibrated hydrological models work quite well as the benchmark data (less than 1% missing) when the missing data rate is less than 10%.

In the hydrological modeling process, calibration of rainfall-runoff models is a critical step. Observed streamflow data is the most common way of calibrating a rainfall-runoff model. When in-situ measurement of streamflow data is not available, calibration becomes challenging. In the LISFLOOD distributed rainfall-runoff routing model, Revilla-romero et al. (2015) evaluated the usefulness of remotely sensed surface water extent from the Global Flood Detection System (GFDS) as a proxy for streamflow. Using raw GFDS data as a proxy for streamflow for calibration enhanced the ability of the simulated streamflow (high flows) for 21 of the 30 sites using correlation as a criterion.

For infilling gaps in daily streamflow records, the Direct Sampling (DS) approach is utilized as a non-parametric stochastic method (Dembélé et al., 2019). Then, utilizing data from the Volta River basin in West Africa, a full gap-filling system is created and deployed, including predictor station selection and DS parameter optimization. After being tested in a variety of hydroclimatic situations in the Volta River basin, the overall performance of the framework was found to be good.

2.5 Secondary Datasets for Hydrological Modeling

Since this study is conducted in a data-scarce region, the secondary (reanalysis) datasets were reviewed to assess the possibility of using secondary datasets when measured datasets are not available.

Water resources reanalysis may be used as a numerical technique to understand hydrological processes in data-scarce areas. However, the outcomes of water resources reanalysis may have uncertainties that must be investigated to improve their applicability in water resources applications (Koukoula et al., 2020). A range of secondary datasets that can be used in rainfall-runoff modeling are freely-available, and some of those datasets are briefly introduced below.

2.5.1 ERA-40 Reanalysis Data

ERA 40 is a second-generation reanalysis and the first reanalysis that directly incorporates satellite radiance data. The result is better circulation over the tropics and southern hemisphere. However, new research should employ the third-generation reanalysis, ERA-Interim or MERRA, unless it is compared to existing ERA-40-based conclusions.

An assessment of the ERA-40 monthly average of 40 years data with the basin average of observed temperature, precipitation, evaporation, and streamflow in the Mackenzie basin shows that reanalysis data varies dramatically over the analysis period (Betts & Ball, 2003). The possibility of calculating monthly terrestrial water storage fluctuations from water balance calculations using Reanalysis ERA-40 data and river runoff of USGS has been studied in the Mississippi River basin (Seneviratne et al., 2004). The results are shown for the whole Mississippi River basin and its subbasins, as well as a smaller area across Illinois that has precise observations of the attributes of terrestrial water storage (soil moisture, groundwater level, and snow cover). Calculations of monthly terrestrial water storage variation water-balance show excellent correspondence with data taken over Illinois.

The hydrometeorology of the Amazon basin is compared to measurements of precipitation, temperature, and streamflow from the ERA-40 reanalysis over the period

1958–2001 (Betts & Ball, 2005). On an annual water-year basis, the results reveal that the reanalysis runoff–precipitation connection is close to the actual streamflow–precipitation relationship. In the rainy season, ERA-40 precipitation for the Amazon is lower by around 1.3 mm/day compared to observational data, and greater by a smaller amount in the dry season. According to a comparison of reanalysis products from the GSFC, NCEP, and ECMWF, ERA-40 has the lowest precipitation bias (Decker et al., 2012).

2.5.2 ERA5 Reanalysis Data

ERA5 is one of the widely used secondary sources of data which is the fifth generation of the European Centre for Medium-Range Weather Forecasts (ECMWF) atmospheric reanalysis of the global climate. It covers the period from January 1950 to the present. ERA5 is a product of the Copernicus Climate Change Service (C3S) at ECMWF.

There is one (hourly, 31 km) high-resolution realization (referred to as "reanalysis" or "HRES") and a lower resolution ten-member ensemble included in the ERA-5 dataset (referred to as "ensemble" or "EDA"). The ensemble is essential for the data assimilation procedure, but it also considers the relative random uncertainty (ECMWF, 2021).

The ERA5 datasets contain biases that should be carefully investigated. Various methods are available to minimize the biases and enhance the accuracy (e.g., linear bias correction method, which is the simplest). Comparing different plots and assessing the correlation between measured and secondary datasets will provide the necessary insights on the correlation of datasets.

The ECMWF (2021) documentation states that “the family of ERA5 datasets is currently comprised of ERA5, ERA5.1, and ERA5-Land” which can be described as follows:

- ERA5 is a comprehensive reanalysis which is available since 1979 (to near real-time), that incorporates all feasible data in the upper atmosphere and near the surface. There are two models included in the ERA5 atmospheric model which are land surface and wave models.

- ERA5 back extension (preliminary version), from 1950 to 1978, is currently made available separately from ERA5 (1979 onwards). Although this dataset's quality is good in many other ways, it encompasses tropical cyclones that are often abnormally intense. Therefore, until a new upgraded version of ERA5 1950 to near real-time is issued, the current version of the back extension is considered tentative.
- ERA5.1 is a re-run of ERA5 for the years 2000 to 2006, which was created to enhance ERA5's lower stratospheric cold bias during this period. In the majority of the troposphere, ERA5 behaves similarly to ERA5.1.
- The ERA5-Land dataset is available from 1950 to near real-time, which is created at a higher resolution (9 km) and is forced by ERA5 atmospheric parameters with lapse rate correction, but without any further data assimilation.

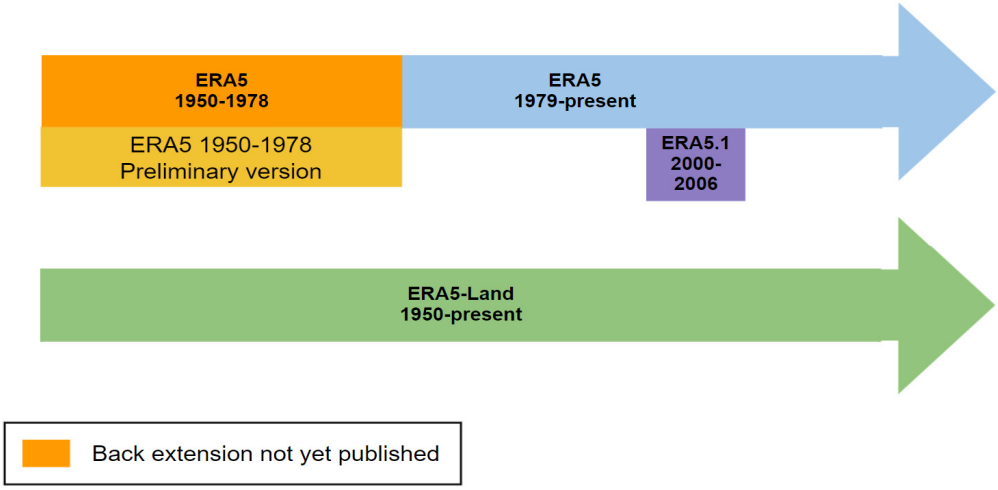

Figure 2-1: ERA5 family timeline (ECMWF, 2021)

CHAPTER 3

3 MATERIALS AND METHODS

As the first step, the data required for the study was collected and verified. Then the following procedures were implemented to achieve the desired outputs:

I. Four scenarios of LULC representing the land cover conditions of the Maduru Oya River Basin in 1976, 1994, 2009, and 2021 were set up to evaluate the effect of deforestation and land cover change on flood peak discharge.

II. The Satellite images are downloaded using Landsat 2 multispectral scanner (MSS), Landsat 5 thematic mapper (TM), and Landsat 8 operational land imager-thermal infrared sensor (OLI-TIRS), and then the supervised image classification method was used to perform land use and land cover classification. The Maximum Likelihood Classifier (MLC) algorithm of supervised classification for land cover classification of each Landsat image was used to obtain highly accurate results. Quantification of all classified LULC maps was performed, and the relative changes between different scenarios were assessed.

III. The vegetation distribution and status in various historical periods are assessed in each scenario using the normalized difference vegetation index (NDVI).

IV. ArcGIS (Version 10.3) Esri Inc. software was used to delineate the catchment from DEM, divide it into sub-basins, and derive the stream network.

V. A hydrological model (i.e., HEC-HMS) was set up, calibrated, and validated to assess the impact of land cover changes on flood peak discharge.

VI. Finally, the impact of deforestation and land cover changes on flood peak discharge of the catchment is assessed and quantified from 1976 to 2021.

The above steps are shown in the methodology flow chart below in Figure 3-1.

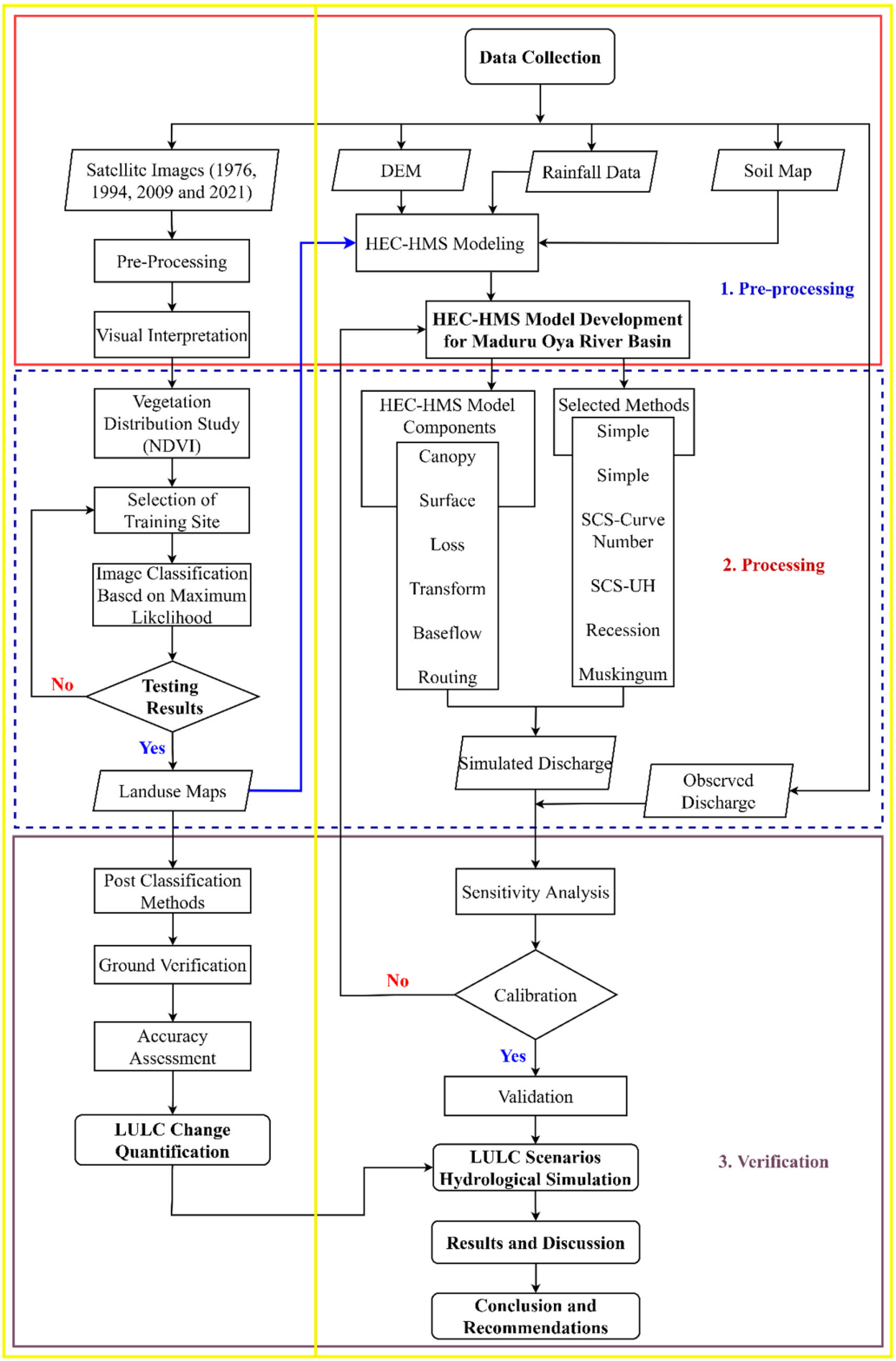

Figure 3-1: Methodology flowchart

In Figure 3-1, the yellow line separates the landuse processing from the hydrological modeling.

3.1 Data Collection and Data Checking

The following data were collected for this study:

- Geometrically corrected Landsat 2 multispectral scanner (MSS), Landsat 5 thematic mapper (TM), and Landsat operational land imager-thermal infrared sensor (OLI-TIRS) satellite images (obtained from http://earthexpolorer.usgs.gov).
- The Shuttle Radar Topography Mission (SRTM) Digital Elevation Model (DEM) is obtained from the US Geological Survey Website.
- Landuse maps of Sri Lanka from the Survey Department and online sources for accuracy assessment of Landsat images.
- Soil data of the Madura Oya River basin from the Survey Department of Sri Lanka.
- Hydrological and meteorological datasets were collected from the Irrigation and Meteorological Departments of Sri Lanka.

Table 3-1: Data collection

Data	Temporal/Spatial Resolution	Sources
Landsat Satellite Images	30 m	earthexpolorer.usgs.gov
Landuse Map	1: 10,000	Survey Department of Sri Lanka
DEM	30 m	SRTM, US Geological Survey Website
Soil Data		Survey Department
Rainfall	Daily	Meteorological Department of Sri Lanka,
Discharge	Daily	Irrigation Department of Sri Lanka

3.1.1 Satellite Data Checking

For LULC change study and quantification, satellite images were acquired from the USGS website (earthexpolorer.usgs.gov). Images were checked according to their coverage and cloud cover. The cloud cover is considered between 0-10 %. Since Sri Lanka is one of the cloudiest places in the world (Nay et al., 2018), only limited images are available within the selected cloud cover. The earliest image that covers the study area was identified in 1976 with a 60 m spatial resolution. The other satellite images covering the study area were identified in 1994, 2009, and 2021 which have a 30 m spatial resolution. The satellite image collected in 1976 contained scanline error, and it was optimized by the Landsat toolbox in ArcGIS 10.3. The other images did not show any significant errors. Moreover, to enhance satellite images quality, accuracy enhancement steps such as noise reduction, haze reduction, and histogram equalization were performed during the process.

3.1.2 Rainfall Data

Following rainfall gauging stations were identified from the Meteorological Department of Sri Lanka website. Then, data availability was checked using the data availability excel sheet provided by the website. In total, 10 rainfall gauging stations were identified within the Maduru Oya River Basin and their details are shown in Table 3-2.

Table 3-2: Data availability of rainfall gauging stations located within the catchment

No.	Rainfall Stations Name	Data Period Available	Data Period Missing	Location (Decimal Degree)
1	Ekiriyankumbura	2008 - 2010	2008 (Jan - June) 2010 (Aug - Dec)	(Upstream) Long: 81.23 E Lat: 7.30 N
2	Kudasigiriya	1993 - 2020	1993 (Jan-Mar) 1994 (Aug) 1998 (Nov)	(Midstream) Long: 81.13 E Lat: 7.68 N

No.	Rainfall Stations Name	Data Period Available	Data Period Missing	Location (Decimal Degree)
			2000 (Apr and Dec) 2003 (Aug) 2007 (Feb and Oct) 2010 (Oct) 2012 (July and Jan) 2015 (Aug) 2020 (Sep - Dec)	
3	Aralaganwila	2003 - 2020	2003 (Jan and Feb) 2020 (Oct - Dec)	(Midstream) Long: 81.15 E Lat: 7.80 N
4	Welikanda	2002 - 2006	2002 (Jan - Nov) 2003 (Dec) 2004 (Sep) 2005 (June) 2006 (Mar - Dec)	(Midstream) Long: 81.25 E Lat: 7.95 N
5	Welikanda (Muthuwella)	2004 (Jun & Sep), 2005 (June), 2017 (Apr), 2019 (Feb)	All Other Months Within the Periods are Unavailable.	(Midstream) Long: 81.22 E Lat: 8.00 N
6	Punani	1990 (Jan), 1992 (Apr), 2002 (Dec), 2003 (Jan – Mar, May, June, Aug)	All Other Months Within the Periods Are Unavailable.	(Downstream) Long: 81.35 E Lat: 7.95 N
7	Vakaneri	2013 – 2020	2014 (Mar) 2019 (Feb & Sep) 2020 (Sep - Dec)	(Downstream) Long: 81.43 E Lat: 7.92 N
8	Valachchenai	1989 - 2000	1989 (Jan)	(Downstream)

No.	Rainfall Stations Name	Data Period Available	Data Period Missing	Location (Decimal Degree)
			1993 (Feb) 1998 (Oct & Nov) 2000 (Jan & May - Dec)	Long: 81.53 E Lat: 7.92 N
9	Passikuda	2004 – 2020	2004 (Jan - Apr, June, Oct - Dec) 2005 (Jan - Apr) 2007 (July) 2010 (Apr) 2012 (June - Dec) 2013 (Jan) 2014 (Feb & Mar) 2015 (Jan) 2020 (Sep - Dec)	(Downstream) Long: 81.55 Lat: 7.93
10	Kalkudah	1996 - 2014	1996 (Jan - May) 1997 (Jan - Aug) 2010 (Mar) 2011 (Nov) 2012 (Dec) 2013 (Dec) 2014 (June - Sep)	(Downstream) Long: 81.55 Lat: 7.88

3.1.3 Maduru Oya rainfall data checking

Following rainfall data were collected to be used in this study. However, except for Batticaloa, which is 38 km far from the catchment, no rainfall gauge station has continuous records for the desired period. Therefore, only the Batticaloa rainfall station data are checked for continuity and consistency errors and used in this study. The details of collected rainfall data are given in Table 3-3.

Table 3-3: Collected rainfall data

No.	Rainfall Stations Name	Period Available	Distance from Catchment Boundary (km)	Long. (Decimal)	Lat. (Decimal)
1	Aluthnuwara	1979 – 2015	18.2	81.00 E	7.32 N
2	Angamedilla	1976 – 2016	23.5	80.92 E	7.85 N
3	Aralaganwila	2003 – 2016	Midstream	81.15 E	7.8 N
4	Bible Agri. Training Center	2000 – 2015	6.2	81.22 E	7.15 N
5	Galoola Estate	1989 – 2015	16.6	81.15 E	7.07 N
6	Galpurayaya - G/Kotte	2002 – 2012	10.3	81.02 E	7.45 N
7	Giradurukotte	1995 – 2015	3.7	81.08 E	7.45 N
8	Hembarawa	1996 – 2016	12.9	80.98 E	7.52 N
9	Kandaketiya	1976 – 2015	20.5	81.02 E	7.17 N
10	Kudasigiriya	1993 – 2016	Midstream	81.13 E	7.68 N
11	Minneriya Tank	1976 – 2016	31.7	80.90 E	8.05 N
12	Passikuda	2004 – 2016	Outlet	81.55 E	7.93 N
13	Polonnaruwa Agri.Station	1976 – 2016	13.4 km	81.03 E	7.92 N
14	Tissapura	2008 – 2015	9.8	81.08 E	7.30 N
15	Valachchenai	1981 – 2000	Outlet	81.53 E	7.92 N
16	Welimada Group	1989 – 2011	48.3	80.90 E	6.90 N
17	Welipitiya Coconut	1992 – 2015	6.5	81.25 E	7.15 N
18	Ekiriyankumbura	2014 – 2016	Upstream	81.23 E	7.30 N
19	Batticaloa	1950 – 1980	38	81.67 E	7.72 N

The rainfall stations which are located within or at a distance of 10 km from the river basin boundary and river gauges are shown in Figure 3-2.

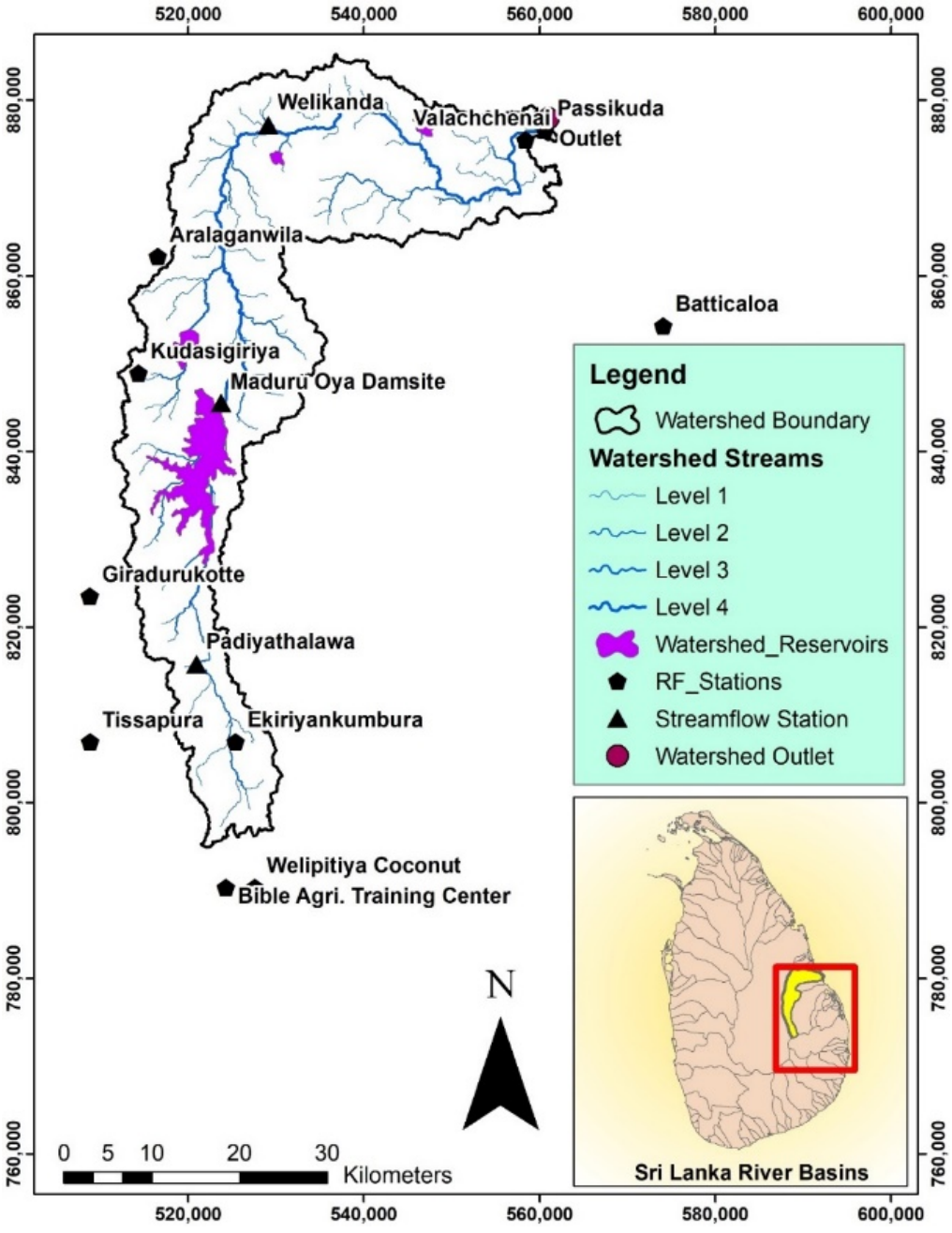

Figure 3-2: Gauging stations

The rainfall data which were collected initially and details are presented in Table 3-3 are shown in Figure 3-3 graphical chart.

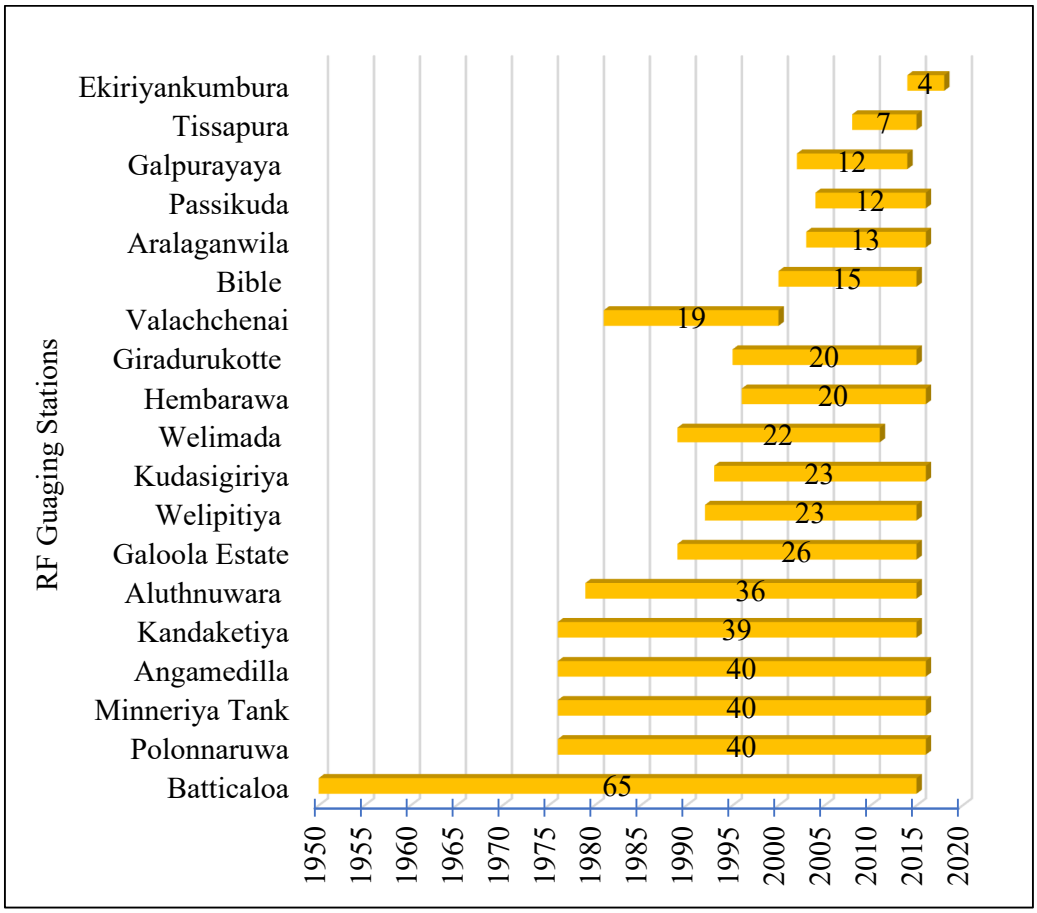

Figure 3-3: Collected rainfall data chart

3.1.4 Visual data inspection

The purpose of visual inspection is to assess the response of the flow to the rainfall which is the fundamental aspect in rainfall-runoff modeling of a watershed. The following procedures are applied for visual data checking:

Initially, visual inspection of the data is accomplished, missing and inconsistencies are identified and highlighted then the collected rainfall data are prepared and converted to an annual and monthly format and plotted in different charts and graphs like yearly, monthly, monthly mean, max, and min, seasonal and box plot to visualize and check inconsistencies and missing values further. The annual rainfall in Figure 3-4, shows

that there were highest rainfalls occurred in 1957, and 1963 while the least rainfall has happened in 1968.

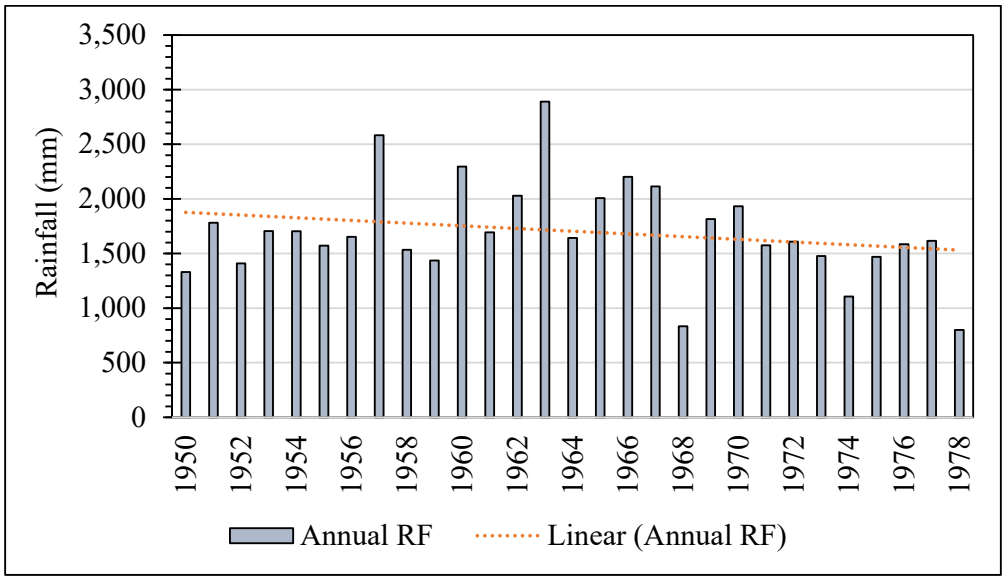

Figure 3-4: Batticaloa station annual rainfall

The monthly average rainfall during the study period which is presented in Figure 3-5, shows that the highest average monthly rainfall in recorded in 1957 and 1963 while the lowest is recorded in 1968.

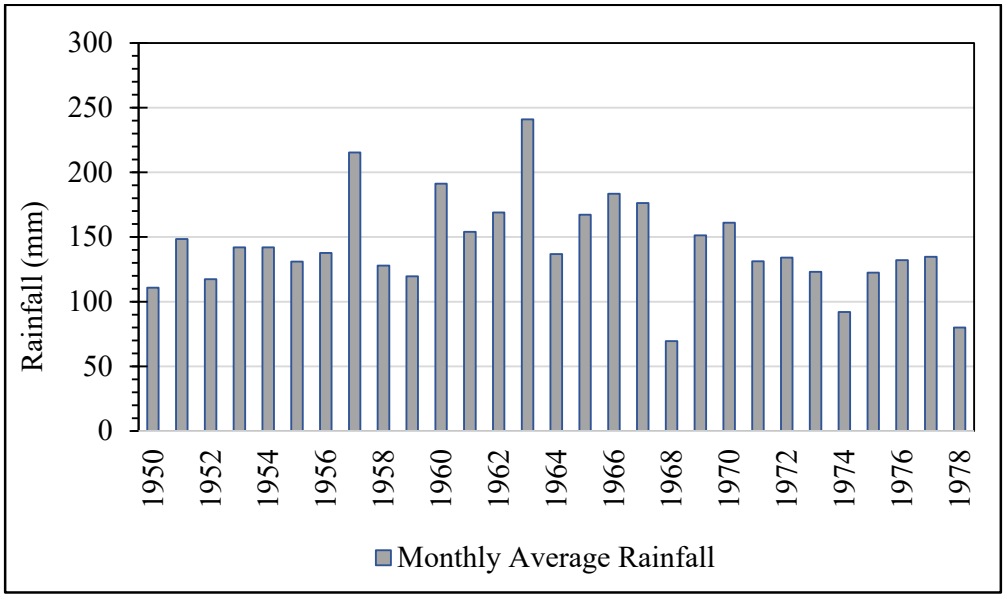

Figure 3-5: Batticaloa station monthly average rainfall

The seasonal variation of rainfall in Batticaloa stations which is presented in Figure 3-6, indicates that the highest rainfall is dominated by the Southwest monsoon followed by the Second inter-monsoon, Northeast monsoon, and First inter-monsoon.

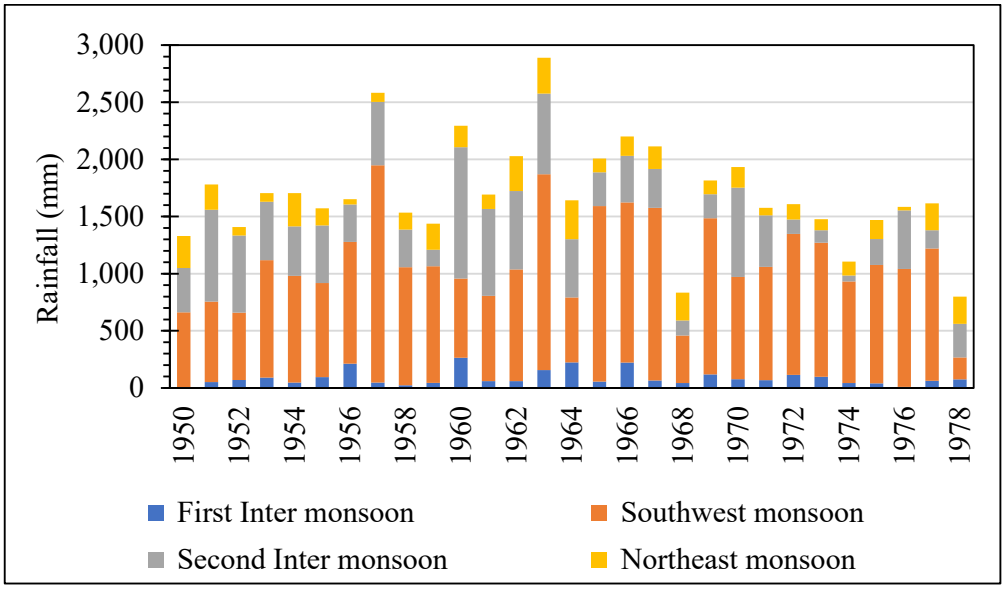

Figure 3-6: Seasonal variation of rainfall at Batticaloa station

The box plot of rainfall recorded in Batticaloa which is presented in Figure 3-7, indicates that the highest rainfalls have happened in the month of September while the lowest have happened in the month of March.

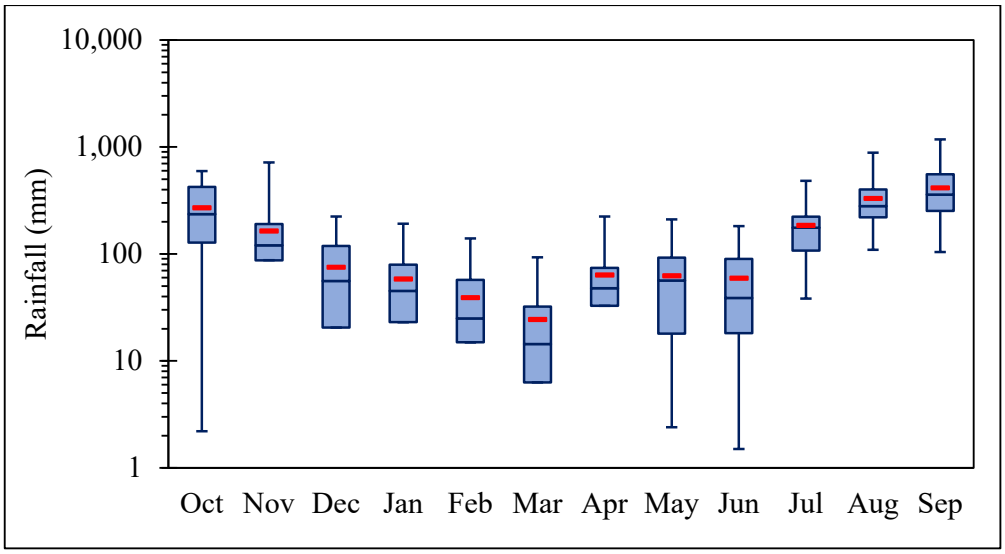

Figure 3-7: Rainfall variation at Batticaloa station

The min, max and mean monthly rainfall recorded at Batticaloa stations indicates that the maximum rainfall has an increasing trend from June to September while the highest is also recorded in the month of September while the lowest is recorded in the month of March. The min, max, and mean graph is presented in Figure 3-8.

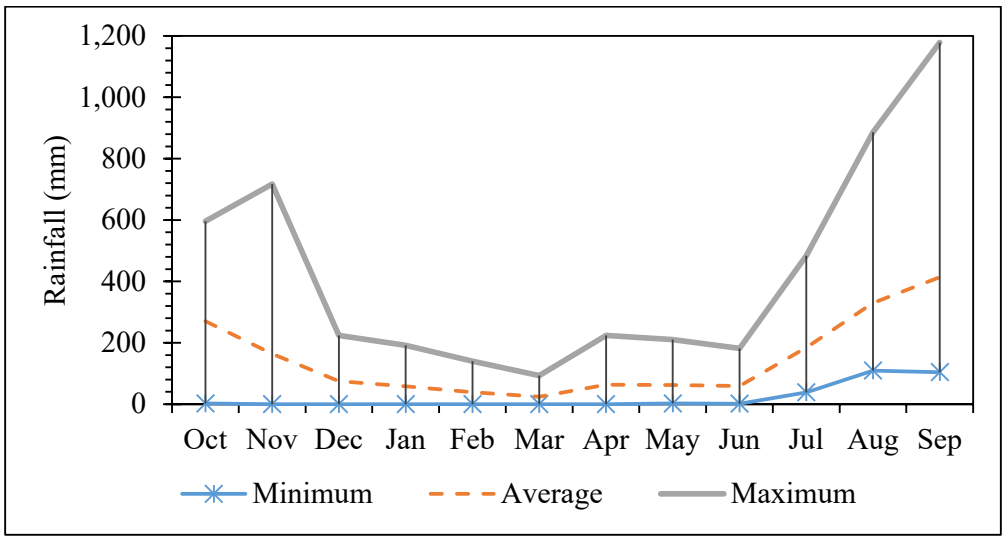

Figure 3-8: Min, max, and average rainfall at Batticaloa station

3.1.5 Streamflow Data

There are several streamflow monitoring locations in the project area, but these measurements are not continuous. There were two river gauges at Welikanda and Maduru Oya dam-site before the reservoir construction. After completing the construction of the Maduru Oya Reservoir, a new gauging station was established at Padiyatalawa in 1984.

The Maduru Oya dam-site station data are missing between 1957 – 1978. The Padiyatalawa station's catchment is very small and does not reflect the river basin's actual landuse change and deforestation. Therefore, the only viable option was to use the Welikanda station's data to calibrate and validate the HEC-HMS model. The details of the available streamflow data are given in Table 3-4 and the locations of rainfall and streamflow gauging stations are shown in Figure 3-2. A summary of the available rainfall and streamflow data is shown in Figure 3-9.

Table 3-4: Collected streamflow data

No.	Station Name	Drainage Area (km^2)	Period Available	Location	Long. (Decimal)	Lat. (Decimal)
1	Padiyathalawa	159	1984 – 2020	Upper Catchment	81.19 E	7.38 N
2	Maduru Oya Damsite	453	1950 – 1978	Midstream	81.21 E	7.65 N
3	Welikanda	1029	1945 – 1978	Downstream	81.25 E	7.93 N

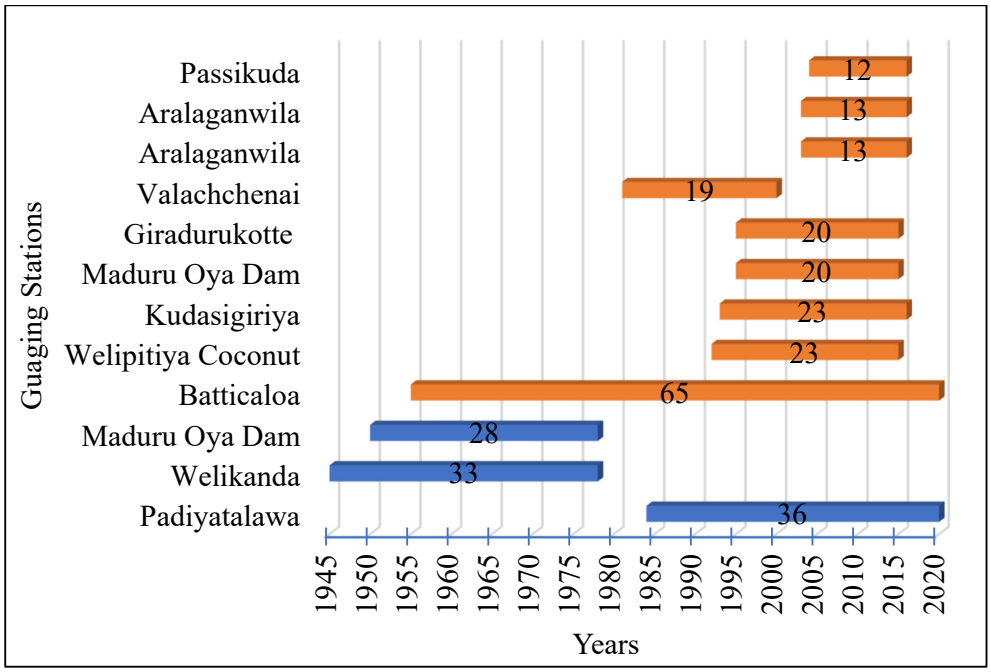

Figure 3-9: Rainfall and Streamflow Data in Maduru Oya

(rainfall in red and streamflow in blue)

From Figure 3-9, it can be observed that there is no concurrent streamflow data available with rainfall in the basin except for Padiyatalawa, which is in the upper catchment with a smaller area, and Welikanda with an earlier period (i.e., prior to the study period). Considering the effect of LULC change impacts on flood peak

discharge, the Welikanda streamflow gauging station with a more extensive area and Batticaloa rainfall station were used in this study for rainfall-runoff modeling.

3.1.6 Maduru Oya streamflow data checking

Streamflow in Welikanda station which is located downstream is checked to analyze the streamflow trend, seasonal pattern, and inconsistencies. Various graphs (annual streamflow, monthly average, seasonal variations, box plot, min, max, and mean) are plotted and shown in Figure 3-10, Figure 3-11, Figure 3-12, Figure 3-13, and Figure 3-14, respectively.

From the annual streamflow graph in Figure 3-10, and monthly average streamflow in Figure 3-11, the major flood event of 1957 which is shown in an orange color circle and happened in the month of December and destroyed a large number of major and minor tank systems in Sri Lanka can be easily distinguished in Maduru Oya basin as well (Wickramasuriya & Fernando, 2012). This event is selected as the major event of the study period for validation of the model.

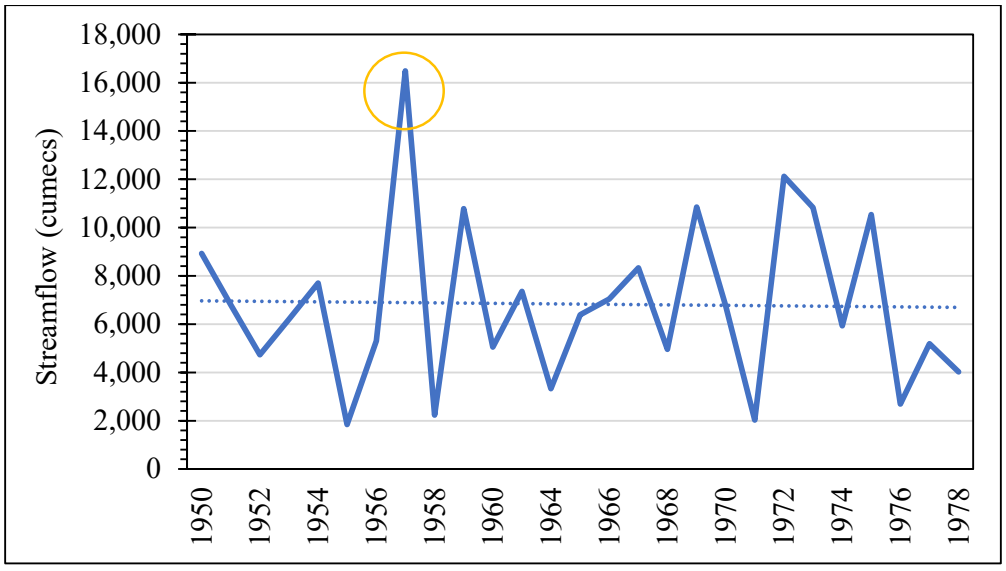

Figure 3-10: Annual streamflow at Welikanda station

The dataset at Welikanda gauging stations contains 15% missing data which is shown in the monthly average streamflow graph in Figure 3-11.

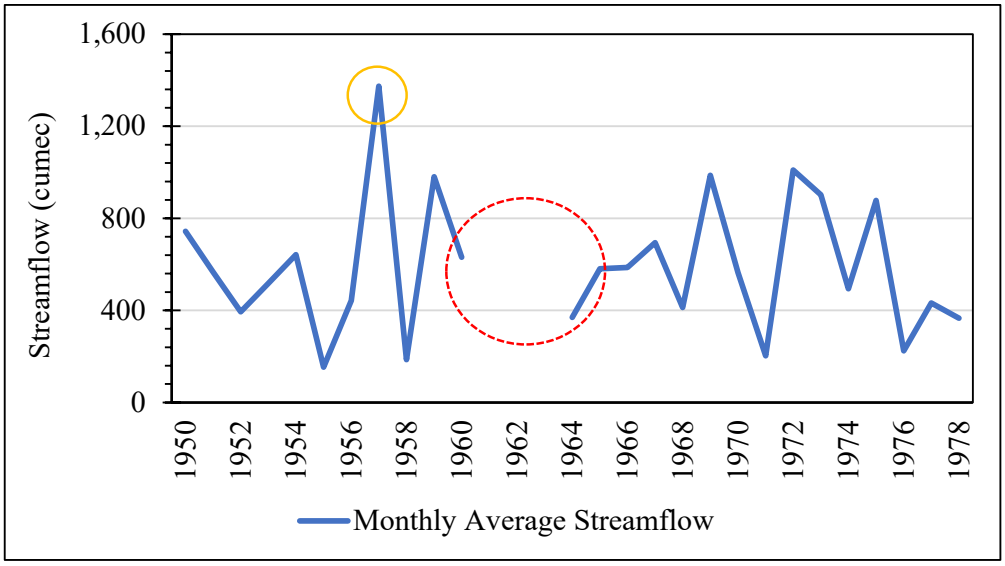

Figure 3-11: Monthly average observed streamflow at Welikanda

The seasonal variation of river discharge at Welikanda station in Figure 3-12, indicates that the highest discharges have happened during the first inter-monsoon (March - April) followed by southwest monsoon (May – September), northeast monsoon (Dec – Feb), and second inter-monsoon seasons in Maduru Oya basin which is shown in Figure 3-12.

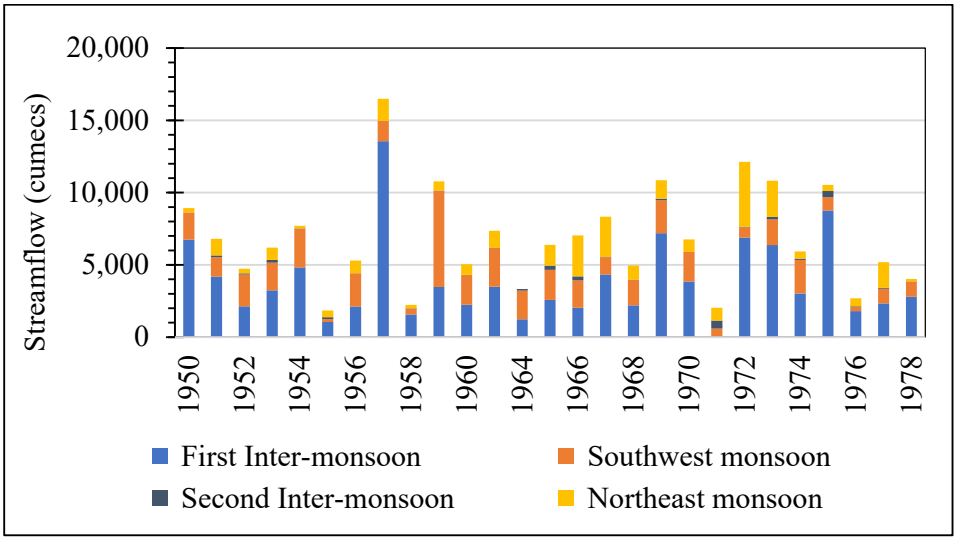

Figure 3-12: Seasonal variation of streamflow at Welikanda station

The box plot of the Welikanda station indicates that the high magnitude of river discharge occurred from February to April in the Maduru Oya basin which is shown in Figure 3-13.

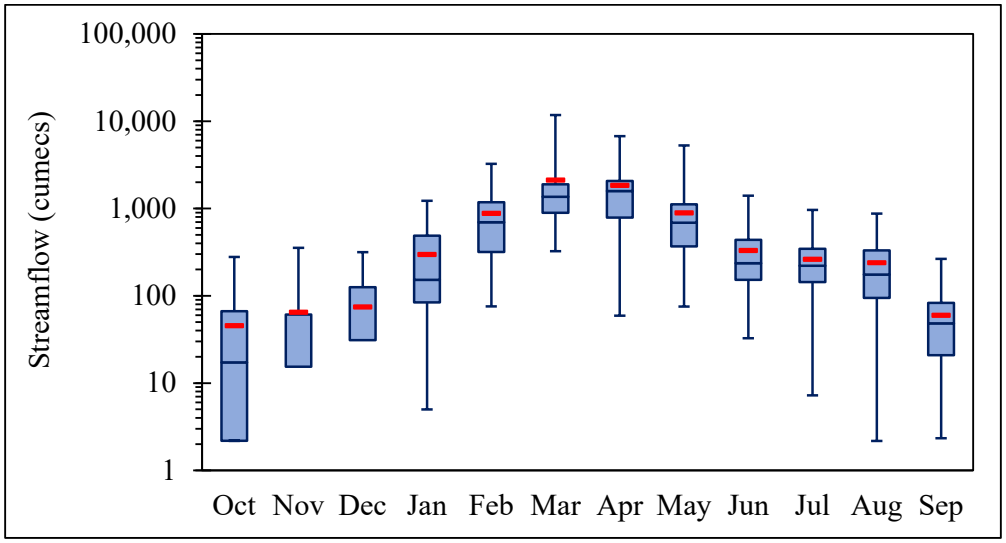

Figure 3-13: Streamflow variation in Welikanda station – box plot

Same as the box plot, the monthly min, max and mean graph shows that the highest discharges were recorded from February to April in the Maduru Oya basin while the lowest is recorded from September to October which is shown in Figure 3-14.

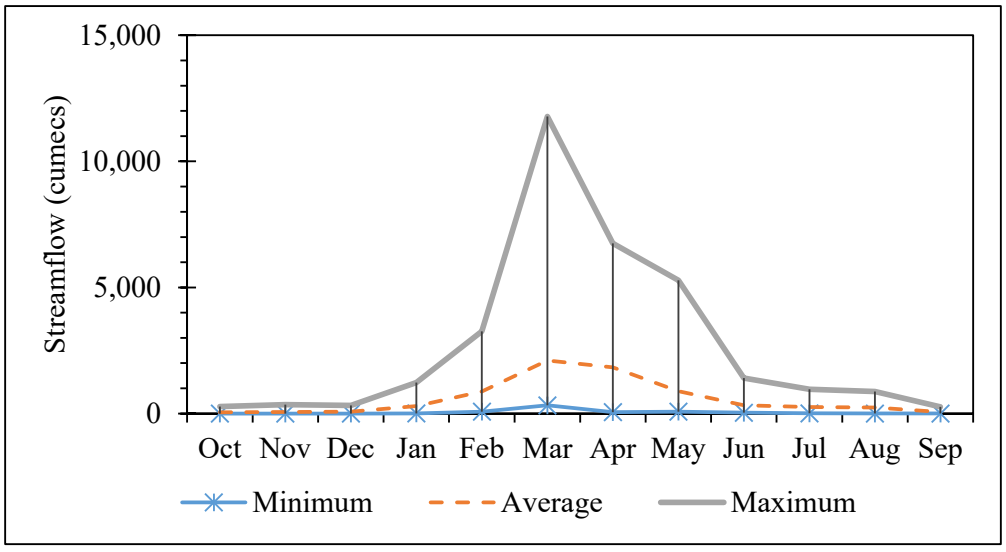

Figure 3-14: Max, min, and average streamflow at Welikanda station

3.2 Single Mass Curve

Rainfall and streamflow data are plotted in a single mass curve to check the inconsistencies where cumulative rainfall data are plotted against time to depict the homogeneity and the results are shown in figure Figure 3-15 and Figure 3-16.

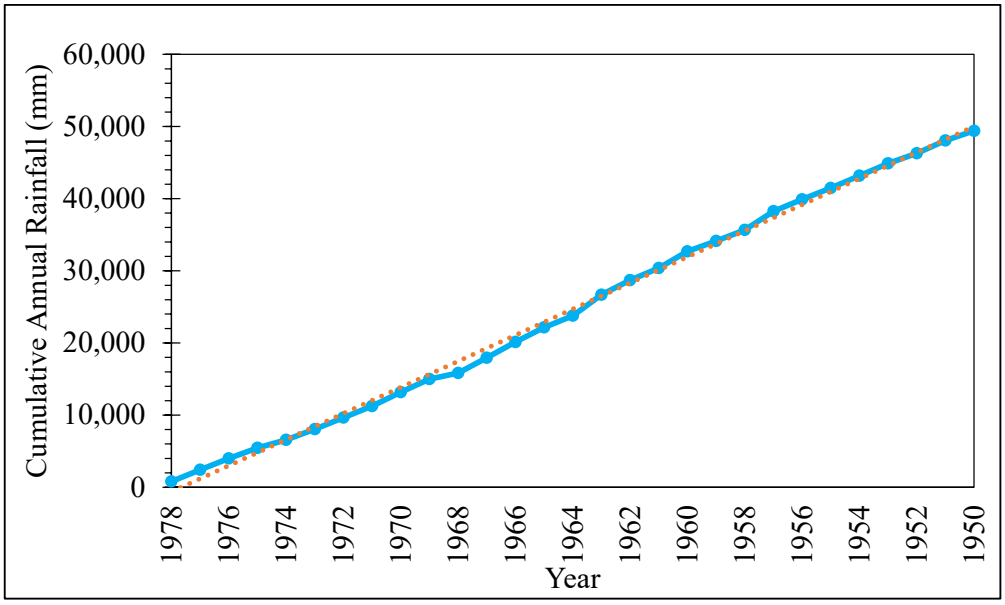

Figure 3-15: Single mass curve of Batticaloa rainfall station

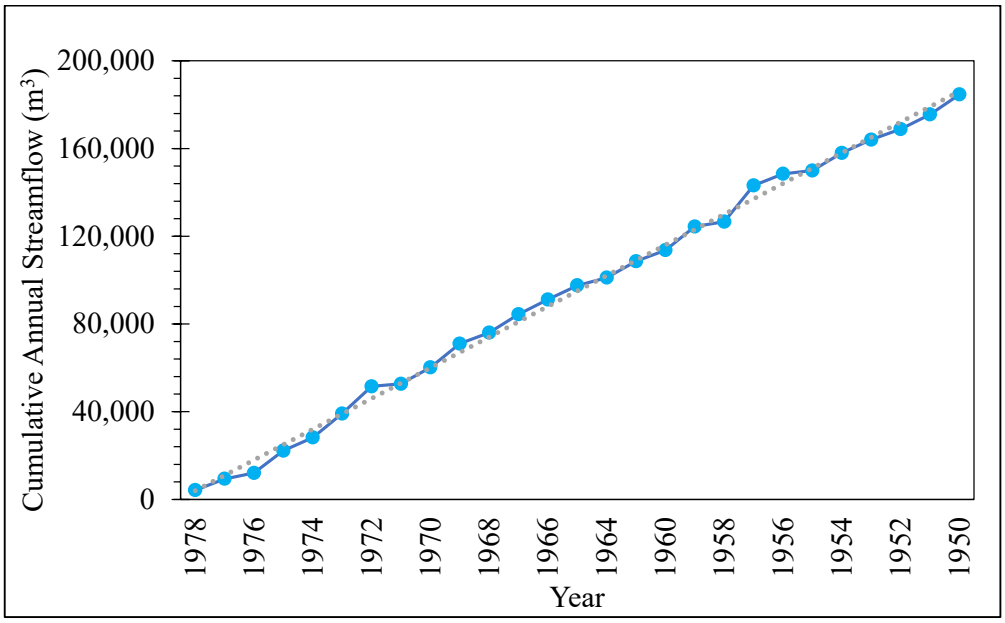

Figure 3-16: Single mass curve of Welikanda streamflow gauging station

The single mass curve graph of rainfall records at Batticaloa stations shows inconsistencies during 1964 – 1968 and from 1975 to 1978. The single mass curve of streamflow records at Welikanda station shows inconsistencies from 1955 – 1958, from 1963 – 1970, from 1972 – 1977. The reason behind the major inconsistency between 1963 – 1970 is the missing data in 1960, 1963, and 1964 which has affected the cumulative rainfall thereafter.

3.3 Correlation Between Rainfall and Streamflow

Correlation between Batticaloa rainfall and Welikanda streamflow gauging stations are checked on a monthly basis and the results are showing a satisfactory correlation which is shown in Figure 3-17.

From the plot, we can observe a good correlation between rainfall and streamflow. There is a high value noticeable which denotes 1178 mm rainfall in the month December 1957 which shows the major flooding event in the respective year.

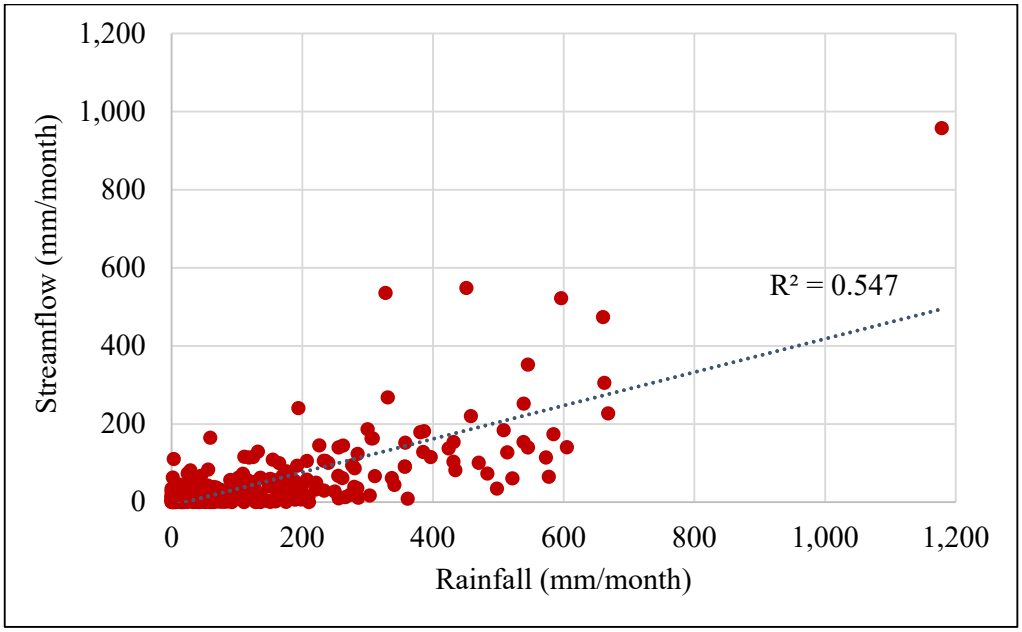

Figure 3-17: Correlation between Batticaloa rainfall and Welikanda streamflow station

3.4 Deforestation and Landuse/Landcover Change Assessment

Deforestation and landuse/landcover are happening in developing countries as a result of the growing need of people for food, shelter, and economic activities. These changes are accompanied by adverse impacts on critical ecosystem services (Kennedy et al., 2015), depletion of biodiversity (Li et al., 2013; Zoran et al., 2012), decreasing land productivity, and changing climatic conditions (Vermote et al., 2016). To enhance a region's economic situation without further deterioration, proper utilization of all available land is crucial (Rawat et al., 2013). Satellite images pave the way to study LULC change in different periods and many researchers (Li et al., 2013; Rwanga & Ndambuki, 2017; Vermote et al., 2016; Zope et al., 2016) have gotten the advantages of using opensource satellite images for LULC studies.

To study the deforestation and landuse change in Maduru Oya river basin Landsat images which are shown in Table 3-5 are acquired. To generate landuse maps, the steps shown in Figure 3-18 are performed, and then the relative changes are calculated, respectively.

Table 3-5: Landsat image acquired for LULC study

No.	Year	Satellite	Date of Acquisition	Resolution
1	1976	Landsat 2 MSS	18-May-76	60m
2	1994	Landsat 5 TM	06-May-94	30m
3	2009	Landsat 5 TM	15-May-09	30m
4	2021	Landsat 8 OLI-TIRS	29-Mar-21	30m

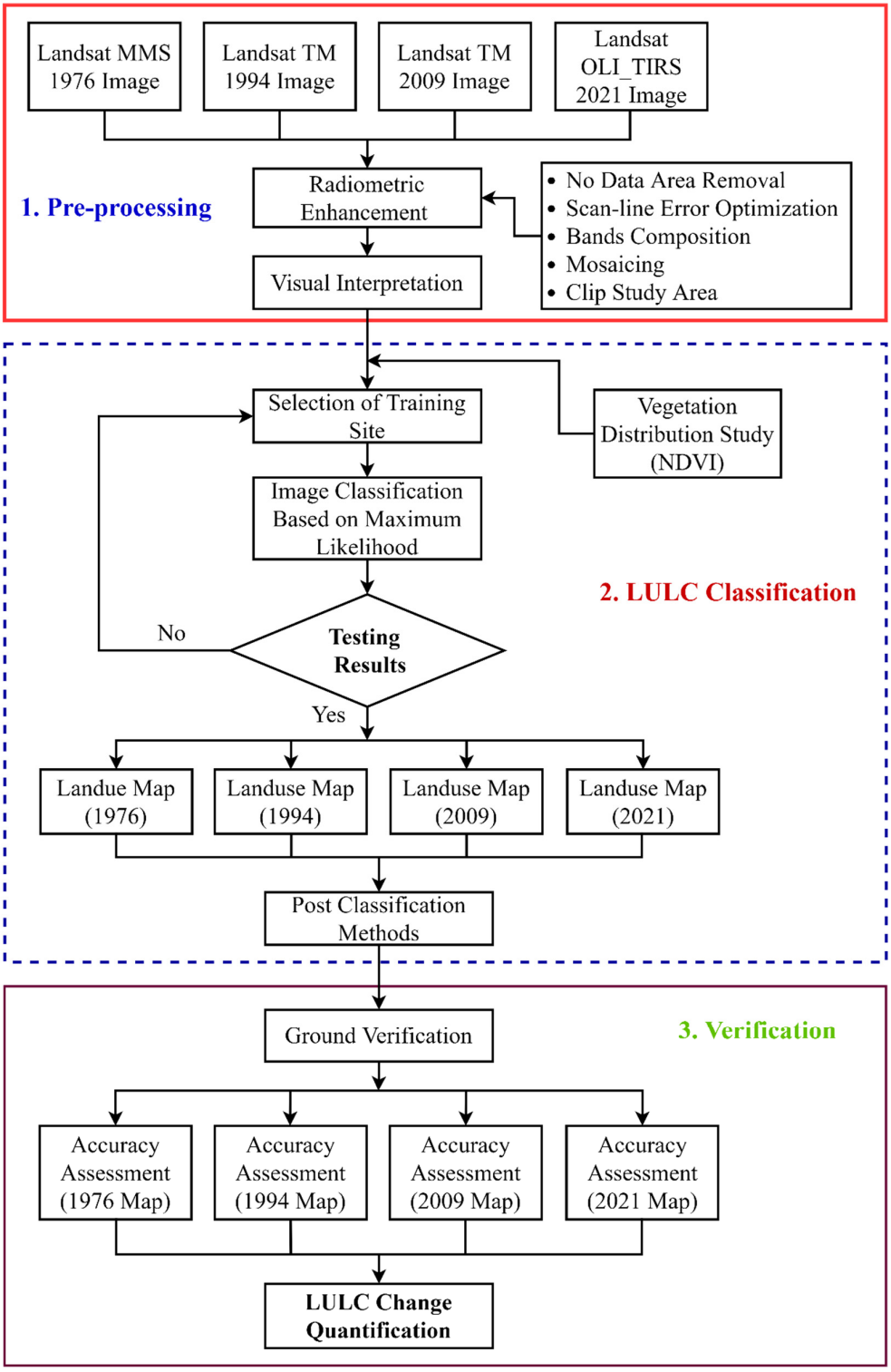

Figure 3-18: LULC classification methodology flowchart

To simplify the quantification of landuse change with a focus on deforestation, LULC change assessment is divided into two major stages considering data availability and Accelerated Mahaweli Program (AMP) implemented in the study area:

1. Landuse/landcover change induced by Accelerated Mahaweli Program (AMP) between 1976 – 1994. In this period, construction of the Maduru Oya reservoir which started in 1979 and finished in 1986 as a development program of the study area is considered as the major LULC changing factor.
2. Landuse/landcover change post-Accelerated Mahaweli Program between 1994 – 2021. To quantify LULC change after AMP to the present, this stage is considered.

3.4.1 Landuse/landcover Change Induced by AMP (1976-1994)

The Mahaweli Development Programme (MDP) would have taken roughly 30 years to implement in stages starting in 1975. However, in 1977, the newly constituted J. R. Jayewardene administration chose to accelerate the project and accomplish it within its six-year term of office. In 1977, the Accelerated Mahaweli Programme (AMP) was undertaken in conjunction with a revision of the Master Plan. The initial works of the program included the construction of the Kotmale, Victoria, Maduru Oya, and Randenigala dams, as well as the downstream development of about 60,000 ha in Systems B and C, which included the Minipe anicut, the Right Bank Transbasin Canal, and the Ulhitiya and Ratkinda reservoirs. The MDP was aimed to achieve Sri Lanka's self-sufficiency in basic food stuffs like rice and sugar, to strengthen the country's foreign exchange position, to mitigate high levels of unemployment, and to foster strongly-based regional economies (ACRES, 1979). A wide landuse change happened in the Maduru Oya river basin due to the activities designed and implemented for Maduru Oya Project.

It is stated in the Maduru Oya Project Feasibility Study that in physical terms, the main element of the Maduru Oya project include the dam, link tunnel, and canal systems (ACRES, 1979). It was considered that the dam would be a rockfill or concrete gravity structure, some 41.5 m in height above the foundation and 1020 -1050 m in length along the crest. The reservoir was designed to have a live storage capacity of 457

MCM, compared to an average annual inflow of 385 MCM. To augment the natural runoff and provide irrigation water for more land in the downstream development area, water would be diverted into the Maduru Oya basin upstream from the dam. This water would be originated in the Mahaweli Ganga at Minipe and would be conveyed by the Minipe right bank trans-basin canal to the Ulhitiya Oya and Patkinda Oya reservoirs. From these reservoirs, the water will enter a 5800 m long, 5.1 m diameter link tunnel, which will deliver the water to the Vila Oya, a minor left bank tributary of the upper Maduru Oya.

Irrigation water was to be discharged from the dam through separate powerhouses into the main canals in the left and right bank. The left bank main canal, which was aimed to serve an irrigable area of about 27,000 hectares, was designed to be about 58 km in length. Major branch canals would total a further 75 km. Laterals and farm ditches, major and minor drainage works, and land improvements were also required.

The right bank main canal was designed to serve a smaller irrigable area of about 18,000 hectares with a length of 53 km, with a major branch canal with a total length of about 33 km. As for the left bank, other works included were laterals, farm ditches, drainage channels, and land improvements.

According to ACRES (1979) in the Maduru Oya project feasibility study, activities within the Maduru Oya project were aimed to support the achievement of the Mahaweli Program as a whole.

In this study, the Maduru Oya project and mainly the Maduru Oya reservoir construction is considered as a leading landuse change factor. Therefore, this stage is considered to assess the landuse change separately from the remaining period. After data collection, data checking, and quality enhancement, satellite images acquired in 1976 and 1994 were classified using a supervised image classification. Five major landuse types were identified in the Maduru Oy river basin: Forest, Homestead/Garden, Paddy, Scrubland, and Water Body. For each landuse type, 50 training samples have been taken and landuse maps are classified accordingly.

3.4.2 Landuse/landcover Change Post-AMP (1994-2021)

To assess the landuse change post-Accelerated Mahaweli Program to the present, this stage is considered. After data collection, data checking, and quality enhancement, satellite images acquired in 2009 and 2021 were classified using a supervised image classification. Five major landuse types are identified in the Maduru Oy river basin: Forest, Homestead/Garden, Paddy, Scrubland, and Water Body. For each landuse type, about 50 training samples have been taken and landuse maps were classified accordingly.

3.4.3 Accuracy Assessment

Accuracy assessment is an important step in landuse/landcover classification which provides useful information on how much the image is classified accurately based on another reference. The accuracy analysis also shows how well the pixels were sampled into the relevant land cover groups (Rwanga & Ndambuki, 2017).

To assess the accuracy of 1976, 1994, 2009, and 2021 landuse maps, 100 samples are taken randomly from all the ground truth points and verified with the available maps. To perform the accuracy assessment of the 1976 image, the district-wise landuse maps of Sri Lanka which are accessible in the 1980s (Panagos et al., 2011) in the European Digital Archive of Soil Maps (EDASM) were collected and georeferenced. For accuracy assessment of the 1994 image, the landuse shapefile of Sri Lanka which was collected from the Survey Department was used and validated with the observations on Google Earth imageries. For the accuracy assessments of 2009 and 2021 images, Google Earth historical imageries were used.

Then, a confusion matrix (error matrix) which quantitively shows the accuracy of the classified images is prepared for each image to evaluate their accuracy. Error matrix for 1976, 1994, 2009, and 2021 landuse maps are shown in Table 3-6, Table 3-7, Table 3-8, and Table 3-9.

Table 3-6: Confusion matrix (error matrix) for accuracy assessment of 1976 image

No.	LULC Type	Forest	Homestead/ Garden	Paddy	Scrubland	Water Body	Total User
1	Forest	17	0	1	2	0	20
2	Homestead/Garden	1	12	4	3	0	20
3	Paddy	0	0	17	3	0	20
4	Scrubland	2	1	0	17	0	20
5	Water Body	0	0	1	0	19	20
Total Producer		20	13	23	25	19	100

Table 3-7: Confusion matrix (error matrix) for accuracy assessment of 1994 image

No.	LULC Type	Forest	Homestead/ Garden	Paddy	Scrubland	Water Body	Total User
1	Forest	20	0	0	0	0	20
2	Homestead/Garden	2	11	2	5	0	20
3	Paddy	0	1	16	3	0	20
4	Scrubland	1	1	1	17	0	20
5	Water Body	0	0	0	0	20	20
Total Producer		23	13	19	25	20	100

Table 3-8: Confusion matrix (error matrix) for accuracy assessment of 2009 image

No.	LULC Type	Forest	Homestead/ Garden	Paddy	Scrubland	Water Body	Total User
1	Forest	20	0	0	0	0	20
2	Homestead/Garden	1	15	2	2	0	20
3	Paddy	0	0	16	4	0	20
4	Scrubland	0	0	1	19	0	20
5	Water Body	1	0	1	0	18	20
Total Producer		22	15	20	25	18	100

Table 3-9: Confusion matrix (error matrix) for accuracy assessment of 2021 image

No.	LULC Type	Forest	Homestead/ Garden	Paddy	Scrubland	Water Body	Total User
1	Forest	20	0	0	0	0	20
2	Homestead/Garden	0	15	3	1	1	20
3	Paddy	0	0	17	3	0	20
4	Scrubland	0	0	1	19	0	20
5	Water Body	0	0	0	0	20	20
Total Producer		20	15	21	23	21	100

Because the two sets of classes have to be similar, the diagonal line (shown in grey) represents the pixels in both data sets that have the same land cover class. Off-diagonals have been classified incorrectly. One method of determining classification accuracy is to calculate the proportion of pixels in the diagonal elements of an error matrix and report it as a percentage of the total number of pixels compared. User

accuracy, producer accuracy, overall accuracy, and kappa coefficient are calculated for each image using equations [3-1], [3-2], [3-3], and [3-4], respectively.

$$User\ Accuracy = \frac{Number\ of\ Correctly\ Classified\ Pixels\ in\ Each\ Class}{Total\ Number\ of\ Classified\ Pixels\ in\ that\ Class} \times 100 \quad [3\text{-}1]$$

$$Producer\ Accuracy = \frac{Number\ of\ Correctly\ Classified\ Pixels\ in\ Each\ Class}{Total\ Number\ of\ Reference\ Pixels\ in\ that\ Class} \times 100 \quad [3\text{-}2]$$

$$Overall\ Accuracy = \frac{Total\ Number\ of\ Correctly\ Classified\ Pixels\ (Diagonal)}{Total\ Number\ of\ Reference\ Pixels} \times 100 \quad [3\text{-}3]$$

$$\hat{k} = \frac{N\sum_{i=1}^{r} x_{ii} - \sum_{i=1}^{r}(x_{i+} \times x_{+i})}{N^2 - \sum_{i=1}^{r}(x_{i+} \times x_{+i})} \quad [3\text{-}4]$$

where r is the number of rows, columns in the error matrix; N is the number of observations (pixels) in the error matrix; x_{ij} is the major diagonal element for class i; x_{i+} is the total number of observations in row i (right margin), and x_{+i} is the total number of observations in column i (bottom margin).

3.5 Normalized Difference Vegetation Index (NDVI)

The "Normalized Difference Vegetation Index (NDVI) is a dimensionless index that describes the difference between visible and near-infrared reflectance of vegetation cover and can be used to estimate the density of green on an area of land" (Weier & Herring, 2000). The NDVI value for a specific pixel is always ranging from minus one (-1) to plus one (+1); nevertheless, no green leaves deliver a number near to zero. A zero denotes no vegetation, whereas a value close to +1 (0.8-0.9) suggests the maximum density of green leaves available. Low NDVI values (0.1 and lower) indicate barren areas of rock, sand, or snow. High levels (0.6 to 0.8) imply temperate and tropical rainforests, whereas moderate values (0.2 to 0.3) indicate shrub and grassland (Dowo & Kativu, 2013). The NDVI is calculated by dividing the total of near-infrared (NIR) and red (RED) reflectance by their difference in Equation [3-5].

$$NDVI = \frac{NIR - RED}{NIR + RED} \quad [3\text{-}5]$$

3.6 HEC-HMS Model Development

The Army Corps of Engineers' Hydrologic Engineering Center (HEC) developed the Hydrologic Modeling System (HMS) to simulate the rainfall-runoff processes in dendritic watershed systems (USACE, 2021). It is produced to address various problems in water resources management, urban hydrology, flood studies, and many more in the water sector.

HEC-HMS contains different models for runoff volume, direct runoff, routing, and baseflow, as well as different tools for calculating hydrological processes. Model development may be broken down into four major components, according to the classification performed by Zema et al. (2016).

- Basin model: For characterizing the physical parameters of the watershed and the topology of the stream network, the basin model is utilized. It includes Modeling components for canopy interception, surface storage, infiltration, surface runoff, baseflow, channel routing, and lakes will be included. It might also include elements to introduce engineered structures like dikes, reservoirs, and pump stations.
- Meteorological model: One of the most important parts of every project is the meteorologic model. The primary objective is to define meteorologic boundary conditions for subbasins.
- Data Input: This module provides the opportunity to enter time-series, gridded data, and paired data as needed data for initial conditions, boundary conditions, or parameters.
- Control specifications: This component helps to manage simulations and run them on multiple timeframes.

In this study, an event-based model is developed. The selected methods for model development and meteorologic model used in this study are shown in Table 3-10 and Table 3-11.

Table 3-10: Selected HEC-HMS methods

Model Type	Loss Method	Transform Method	Routing Method	Baseflow Method	Canopy	Surface
Event-Based	SCS-CN	SCS Unit Hydrograph	Muskingum	Recession	Simple Canopy	Simple Surface

Table 3-11: Selected meteorologic models' methods

Model Type	Precipitation	Evapotranspiration	Snowmelt
Event-Based	Specified Hyetograph	Monthly Average	Not Used

3.6.1 Model Setup

The model setup is a composition of the basin and meteorological models to simulate a hydrological event. A brief explanation of the HEC-HMS main components is given in the following sections.

3.6.2 Assumptions

To set up a model in a data-scarce situation, the hydrologists and water engineers rely on realistic assumptions which make the process of modeling easy. To simplify the model and overcome the lack of data in the Maduru Oya river basin, the following assumptions are made during the HEC-HMS model setup in this study.

- The major rainstorms at Batticaloa gauge station correspond to the records in Welikanda river gauging station and the rainfall is distributed uniformly across the river basin.
- The Maduru Oya reservoir is operating at its maximum capacity level during the flood events therefore, the inflow is equal to outflow from the reservoir and its detention capacity is neglected.

3.6.3 Basin Model

The HEC-HMS version 4.8 which is used in this study enables the users to delineate basin elements such as subbasins, reaches, junctions, sources, sinks, reservoirs, and diversions using a digital elevation model which can be easily input into the model. It also provides information about the above components which eases further calculations and computation of parameters.

For HEC-HMS model development, the Welikanda river flow gauging station is considered as the outlet which consists of data between 1945 - 1978. The Batticaloa rainfall station is considered as the only rainfall station available during the same period and the catchment is divided into five sub-catchments which the characteristics are shown in Table 3-12 and Figure 3-19.

Table 3-12: Sub-catchments characteristics

Sub-Catchments	Area (km^2)
Sub-catchment 1	335.66
Sub-catchment 2	88.10
Sub-catchment 3	216.46
Sub-catchment 4	162.34
Sub-catchment 5	226.96
Total	**1029**

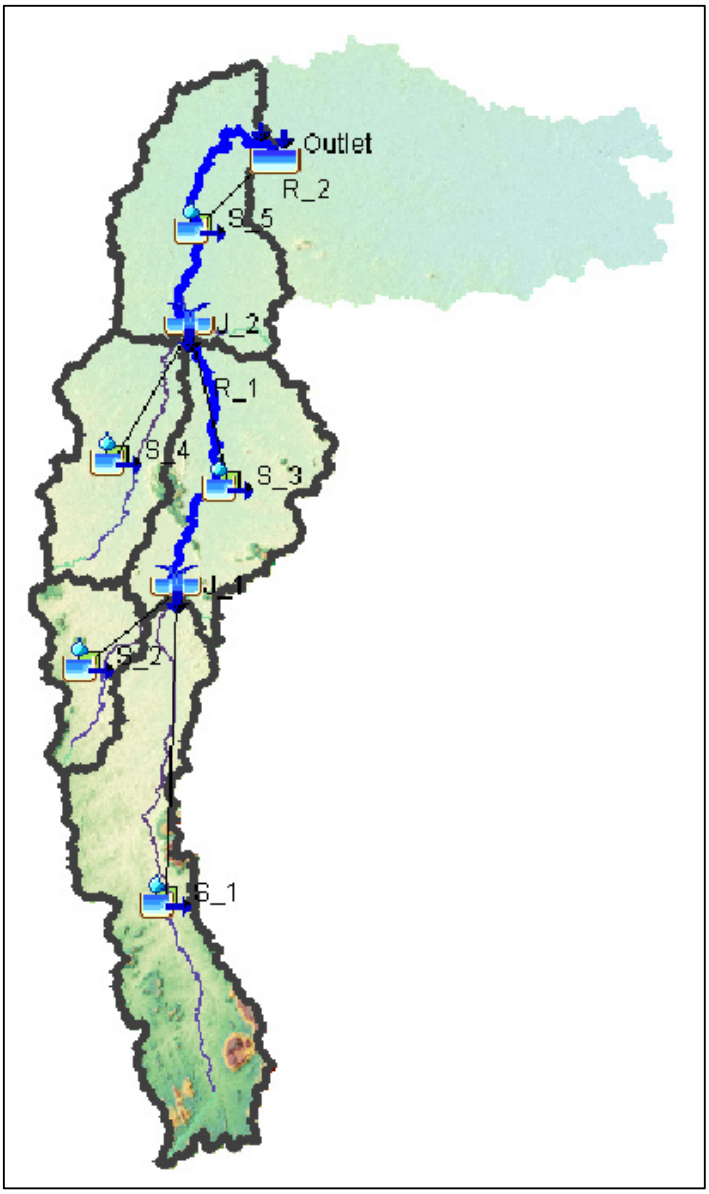

Figure 3-19: HEC-HMS model setup (subcatchments, reaches, junction, and streams)

As it is previously indicated that SCS CN, SCS UH, Muskingum, and Recession methods are selected for loss, transform, routing, and baseflow in this study, the mechanism, and formulation of them are explained in the following sections.

3.6.3.1 Soil Conservation Service Curve Number Loss Method

While a subbasin element illustrates the interaction of infiltration, surface runoff, and subsurface processes, the actual infiltration computations are carried out by a loss

method embedded inside the subbasin (USACE, 2021). The incremental losses for each sub-basin are estimated using appropriate curve numbers in the Soil Conservation Service Curve Number technique in this study, given the fact that HEC-HMS supports twelve loss methods.

The USACE Users' Manual (2021), recommends the SCS curve number loss approach for an event-based simulation. The approach was designed to quantify overall infiltration during a storm. By recalculating the infiltration volume at the end of each time period, the software calculates incremental precipitation during a storm. "Infiltration during each time interval is the difference in volume at the end of two adjacent time intervals" (USACE, 2021).

Precipitation excess is calculated using the SCS CN values, which are based on cumulative precipitation, soil cover, land use, and antecedent moisture. Empirical formulas are used to calculate the infiltration loss (USACE, 2018) in Equation [3-6].

$$Pe = \frac{(P - I_a)^2}{(P - I_a) + S} \quad [3\text{-}6]$$

where P_e is accumulated precipitation excess at time t, P is the accumulated rainfall depth at time t, I_a is the initial abstraction (initial loss), and S is the potential maximum retention, a measure of the ability of a basin to abstract and retain storm precipitation.

According to this formulation, the accumulated precipitation excess and consequently the runoff is zero until the accumulated rainfall exceeds the initial abstraction. The relationship between the initial abstraction and potential maximum retention is given in Equation [3-7]:

$$I_a = 0.2 \times S \quad [3\text{-}7]$$

Therefore, cumulative excess at time t is estimated using Equation [3-8]:

$$Pe = \frac{(P\ - 0.2 \times S)^2}{(P + \ 0.8 \times S)} \quad [3\text{-}8]$$

The maximum retention, S, and basin characters are related to the curve number as in Equation [3-9]:

$$S = \frac{25400 - 254\,CN}{CN}\ (in\ SI\ units) \qquad [3\text{-}9]$$

According to USDA (2009), the hydrological soil groups are categorized into four following categories:

- Group A: Soils in this group are described as having low runoff potential when thoroughly wet. The soil allows water to freely pass through it. The soils in this group are composed of less than 10% clay and more than 90% sand or gravel, with a gravel or sand texture.
- Group B: Soils in this group are described as having moderately low runoff potential when thoroughly wet. Water transmission through the soil is unimpeded. Group B soils feature loamy sand or sandy loam textures and include between 10% and 20% clay and 50% to 90% sand.
- Group C: When saturated, the soils in this group are described by a high runoff potential. The ability of water to pass through the soil is limited. Group C soils are loam, silt loam, sandy clay loam, clay loam, and silty clay loam in texture, with 20 - 40% clay and less than 50% sand.
- Group D: When completely saturated, these soils have a significant runoff potential. The circulation of water through the soil is limited or non-existent. Clayey textures are common in Group D soils, which include more than 40% clay and less than 50% sand.

Based on findings of Withanage et al. (2018), the prominent soil types in the basin are Reddish Brown Earths and Immature Brown Loams and can be considered as moderately permeable soils. Therefore, the soil type for the study area is considered type C.

The summary of the CN weighted averages for each scenario are shown in Table 3-13, Table 3-14, Table 3-15, Table 3-16, and the details are given in Annexure 1.

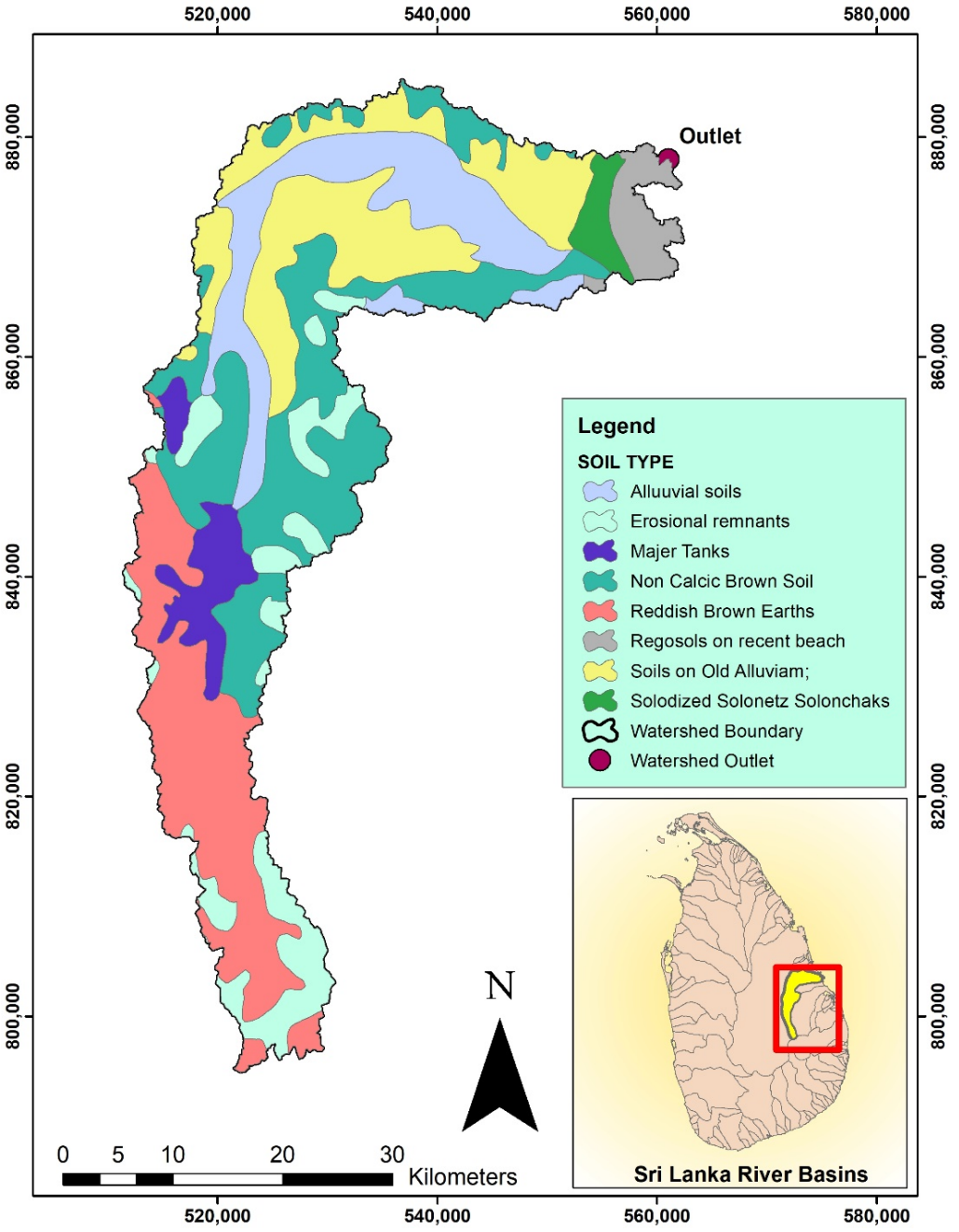

Figure 3-20: Maduru Oya soil map (Source: Survey Department)

Table 3-13: Curve number calculations for 1976 LU scenario

1976 LU Scenario					
Sub-catchment	**Area (km^2)**	**Soil Group**	**CN x A**	**Impervious Area (km^2)**	**Impervious Area (%)**
Sub catchment 1	335.18	C	61.43	3.0679	0.92
Sub catchment 2	87.89	C	60.09	0.0832	0.09
Sub catchment 3	216.61	C	60.41	0.9025	0.42
Sub catchment 4	161.74	C	65.45	5.6491	3.49
Sub catchment 5	226.46	C	62.82	3.0485	1.35
Total	**1027.87**	**C**	**62.04**	**12.751**	**1.24**

Table 3-14: Curve number calculations for 1994 LU scenario

1994 LU Scenario					
Sub-catchment	**Area (km^2)**	**Soil Group**	**CN x A**	**Impervious Area (km^2)**	**Impervious Area (%)**
Sub catchment 1	335.6	C	63.3	26.45	7.9
Sub catchment 2	88.1	C	65.8	10.26	11.6
Sub catchment 3	216.3	C	72.4	35.77	16.5
Sub catchment 4	162.4	C	73.0	14.75	9.1
Sub catchment 5	227.0	C	71.9	4.10	1.8
Total	**1029.34**	**C**	**69.29**	**91.330**	**8.87**

Table 3-15: Curve number calculations for 2009 LU scenario

2009 LU Scenario					
Sub-catchment	**Area (km^2)**	**Soil Group**	**CN x A**	**Impervious Area (km^2)**	**Impervious Area (%)**
Sub catchment 1	335.6	C	64.1	14.3	4.3
Sub catchment 2	88.1	C	63.5	3.7	4.2
Sub catchment 3	216.4	C	72.0	28.4	13.1
Sub catchment 4	162.4	C	75.0	15.9	9.8
Sub catchment 5	227.0	C	74.7	8.6	3.8
Total	**1029.4**	**C**	**69.9**	**70.8**	**6.9**

Table 3-16: Curve number calculations for 2021 LU scenario

2021 LU Scenario					
Sub-catchment	**Area (km^2)**	**Soil Group**	**CN x A**	**Impervious Area (km^2)**	**Impervious Area (%)**
Sub catchment 1	335.6	C	65.7	28.4	8.5
Sub catchment 2	88.1	C	64.2	8.5	9.6
Sub catchment 3	216.4	C	73.1	36.2	16.7
Sub catchment 4	162.4	C	75.9	18.8	11.6
Sub catchment 5	227.0	C	74.7	9.6	4.2
Total	**1029.4**	**C**	**70.7**	**101.5**	**9.9**

3.6.3.2 Soil Conservation Service Unit Hydrograph Transform Method

The unit hydrograph method of the Soil Conservation Service (SCS) defines a curvilinear unit hydrograph by first determining the percentage of unit runoff that takes

place before the peak flow, and then fitting a triangular unit hydrograph to the curvilinear unit hydrograph to determine the total time base of the unit hydrograph (USACE, 2021).

The lag time in minutes is the sole parameter required for SCS UH. The standard lag is the period between the centroid of precipitation mass and the peak flow of the corresponding hydrograph. The lag time may be calculated by dividing the period of unit precipitation by two, plus 60 percent of the time of concentration, according to the formulas used to get the curvilinear unit hydrograph (USACE, 2021).

Furthermore, the default Peak Rate Factor (PRF) of 484 can vary from one watershed to the next depending on topography, with flat basins having a lower PRF and steeper basins having higher PRFs up to 600.

According to USDA-NRCS (2010), "Time of concentration (Tc) is the time required for runoff to travel from the hydraulically most remote point in the watershed to the outlet". The site with the longest traveling time to the watershed outlet is the hydraulically most remote location, not necessarily the place with the longest flow distance to the outlet. Time of concentration is calculated using the Kiripich formula in Equation [3-10].

$$t = 0.0194\, L^{0.77} S^{-0.385} \qquad [3\text{-}10]$$

where t is the time of concentration in minutes, L is the maximum length of water travel in m, and S is the slope of the catchment and is given in Equation [3-11].

$$S = \frac{\Delta H}{L} \qquad [3\text{-}11]$$

ΔH is the difference in elevation between most remote points on the catchment outlet.

Lag time is being calculated using Equation [3-12].

$$T = 0.6 \times T_c \qquad [3\text{-}12]$$

Time of concentration, maximum potential retention, and lag time are calculated based on the above equations and shown in Table 3-17.

Table 3-17: Time of concentration and lag time calculations

Subbasin	Area (km^2)	Longest flow path length (m)	Basin slope	Time of concentration (min)	Time lag (min)
Subbasin 1	335.66	30095.9	0.055	166.10	99.66
Subbasin 2	88.10	21432.4	0.081	110.04	66.02
Subbasin 3	216.46	60412.9	0.115	213.69	128.21
Subbasin 4	162.34	34959.0	0.073	167.30	100.38
Subbasin 5	226.96	36740.0	0.042	214.01	128.41

3.6.3.3 Recession Baseflow Method

The recession baseflow approach is intended to simulate the normal behavior seen in watersheds when channel flow decreases exponentially after an event. This approach is basically aimed to simulate events (USACE, 2021). The initial condition can be specified using one of two methods: initial discharge or initial discharge per area. In the first method, the initial baseflow should be specified as a discharge with units of volume per time. This approach is especially useful for calculating the initial flow in a channel when streamflow data is available at the subbasin's outlet. The initial baseflow is specified as a volume per area per time in the second method. When generalized criteria for watershed yield are utilized to calculate the initial flow, this technique is more suited.

3.6.3.4 Muskingum Routing Method

The "Muskingum" routing method routes the flow along the stream reach using mass balance. This mathematical formulation is developed by McCarthy (1938). By adding a travel time for the reach and weighing between the effect of inflow and outflow, it assumes a linear technique accounts for increasing and decreasing storage during flood waves (USACE, 2018). The following is a derivation of the mathematical formulation

of the approach. The Mass balance is given in Equation [3-13] and channel storage volume in Equation [3-14].

$$\frac{dS}{dt} = I - Q \quad [3\text{-}13]$$

$$S = K\,[xI + (1 - x)\,Q] \quad [3\text{-}14]$$

where S is the water storage, t is the time (hr), I is the inflow (m^3/s), Q is the outflow (m^3/s), K is the storage constant (hr), and x is the weighting factor. The storage volume is the simple linear combination of the inflow of the upstream and outflow of the downstream. Parameter K reflects the wave travel time, and parameter x reflects the flood peak attenuation and hydrograph shape flattening of a diffusion wave in motion. Two model parameters, K, and x, can be determined from observations.

3.6.3.5 Simple Canopy Method

The simple canopy method is a simple illustration of a plant canopy. Until the canopy storage capacity is filled, all precipitation will be intercepted. All subsequent precipitation will fall to the surface, or straight to the soil if no description of the surface is given after the storage is full. All evapotranspiration will be utilized to drain the canopy storage until all water in storage is drained out (USACE, 2021).

There are five components to be set up in the simple canopy method:

- The initial condition of the canopy is the percentage of the canopy storage that is full of water at the beginning of the simulation.
- Canopy storage refers to the quantity of water that can be stored on leaves before it falls on the surface.
- When calculating the amount of water to extract from the soil, the crop coefficient is a ratio applied to the potential evapotranspiration.
- Evapotranspiration, which may be set to evaporate stored water and extract water from the soil just during dry periods without precipitation, or to evaporate stored water and remove water from the soil during both dry and wet periods.

- Uptake method: There are two ways of extracting water from the soil. The Simple approach extracts water at the potential evapotranspiration rate and can be combined with the deficit constant or soil moisture accounting loss rate methods to get the best results. The Tension Reduction method which can be used with the soil moisture accounting method collects water from the gravity zone at the potential evapotranspiration rate but decreases the rate when extracting from the tension zone. Unless Simple or Tension Reduction methods are used, no water will be extracted from the soil. The canopy parameters are found through the calibration process.

3.6.3.6 Simple Surface Method

This method depicts the soil surface in a concise manner. All precipitation that falls on the soil surface is trapped and stored until the surface's storage capacity is reached. Whenever there is water in surface storage, it infiltrates into the soil. That is, even if the storage capacity is not full, water will penetrate. When the capacity of storage is satisfied and the precipitation through-fall rate exceeds the infiltration rate, the surface runoff will occur (USACE, 2021).

There are two parameters in the simple surface: Surface storage, which reflects the maximum quantity of water that can be stored on the soil surface before surface runoff begins, and initial storage, which represents the proportion of the surface storage that is full with water at the start of the simulation. Both parameters are adjusted through calibration of the model.

3.6.4 Event Selection

Since this study is focusing on flood peak discharge, the flood events are selected based on return period estimation using Gambel's method from the available datasets.

Gumbel defined a flood as "the largest of the 365 daily flows and the annual series of flood flows constitute a series of largest values of flows" (Subramanya, 2013). According to this theory of extreme events, the probability of occurrence of an event is equal to or larger than a value x_0 which is,

$$P(X \geq x_0) = 1 - e^{-e^{-y}} \quad [3\text{-}15]$$

in which y is a dimensionless variable given by

$$y = \alpha(x - a); \quad [3\text{-}16]$$

$$a = \bar{x} - 0.45005\,\sigma_x \quad [3\text{-}17]$$

$$\alpha = \frac{1.2825}{\sigma_x} \quad [3\text{-}18]$$

Thus,

$$y = \frac{1.285(x - \bar{x})}{\sigma_x} + 0.577 \quad [3\text{-}19]$$

Where $\bar{x}$ = mean, σ_x = standard deviation of variate X. The value of X for a given P that is required is transposed as:

$$y_P = -ln(-ln(1 - P)) \quad [3\text{-}20]$$

Return period, T = 1/P and y_T = value of y called reduced variate for a given T

Therefore,

$$y_T = -\left(l_n \cdot l_n \frac{T}{T-1}\right) \quad [3\text{-}21]$$

Or:

$$y_T = -\left(0.834 + 2.303\, log\, log \frac{T}{T-1}\right) \quad [3\text{-}22]$$

Now rearranging the value of variate x with return period T is given by:

$$x_T = \bar{x} + K\sigma_x \quad [3\text{-}23]$$

Where,

$$K = \frac{y_T - \overline{y_n}}{s_n} \quad [3\text{-}24]$$

$\overline{y_n}$ =reduced mean and s_n = reduced standard deviation

To calculate the return period, the following parameters are calculated.

Table 3-18: Parameters calculations for flood return period estimation

Year	Max SF (m^3/day)	Rank (M)	Recurrence Interval (T)	Reduced variate (Yt)	Frequency factor (K)	Xt
1957	1798.87	1	30.0	3.4	2.6	1612.2
1976	1554.82	2	15.0	2.7	1.9	1332.1
1960	1120.68	3	10.0	2.3	1.5	1165.3
1972	932.49	4	7.5	1.9	1.3	1044.6
1969	908.87	5	6.0	1.7	1.1	949.1
1951	864.08	6	5.0	1.5	0.9	869.5
1961	819.75	7	4.3	1.3	0.7	800.7
1952	597.73	8	3.8	1.2	0.6	739.7
1966	507.59	9	3.3	1.0	0.4	684.7
1971	498.3	10	3.0	0.9	0.3	634.1
1955	495.75	11	2.7	0.8	0.2	587.2
1967	448.58	12	2.5	0.7	0.1	543.1
1975	437.82	13	2.3	0.6	0.0	501.3
1954	401.42	14	2.1	0.5	-0.1	461.3
1973	354.11	15	2.0	0.4	-0.2	422.8
1974	264.87	16	1.9	0.3	-0.2	385.4

Year	Max SF (m^3/day)	Rank (M)	Recurrence Interval (T)	Reduced variate (Yt)	Frequency factor (K)	Xt
1962	234.56	17	1.8	0.2	-0.3	348.8
1956	224.65	18	1.7	0.1	-0.4	312.8
1958	212.63	19	1.6	0.0	-0.5	277.1
1953	212.46	20	1.5	-0.1	-0.6	241.3
1959	201.61	21	1.4	-0.2	-0.7	205.2
1970	188.87	22	1.4	-0.3	-0.7	168.4
1964	175.44	23	1.3	-0.4	-0.8	130.5
1950	169.12	24	1.3	-0.5	-0.9	90.8
1965	162.18	25	1.2	-0.6	-1.0	48.5
1977	161.19	26	1.2	-0.7	-1.1	2.2
1968	130.03	27	1.1	-0.8	-1.2	-50.4
1979	61.19	28	1.1	-1.0	-1.4	-114.3
1978	50.82	29	1.0	-1.2	-1.6	-204.1

A summary of , for 2, 5, 10, 15, 20, 25, 50 and 100 year return periods are shown in Table 3-19.

Table 3-19: Flood return period estimation

Return Period(T)	Flood Discharge (Xt)
2	422.8
5	869.5
10	1165.3
15	1332.1
20	1449.0

Return Period(T)	Flood Discharge (Xt)
25	1539.0
50	1816.2
100	2091.4

The Gumbel's probability distribution is shown in Figure 3-21.

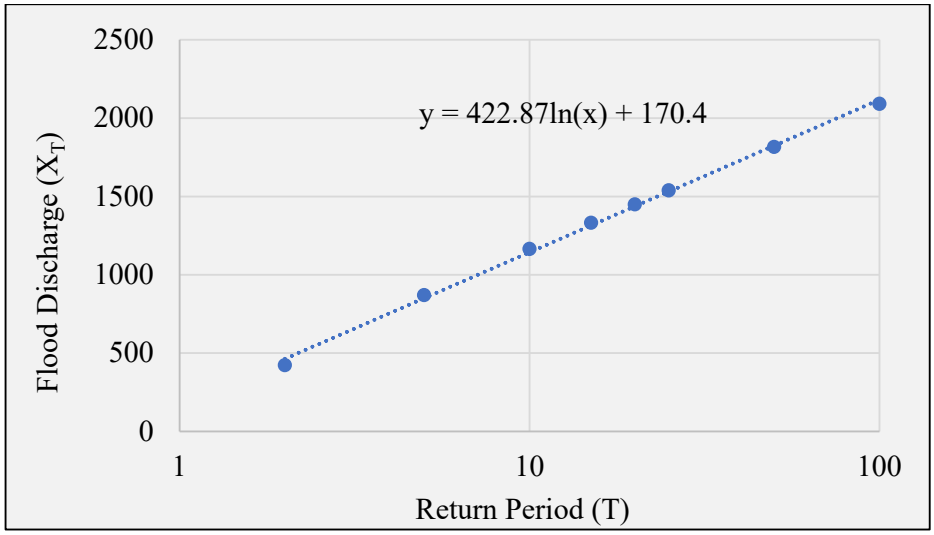

Figure 3-21: Gumbel's probability distribution

Due to limited sample data utilized in Gumbel's approach, the value of the variate for a particular return time, X_T, might have errors therefore, an estimate of the confidence intervals is needed. (Subramanya, 2013). The author discusses that the confidence interval denotes the range of values within which the real value may be claimed to lie with a certain probability based on sampling errors. For confidence probability c, the confidence interval of the variate X_T is bounded by values x_1 and x_2 given by:

$$x_{\frac{1}{2}} = x_T \pm f(c)\, Se \qquad [3\text{-}25]$$

S_e = probable error = $b\frac{\sigma_{n-1}}{\sqrt{N}}$ [3-26]

$$b = \sqrt{1 + 1.3k + 1.1k^2} \qquad [3\text{-}27]$$

where σ_{n-1} is the Standard deviation of the sample, K is the Frequency factor, and N is the sample size.

The confidence limits are estimated for 99%, and 95% confidence probability which is shown in Table 3-20.

Table 3-20: Estimation of confidence probability limits

Return Period	b	Probable Error (Se)	99% Confidence Probability (X1)	99% Confidence Probability (X2)	95% Confidence Probability (X1)	95% Confidence Probability (X2)
2	0.9	73.8	629.5	216.1	567.5	278.1
5	1.7	139.7	1260.6	478.4	1143.3	595.7
10	2.4	192.8	1705.0	625.6	1543.1	787.5
15	2.8	223.7	1958.5	705.8	1770.6	893.7
20	3.0	245.6	2136.6	761.3	1930.3	967.6
25	3.2	262.6	2274.1	803.8	2053.6	1024.4
50	3.9	315.2	2698.8	933.6	2434.0	1198.4
100	4.5	367.9	3121.4	1061.4	2812.4	1370.4

Based on the 99% confidence probability limits, the following events are selected for model calibration and validation.

Table 3-21: Selected events for model calibration and validation

No.	Event	Return Period	Time Period
1	1957	50	17 days
2	1960	50	12 days
3	1961	25	14 days
4	1966	5	13 days
5	1967	2	12 days

3.6.5 Model Calibration and Validation

Calibration is the operation of modifying input parameter values and initial boundary conditions within acceptable intervals until the simulated results sharply match the observed variables, and it is usually performed for the parameters which their measurement is complicated (Zeckoski et al., 2015). Validation is the operation of indicating that a calibrated model can reproduce a group of field measurements or anticipate future circumstances without requiring any additional adjustments to the calibrated parameters (Zheng et al., 2012).

The HEC-HMS optimization component enables users to look for the optimum parameters of calibration and assess the model goodness of fit compared to observed data using different objective functions. The calibration procedure is repeated until an acceptable fit is achieved. Following that, the calibrated parameters are presented. The schematic of a calibration procedure is shown in Figure 3-22.

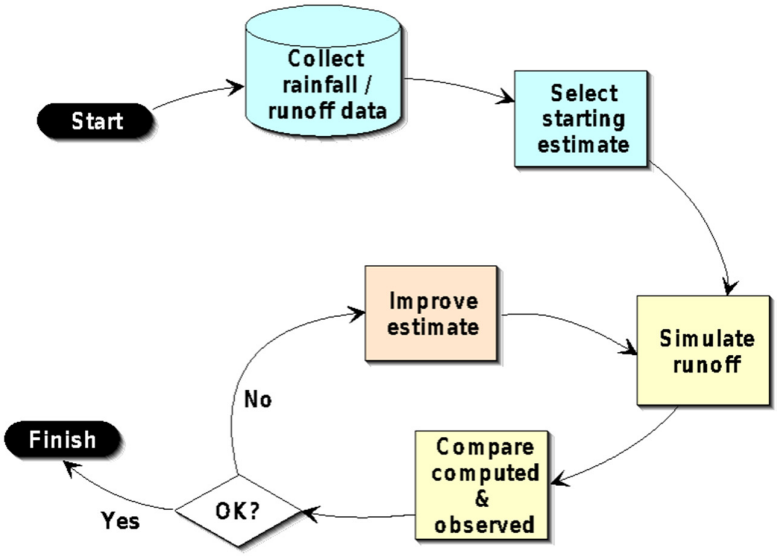

Figure 3-22: Schematic of calibration procedure (USACE, 2000)

3.6.6 Model Sensitivity Analysis

Model sensitivity analysis is one of the critical steps in hydrological modeling. It ranks model parameters according to their impact on total model prediction errors (Belayneh et al., 2020). Some of the model parameters can show high sensitivity to a minor

change while the others can show low or even neglectable changes. Therefore, to understand each parameter sensitivity, it is required to perform a sensitivity analysis. It helps the modeler to find out the most sensitive parameters which can make a big difference in the model simulated results.

Sensitivity analysis, according to Hann (2002) might be local or global. The importance of each input parameter is assessed separately in the local sensitivity analysis by leaving other model parameters constant whilst all model inputs are permitted to fluctuate across their ranges simultaneously in the global sensitivity analysis. The event model was evaluated using local sensitivity analysis in this study. As it can be seen in several studies (Belayneh et al., 2020; Ouédraogo et al., 2018), the calibrated model's final set of parameters was regarded as the baseline/nominal parameter set. To acquire the desired simulated outcomes, each of the optimized parameters must be utilized as inputs into the model (Ouédraogo et al., 2018). To do so, the model was first run with the calibrated and validated model parameters. Then, using one parameter at a time technique, the value of each parameter was adjusted from -30% to +30% in 10% increments while all other parameters were held unchanged.

3.6.7 Model Performance Evaluation

The model performance should be checked for its correctness, consistency, and adaptability to rely on its simulation results. The performance of the HEC-HMS model was assessed through visual inspection of the simulated and observed hydrographs and using several objective functions to determine the goodness-of-fit between simulated and observed hydrographs. Efficiency criteria such as Nash-Sutcliffe Simulation Efficiency (NSE), RMSE Observations Standard Deviation Ratio (RSR), Coefficient of Determination (R^2), and percentage bias (PBIAS) were used to evaluate the model performance. The Nash–Sutcliffe coefficient of efficiency (NSE) is estimated by Equation [3-28]:

$$NSE = 1 - \frac{\sum_{i=1}^{n} \left(Q_{obs,i} - Q_{sim,i}\right)^2}{\sum_{i=1}^{n} \left(Q_{obs,i} - \bar{Q}_{sim,i}\right)^2} \qquad [3\text{-}28]$$

NSE is a number that varies from 0 to 1, with 1 being the intended value. NSE values between 0.6 to 1.0 are regarded as good. However, NSE = 0 shows that the mean observed value is a stronger predictor of hydrological data than the simulated value, suggesting poor performance.

RMSE Observations Standard Deviation Ratio (RSR) is given by Equation [3-29]:

$$RSR = \frac{\sqrt{\sum_{i=1}^{n}(Q_{obs,i}-Q_{sim,i})^2}}{\sqrt{\sum_{i=1}^{n}(Q_{obs,i}-\bar{Q}_{obs})^2}} \quad [3\text{-}29]$$

where: the benefits of error index statistics are combined with a normalization factor in RSR, resulting in a statistic and reported values that may be applied to a variety of components (Koutsovili et al., 2021). The RSR ranges from 0 to a big positive number. Reduced RSR values imply a lower root mean square error normalized by the standard deviation of the data, indicating the model simulation's adequacy (Moriasi et al., 2007).

The average likelihood of the simulated data to be bigger or smaller than their observed counterparts is estimated by PBIAS. PBIAS has a range of –∞ to ∞, with 0 being the best value, and is calculated by Equation [3-30]:

$$PBIAS = \frac{\sum_{i=1}^{n}(Q_{obs,i} - Q_{sim,i})}{\sum_{i=1}^{n}(Q_{obs,i})} \times 100 \quad [3\text{-}30]$$

The coefficient of determination R^2 is a number that varies from 0 to 1 and reflects how much of the variation in the observed measurements is described by the model, with larger numbers suggesting less error variance. $R^2 > 0.5$ is usually regarded as acceptable. R^2 is used to calculate the coefficient of determination in Equation [3-31]:

$$R^2 = \frac{\left[\sum_{i=1}^{n}(Q_{sim,i} - \bar{Q}_{sim,i})(Q_{obs,i} - \bar{Q}_{obs,i})\right]^2}{\sum_{i=1}^{n}\left[(Q_{sim,i} - \bar{Q}_{sim,i})\right]^2 \sum_{i=1}^{n}\left[(Q_{obs,i} - \bar{Q}_{obs,i})\right]^2} \quad [3\text{-}31]$$

In the above equations, $Q_{obs,I}$ is the observed discharge at the time step I, $\bar{Q}_{obs}$ is the mean of the observed discharge, $Q_{sim,I}$ is the simulation discharge at the time step I, $\bar{Q}_{sim,I}$ is the mean of the simulated discharge and n is the number of observations.

CHAPTER 4

4 RESULTS AND ANALYSIS

4.1 Deforestation and Landuse Change

The analysis of deforestation and landuse change obtained in this study show that deforestation has occurred around 25% in the Maduru Oya river basin. The detailed analysis is presented in the following sections.

4.1.1 Landuse Change Between 1976 – 1994

The results of the landuse change assessment show that major deforestation has occurred between 1976 to 1994 as a result of AMP implemented in the basin. The forest area has decreased from 878 km^2 to 500.3 km^2 which accounts for 24.9 % of deforestation in the whole river basin. The homestead/garden, paddy, scrubland, and water bodies have increased by 2.2%, 9.8%, 8.4%, 4.5% during this period, respectively. The increment of the water body from 26.5 km^2 to 96.1 km^2 is due to the construction of the Maduru Oya reservoir and other minor tanks. The details of relative changes between landuse types are given in Table 4-1 and Figure 4-1.

Table 4-1: Modelling comparison of 1976 and 1994 landuse change scenarios in Maduru Oya basin

	1976 Landuse		1994 Landuse		
LULC Classes	**Area (km^2)**	**Area (%)**	**Area (km^2)**	**Area (%)**	**Relative Change (%)**
Forest	878.0	57.6	500.3	32.7	-24.9
Homestead/Garden	32.9	2.2	66.0	4.3	2.2
Paddy	113.0	7.4	263.5	17.2	9.8
Scrubland	473.4	31.1	603.0	39.4	8.4
Water Body	26.5	1.7	96.1	6.3	4.5

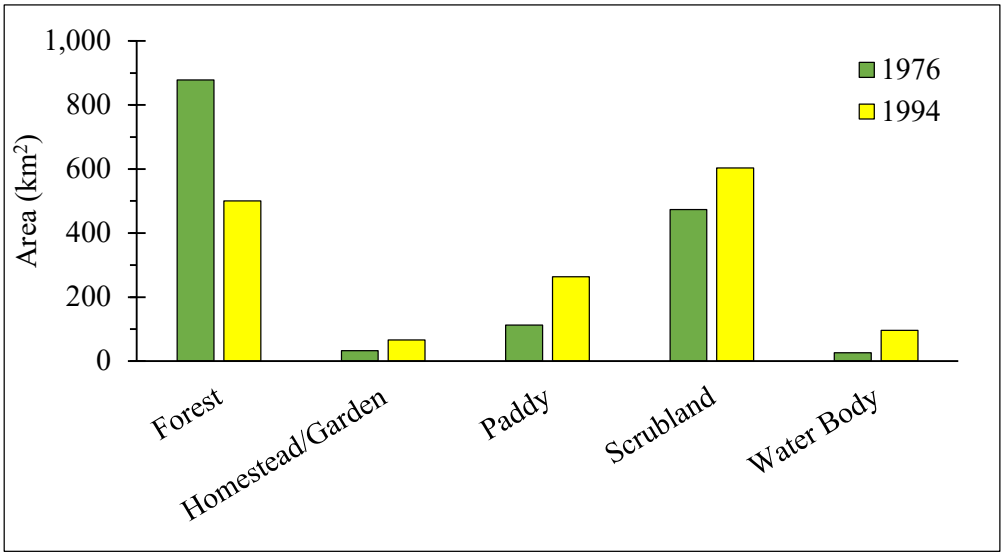

Figure 4-1: LULC Change from 1976 – 1994

4.1.2 Landuse Change Between 1994 – 2009

A comparison of LULC maps between 1994 – 2009 reveals that the forests have reduced from 500.3 km^2 to 435.6 km^2 between the respective years which accounts for 4.1 % of deforestation. Similarly, the water body also shows a decrease from 96.1 km^2 to 65.9 km^2 which stands for a 2% relative change. The homestead/garden, paddy, and scrubland have increased by 3.5%, 1.4%, and 1.5%, respectively. The details are given in Table 4-2 and Figure 4-2.

Table 4-2: Modelling comparison of 1994 and 2009 landuse change scenarios in Maduru Oya basin

	1994 Landuse		2009 Landuse		
LULC Classes	**Area (km^2)**	**Area (%)**	**Area (km^2)**	**Area (%)**	**Relative Change (%)**
Forest	500.3	32.7	435.6	28.6	-4.1
Homestead/Garden	66.0	4.3	119.8	7.9	3.5
Paddy	263.5	17.2	284.2	18.6	1.4
Scrubland	603.0	39.4	623.5	40.9	1.5
Water Body	96.1	6.3	65.9	4.3	-2.0

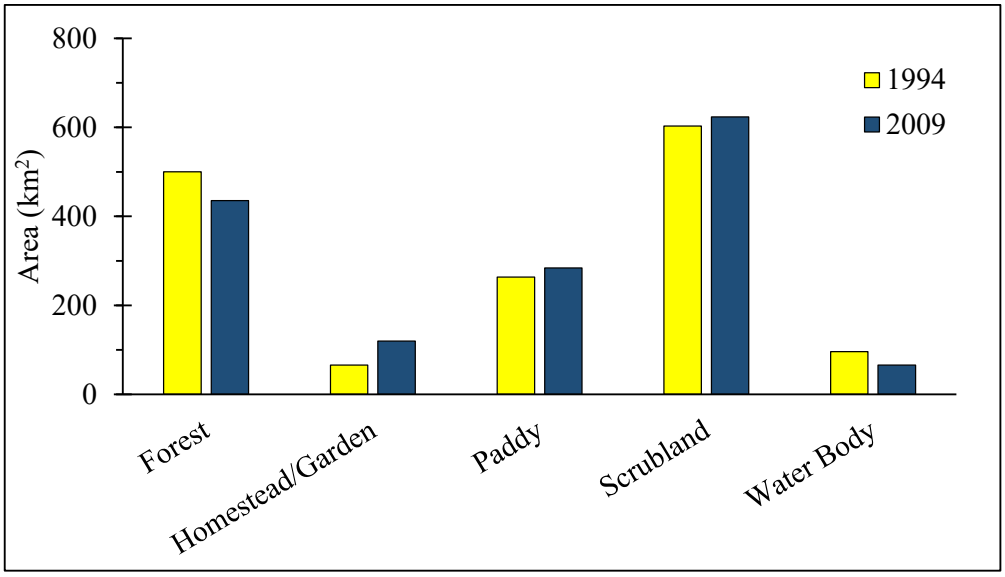

Figure 4-2: LULC Change from 1994 – 2009

4.1.3 Landuse Change Between 2009 – 2021

A comparison of LULC maps in 2009 and 2021 shows an increment of forests from 435.6 km^2 to 492.7 km^2 which stands for 3.6% of relative change. Similarly, homestead/garden, paddy, and water body indicate increment by 0.5%, 1.5%, and 1.8%, respectively. Only scrubland shows a decrease of 7.8% during this period. The details are given in Table 4-3 and Figure 4-3.

Table 4-3: Modelling comparison of 2009 and 2021 landuse change scenarios in Maduru Oya basin

	2009 Landuse		**2021 Landuse**		
LULC Classes	**Area (km^2)**	**Area (%)**	**Area (km^2)**	**Area (%)**	**Relative Change (%)**
Forest	435.6	28.6	492.7	32.2	3.6
Homestead/Garden	119.8	7.9	128.3	8.4	0.5
Paddy	284.2	18.6	307.5	20.1	1.5
Scrubland	623.5	40.9	509.1	33.3	-7.6
Water Body	65.9	4.3	93.4	6.1	1.8

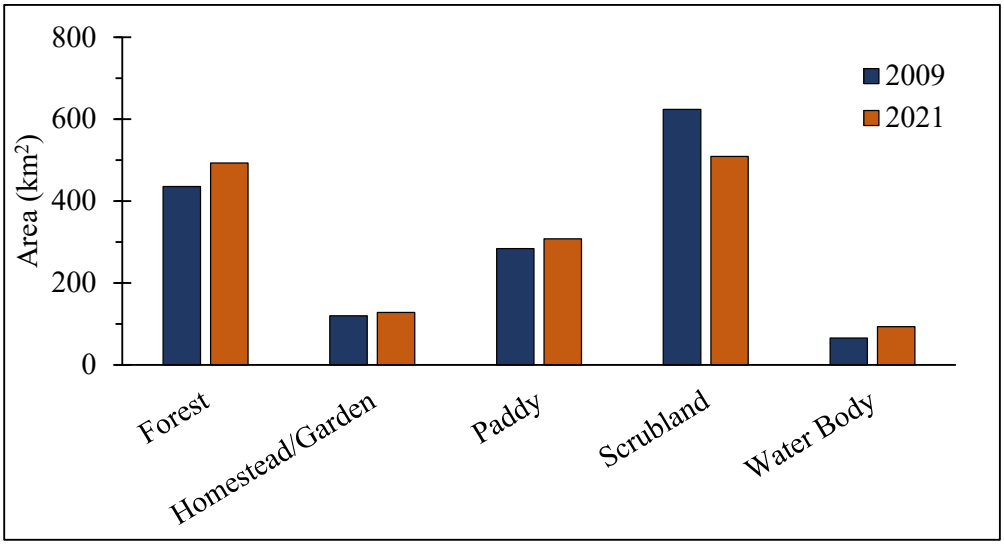

Figure 4-3: LULC Change from 2009 – 2021

4.1.4 Landuse Change Between 1976 – 2021

A comparison of landuse scenarios of 1976 and 2021 shows that forest areas have been decreased significantly by 25.4% while other landuse types have been increased by 6.2%, 12.7%, 2.2%, and 4.4%, respectively. The details are shown in Table 4-4 and Figure 4-4.

Table 4-4: Modelling comparison of 1976 and 2021 landuse change scenarios in Maduru Oya basin

	1976 Landuse		2021 Landuse		
LULC Classes	**Area (km^2)**	**Area (%)**	**Area (km^2)**	**Area (%)**	**Relative Change (%)**
Forest	878.0	57.6	492.7	32.2	-25.4
Homestead/Garden	32.9	2.2	128.3	8.4	6.2
Paddy	113.0	7.4	307.5	20.1	12.7
Scrubland	473.4	31.1	509.1	33.3	2.2
Water Body	26.5	1.7	93.4	6.1	4.4

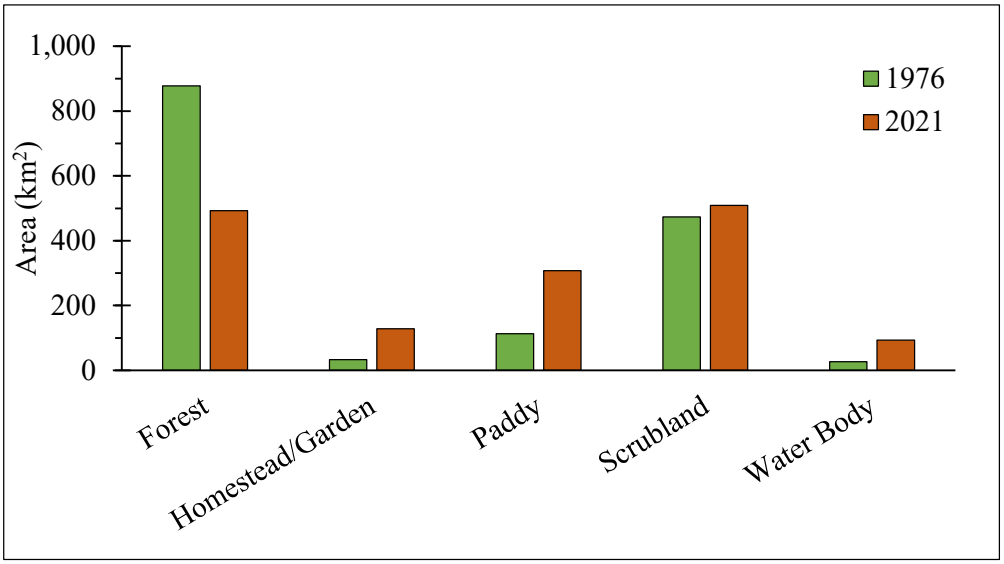

Figure 4-4: LULC Change from 1976 – 2021

Considering landuse variations in all scenarios, deforestation has been prominent in the study area. Homestead/Garden and paddy have had an ascending trend while scrubland and water bodies were variating which can be seen in Figure 4-5 and landuse maps of 1976, 1994, 2009 and 2021 in Figure 4-6, Figure 4-7, Figure 4-8, and Figure 4-9, respectively.

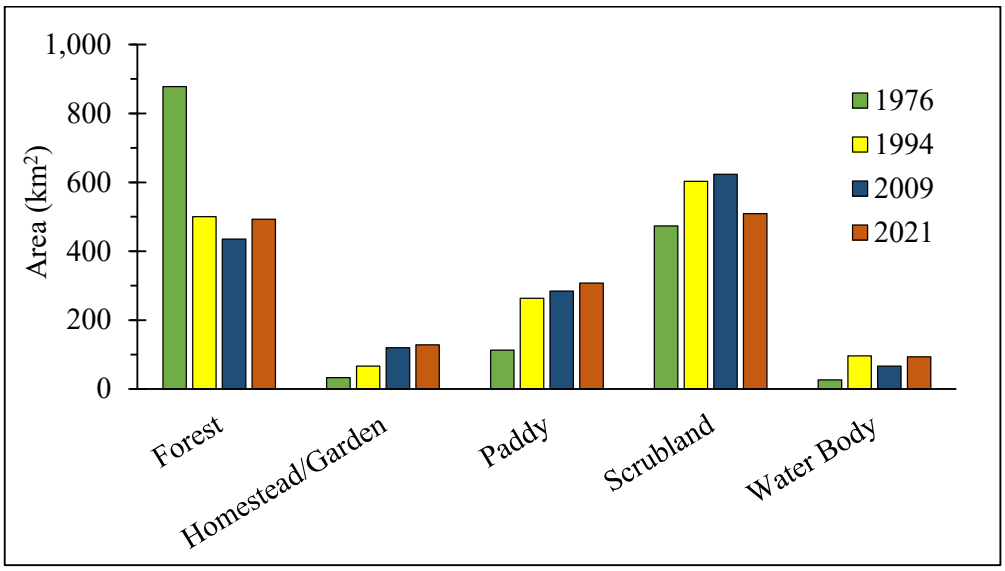

Figure 4-5: LULC Change from 1976 – 2021

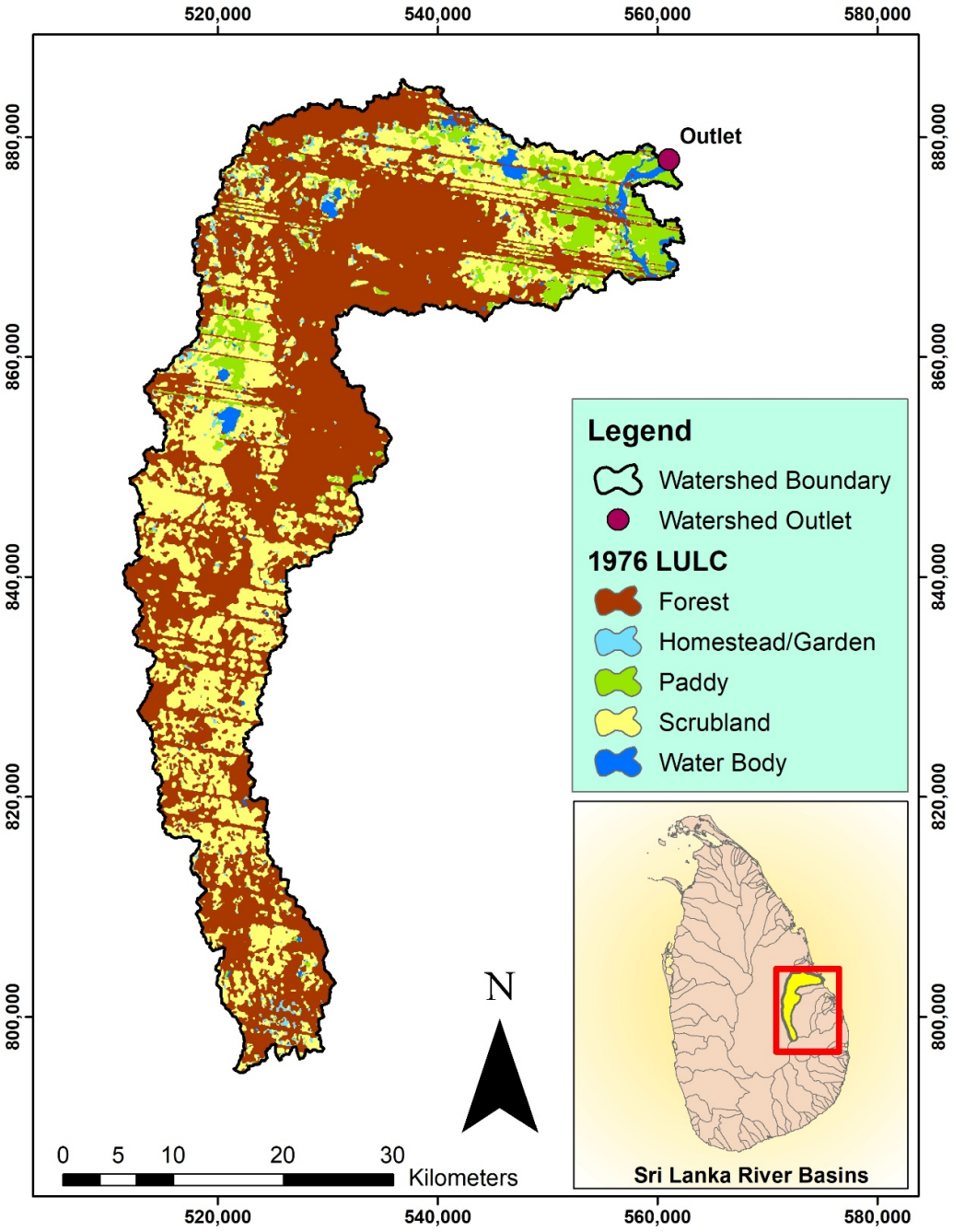

Figure 4-6: Landuse map of Maduru Oya basin (1976 scenario)

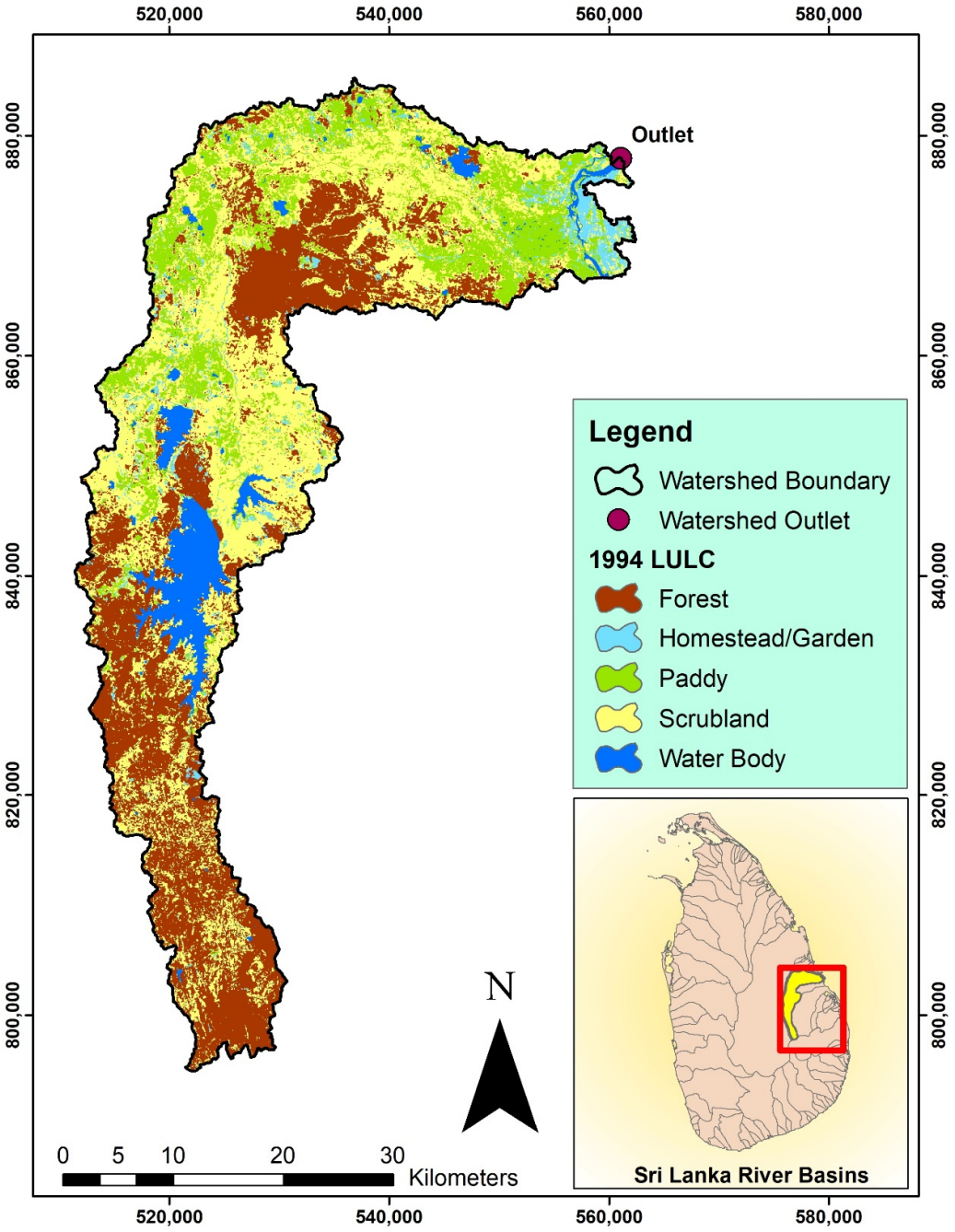

Figure 4-7: Landuse map of Maduru Oya basin (1994 scenario)

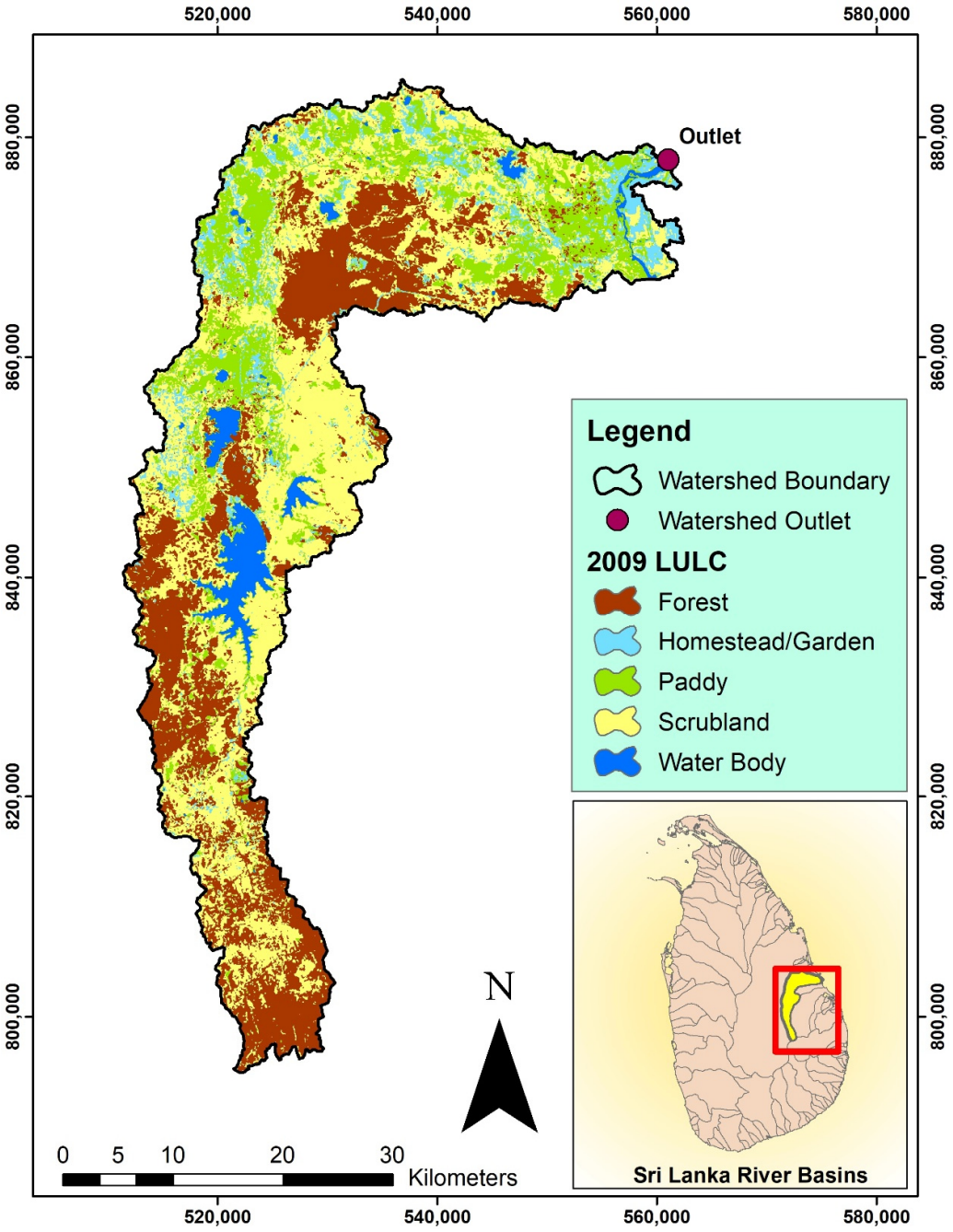

Figure 4-8: Landuse map of Maduru Oya basin (2009 scenario)

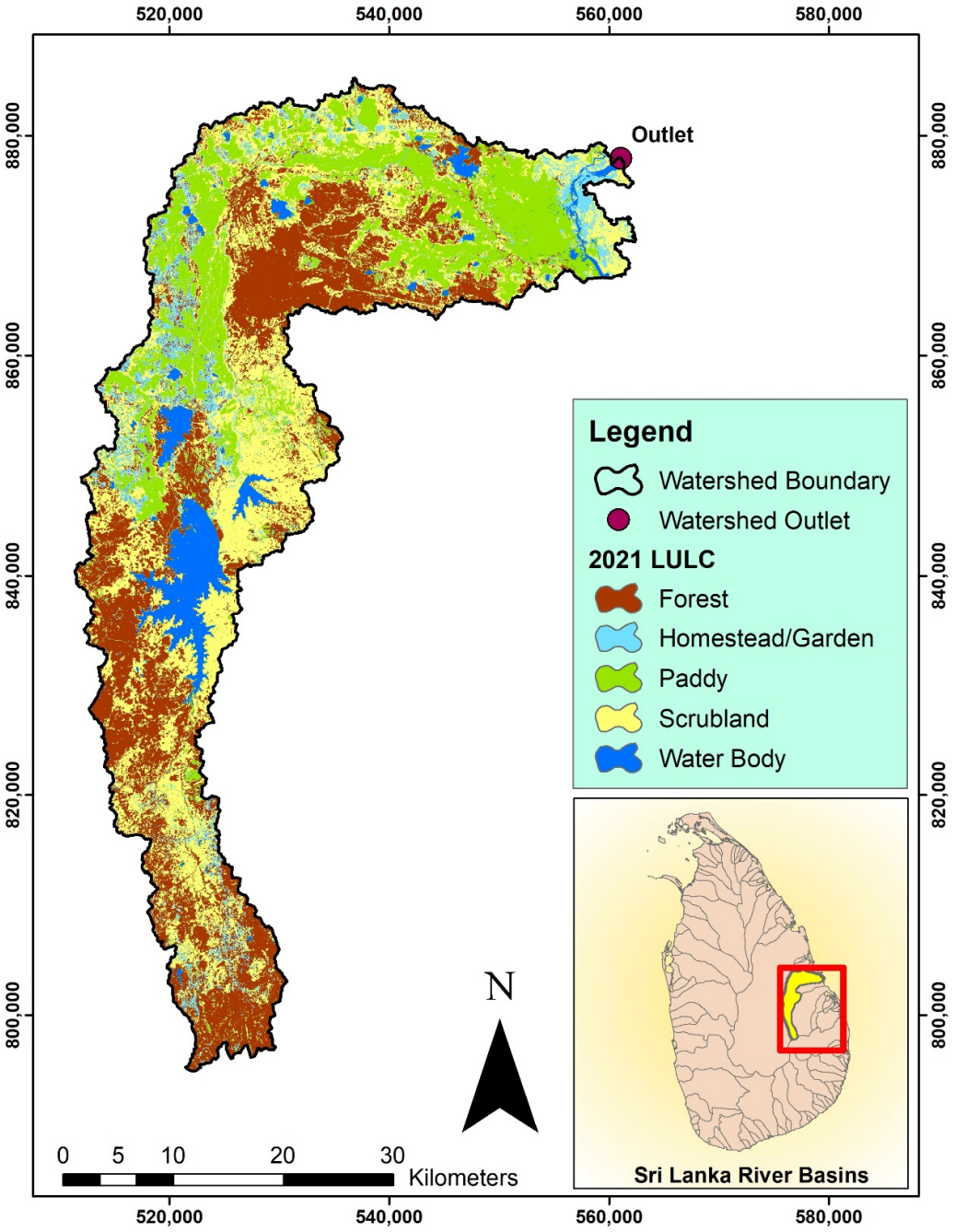

Figure 4-9: Landuse map of Maduru Oya basin (2021 scenario)

4.1.5 Accuracy Assessment Results

The accuracy results (User Accuracy, Producer Accuracy, Overall Accuracy, and Kappa Coefficient) for landuse maps of 1976, 1994, 2009, and 2021 are shown in Table 4-5, Table 4-6, Table 4-7, and Table 4-8, respectively. The overall accuracies of classified images are within good to very good range.

Table 4-5: Accuracy assessment results for 1976 scenario

No.	LULC Type	User Accuracy (%)	Producer Accuracy (%)	Overall Accuracy (%)	Kappa Coefficient
1	Forest	85.0	85.0		
2	Homestead/Garden	60.0	92.3		
3	Paddy	85.0	73.9	**82**	**0.78**
4	Scrubland	85.0	68.0		
5	Water Body	95.0	100.0		

Table 4-6: Accuracy assessment results for 1994 scenario

No.	LULC Type	User Accuracy (%)	Producer Accuracy (%)	Overall Accuracy (%)	Kappa Coefficient
1	Forest	100.0	87.0		
2	Homestead/Garden	55.0	84.6		
3	Paddy	80.0	84.2	**84**	**0.80**
4	Scrubland	85.0	68.0		
5	Water Body	100.0	100.0		

The overall accuracy and Kappa coefficient of the 1976 landuse map is the lowest among the other scenarios while the landuse map of 2021 has the highest overall accuracy and Kappa coefficient. The reason for the lower accuracy of the 1976 landuse map is the lower resolution of the image acquired, while the satellite image in 2021 provides a higher resolution. Therefore, the finer elements were not easily detectable in the 1976 scenario while they could be easily classified in the 2021 scenario.

Table 4-7: Accuracy assessment results for 2009 scenario

No.	LULC Type	User Accuracy (%)	Producer Accuracy (%)	Overall Accuracy (%)	Kappa Coefficient
1	Forest	100.0	90.9		
2	Homestead/Garden	75.0	100.0		
3	Paddy	80.0	80.0	**88**	**0.85**
4	Scrubland	95.0	76.0		
5	Water Body	90.0	100.0		

Table 4-8: Accuracy assessment results for 2021 scenario

No.	LULC Type	User Accuracy (%)	Producer Accuracy (%)	Overall Accuracy (%)	Kappa Coefficient
1	Forest	100.0	100.0		
2	Homestead/Garden	75.0	100.0		
3	Paddy	85.0	81.0	**91**	**0.89**
4	Scrubland	95.0	82.6		
5	Water Body	100.0	95.2		

4.2 Normalized Difference Vegetation Index (NDVI)

Normalized difference vegetation index which measures the plants' greenness is assessed in each landuse scenario.

- The NDVI is ranging from -0.975 to 0.818 in the 1976 landuse scenario. It indicates that the study area vegetation is varying from very dry to very dense vegetated areas. The NDVI map of the Maduru Oya basin in 1976 is shown in Figure 4-10.
- The vegetation index varies from -0.088 to 0.509 in the 1994 scenario which shows a decline of the highest NDVI (0.309) compared to the 1976 scenario while a positive change in the lowest NDVI is the result of an increase in the paddy lands. It is in good agreement with the results of landuse classified images which shows a 24.9% decrease in the forested areas and an increase of 9.8% in the paddy areas between the respective scenarios. The NDVI map of the Maduru Oya basin in 1994 is shown in Figure 4-11.
- The NDVI is ranging from -0.207 to 0.655 in 2009. It indicates an increase of 0.146 in the high NDVI values while a negative change compared to the 1994 scenario. In this period the landuse classified image shows an increase in the scrubland and paddy lands that may have contributed to the changes in the NDVI between the two scenarios. The NDVI map of the Maduru Oya basin in 2009 is shown in Figure 4-12.
- The NDVI is ranging from -0.203 to 0.618 in 2021. It indicates a minor change in the vegetation index between the 2009 and 2021 scenarios which is in agreement with the landuse classified images. The NDVI map of the Maduru Oya basin in 2021 is shown in Figure 4-13.

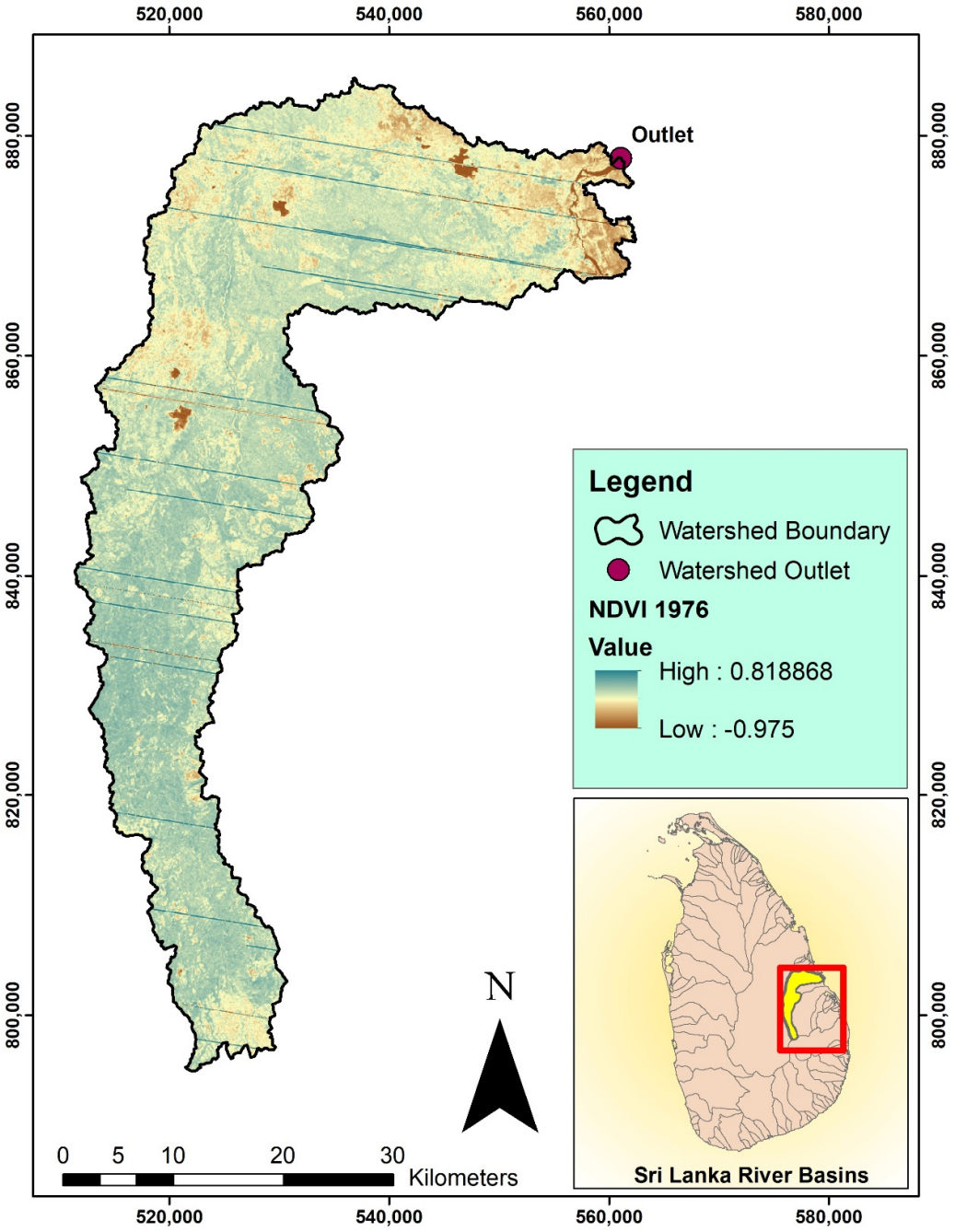

Figure 4-10: NDVI map of Maduru Oya basin (1976 scenario)

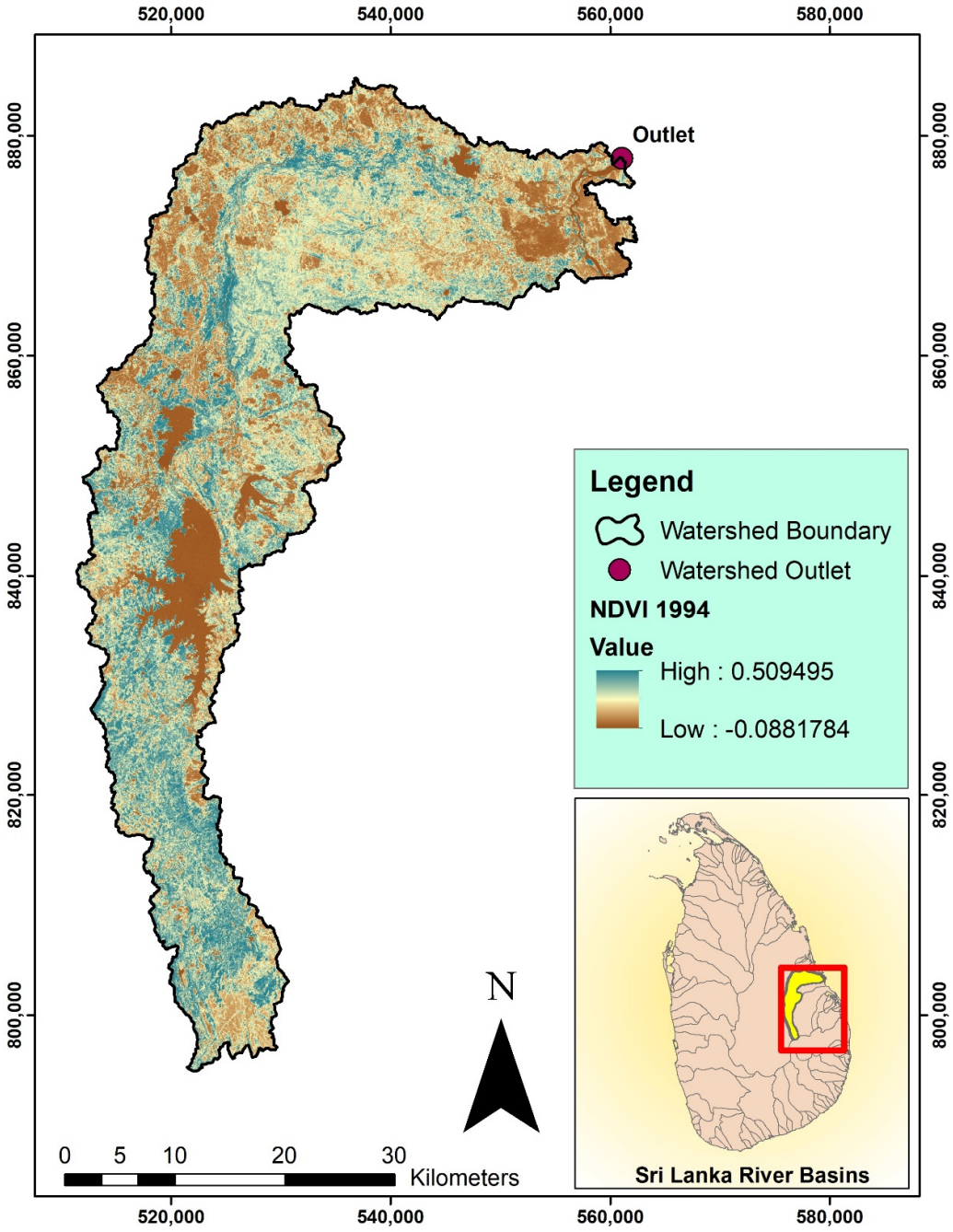

Figure 4-11: NDVI map of Maduru Oya basin (1994 scenario)

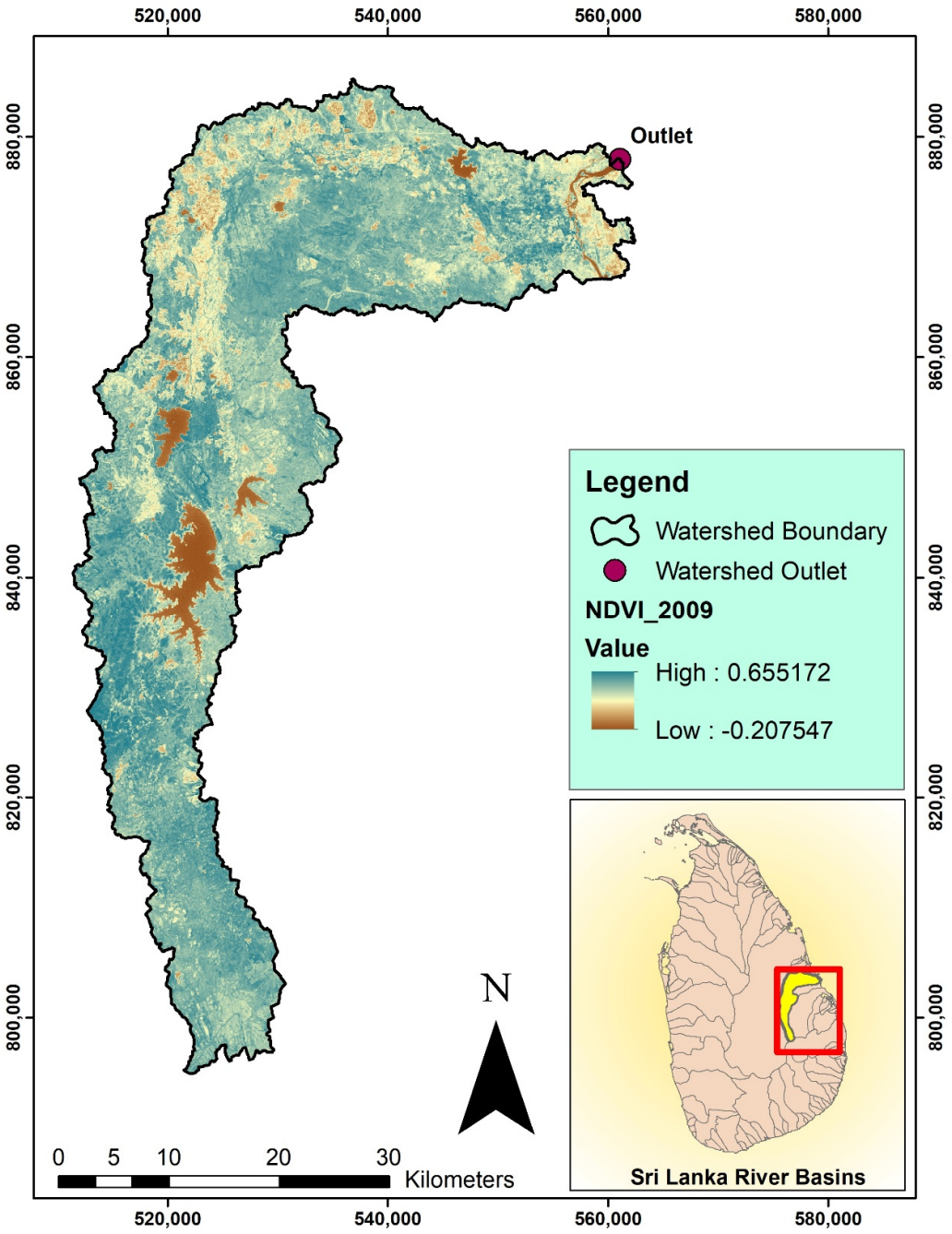

Figure 4-12: NDVI map of Maduru Oya basin (2009 scenario)

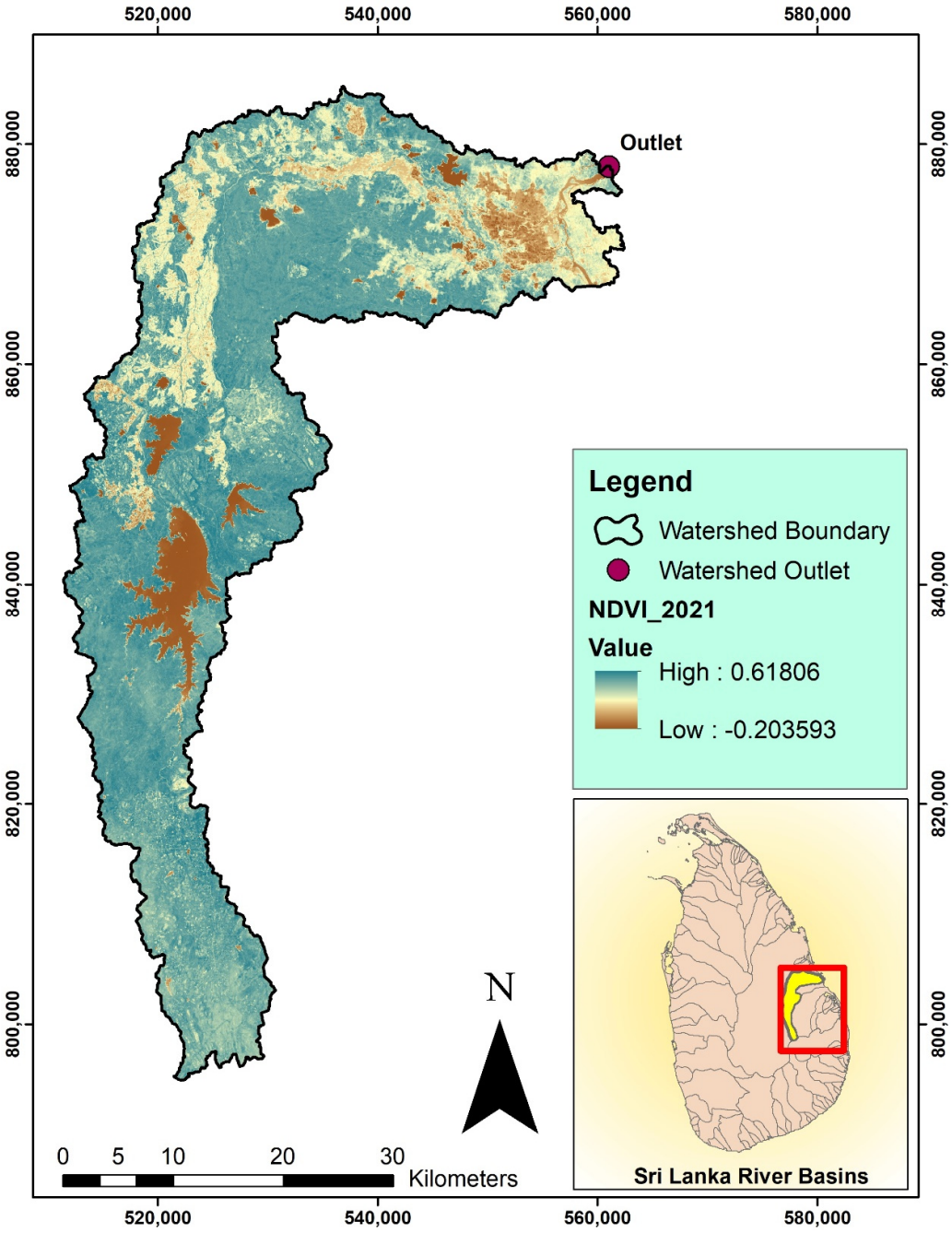

Figure 4-13: NDVI map of Maduru Oya basin (2021 scenario)

4.3 Hydrological Modeling Results

The HEC-HMS model is calibrated for the events in 1961 and 1967 and validated in 1957, 1960, and 1966. The results are rated based on the NSE, RSR, PBIAS, and R^2 objective functions.

The results of calibration and validation are assessed based on the performance rating of each objective function. The criteria for assessing the model performance is considered as described by Moriasi et al. (2007) in Table 4-9.

Table 4-9: Performance rating for evaluation metrics

Performance Rating	**NSE**	**RSR**	**PBIAS**	**R^2**
Very Good	$0.75 < NSE \leq 1$	$0 < RSR \leq 0.50$	$PBIAS < \pm 10$	$0.75 < R^2 \leq 1$
Good	$0.65 < NSE \leq 0.75$	$0.50 < RSR \leq 0.60$	$\pm 10 \leq PBIAS < \pm 15$	$0.65 < R^2 \leq 0.75$
Satisfactory	$0.50 < NSE \leq 0.65$	$0.60 < RSR \leq 0.70$	$\pm 15 \leq PBIAS < \pm 25$	$0.50 < R^2 \leq 0.65$
Unsatisfactory	$NSE \leq 0.50$	$RSR > 0.70$	$PBIAS \geq \pm 25$	$R^2 \leq 0.50$

4.3.1 HEC-HMS Model Calibration

The HEC-HMS model is calibrated for the events of 1961 and 1967. The calibration has been performed manually and using the optimization manager in HEC-HMS to find the optimum values.

The NSE, RSR, PBIAS, and R^2 are found to be 0.95, 0.2, 17.47, and 0.97 for event 1961, respectively which all can be rated very good correlation and goodness of fit between observed and simulation except for PBIAS which can be rated as satisfactory.

The output of model calibration (observed vs. simulated hydrograph) for the 1961 event is shown in Figure 4-14, and Figure 4-15, respectively.

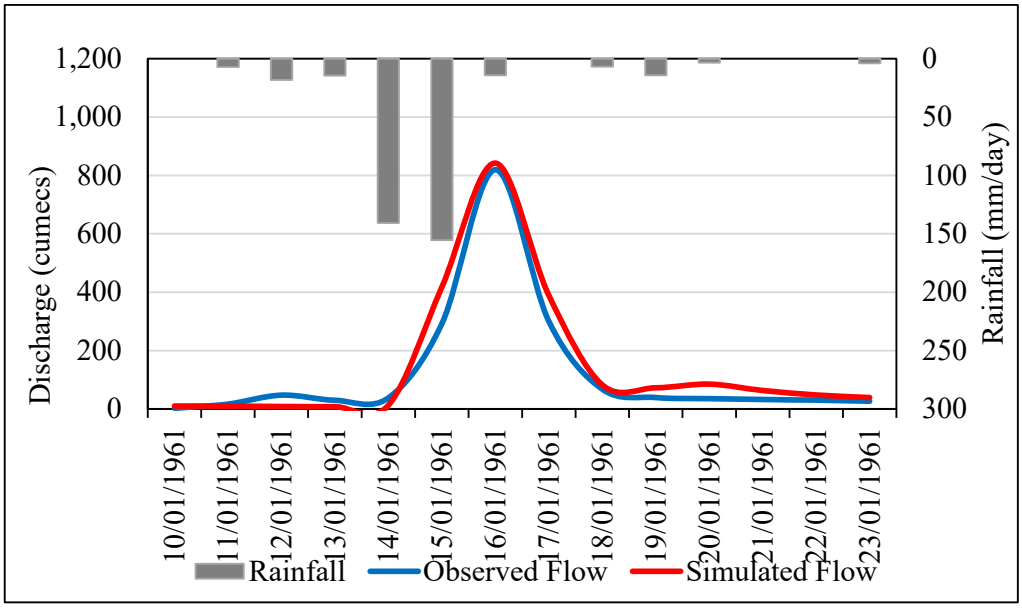

Figure 4-14: Calibration output (1961 Event)

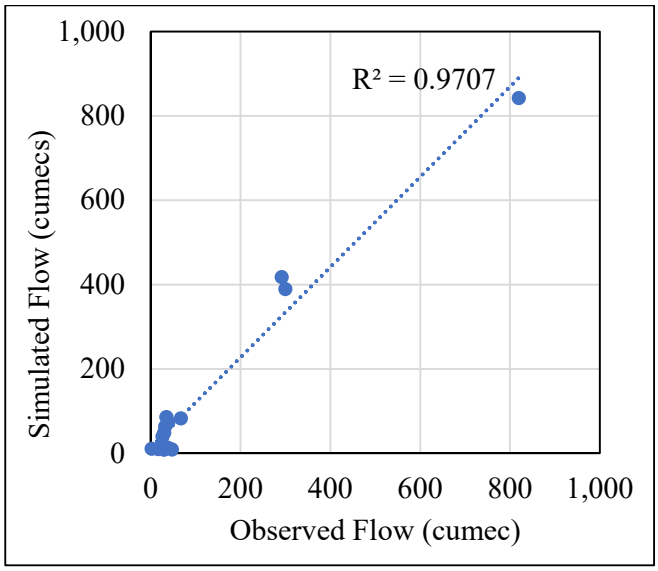

Figure 4-15: Scatter plot for calibration (Event 1961)

The NSE, RSR, PBIAS, and R^2 are found to be 0.89, 0.3, 17.82, and 0.91 for event 1967, respectively which all can be rated very good correlation and goodness of fit between observed and simulation except for PBIAS which can be rated as satisfactory.

The output of model calibration (observed vs. simulated hydrograph) for the 1967 event is shown in Figure 4-16, and Figure 4-17, respectively.

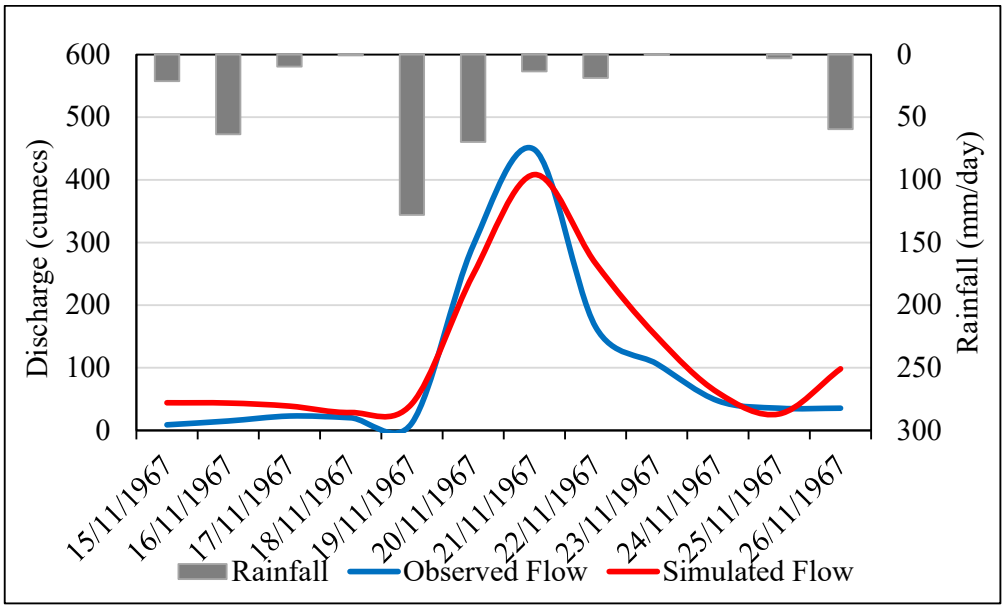

Figure 4-16: Calibration output (1967 Event)

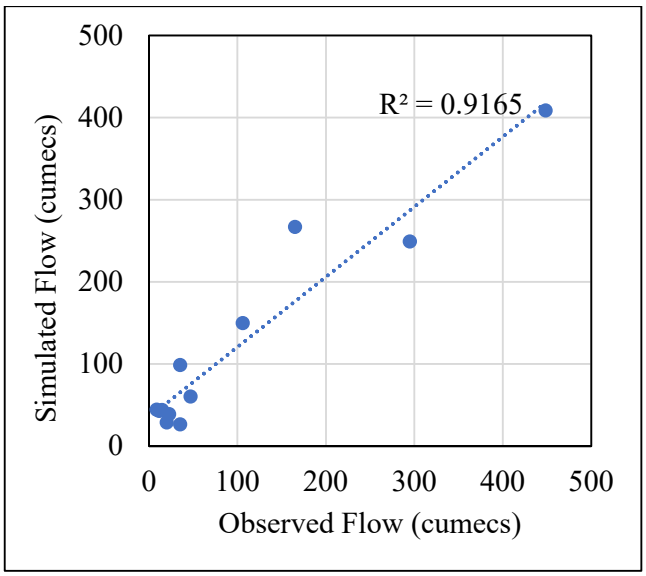

Figure 4-17: Scatter plot for calibration (Event 1967)

The model performance in calibration events are evaluated in Table 4-10 which both events indicate a very good overall performance.

Table 4-10: Performance rating of objective functions for calibration events

Objective Functions					
Year	**NSE**	**RSR**	**PBIAS**	**R^2**	**Overall Performance**
1961	0.95 (Very Good)	0.2 (Very Good)	17.47 (Satisfactory)	0.97 (Very Good)	Very Good
1967	0.899 (Very Good)	0.3 (Very Good)	17.82 (Satisfactory)	0.91 (Very Good)	Very Good

4.3.2 HEC-HMS Model Validation

The optimized parameters found during the calibration process are examined in other events with different periods, and the results are rated based on objective functions. The events in 1957, 1960, and 1966 are selected for model validation. The NSE, RSR, PBIAS, and R^2 are 0.76, 0.5, -16.99, and 0.81 for event 1957, respectively which all can be rated very good correlation and goodness of fit between observed and simulation except for PBIAS which can be rated as satisfactory. The model output for the 1957 event is shown in Figure 4-18, and Figure 4-19.

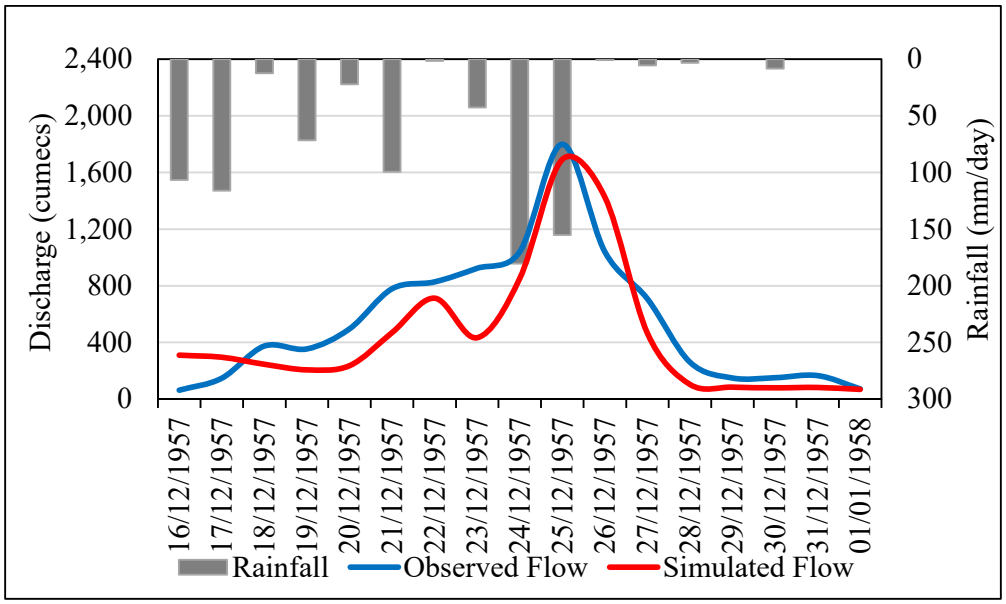

Figure 4-18: Validation output (1957 Event)

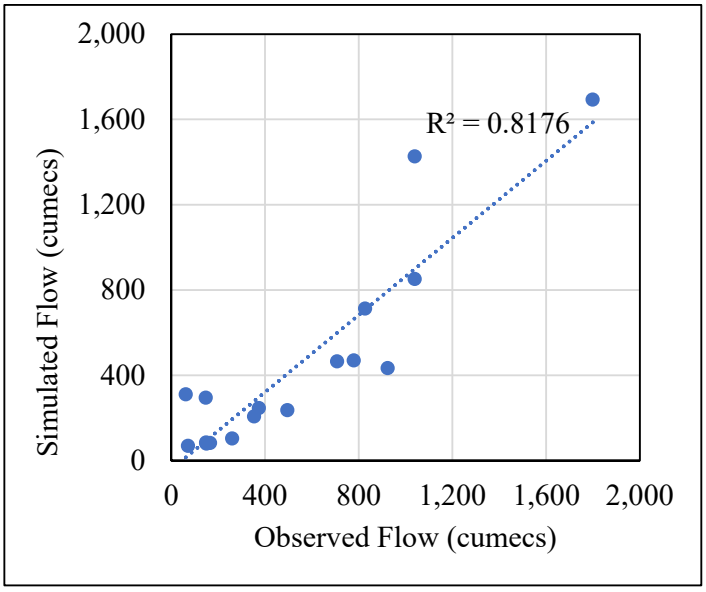

Figure 4-19: Scatter plot for validation (1957 Event)

The NSE, RSR, PBIAS, and R^2 are found 0.69, 0.5, -11.4, and 0.77 for event 1960, respectively which RSR and R^2 show very good correlation and goodness of fit between observed and simulation while NSE and PBIAS are rated as good. The model output for the event in 1960 is shown in Figure 4-20, and Figure 4-21.

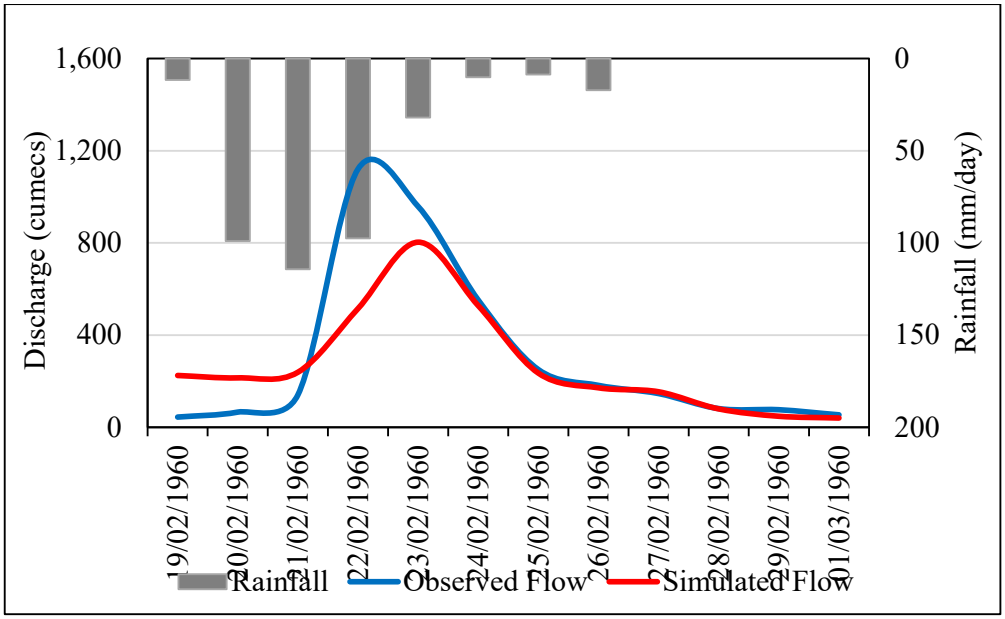

Figure 4-20: Validation output (1960 Event)

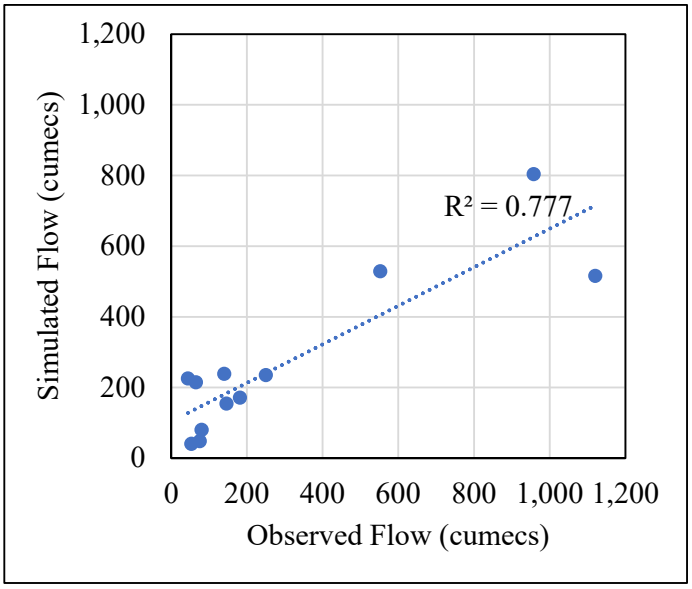

Figure 4-21: Scatter plot for validation (1960 Event)

The NSE, RSR, PBIAS, and R^2 are 0.73, 0.5, 19.29, and 0.78 for event 1966, respectively which RSR and R^2 can be rated as very good while NSE can be rated good and PBIAS as satisfactory. The model output for the event in 1966 is shown in Figure 4-22, and Figure 4-23.

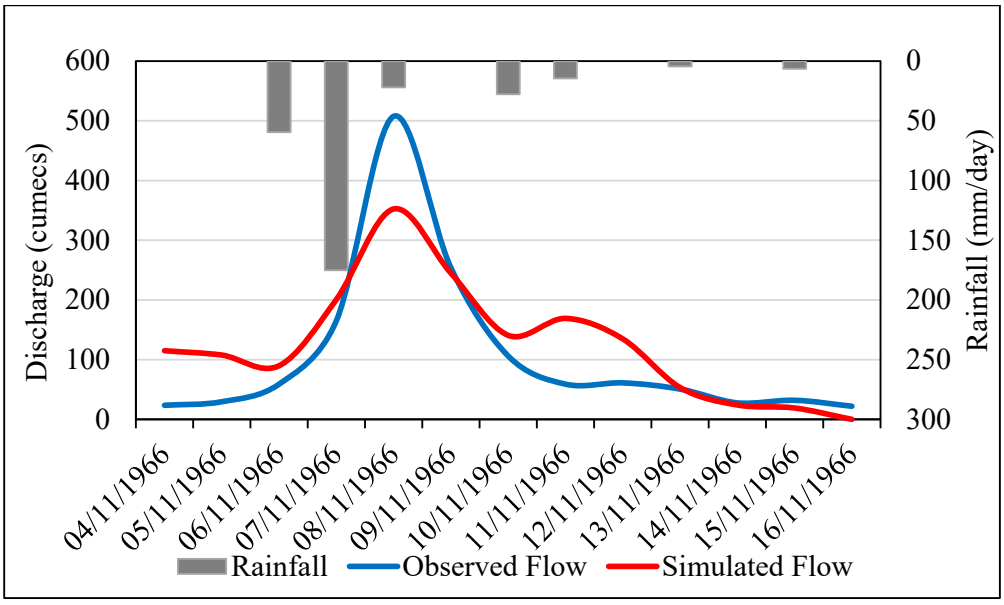

Figure 4-22: Validation output (1966 Event)

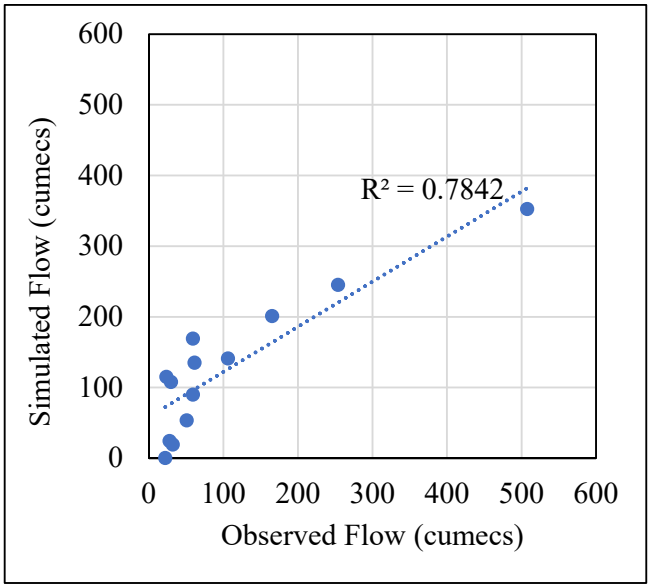

Figure 4-23: Scatter plot for validation (1966 Event)

The results of the validation process are assessed based on objective functions and the performance rating is shown in Table 4-11.

Table 4-11: Performance rating of objective functions for validation events

Objective Functions					
Year	**NSE**	**RSR**	**PBIAS**	**R^2**	**Overall Performance**
1957	0.76 (Very Good)	0.5 (Very Good)	-16.99 (Satisfactory)	0.81 (Very Good)	Good
1960	0.69 (Good)	0.5 (Very Good)	-11.4 (Good)	0.77 (Very Good)	Good
1966	0.73 (Good)	0.5 (Very Good)	19.29 (Satisfactory)	0.78 (Very Good)	Good

4.4 Sensitivity Analysis

The sensitivity of the HEC-HMS model is checked for all the parameters which are optimized through calibration and validation. The sensitivity of each parameter is tested independently by altering it from +30 to -30 in 10% increments. The percentage of variation in simulated peak, volume, NSE, RSR Std. Dev and PBIAS were plotted against the percentage of variation in each parameter.

The sensitivity graph of variations in simulated peak, volume, NSE, RSR, and PBIAS are shown in Figure 4-24, Figure 4-25, Figure 4-26, Figure 4-27, Figure 4-28.

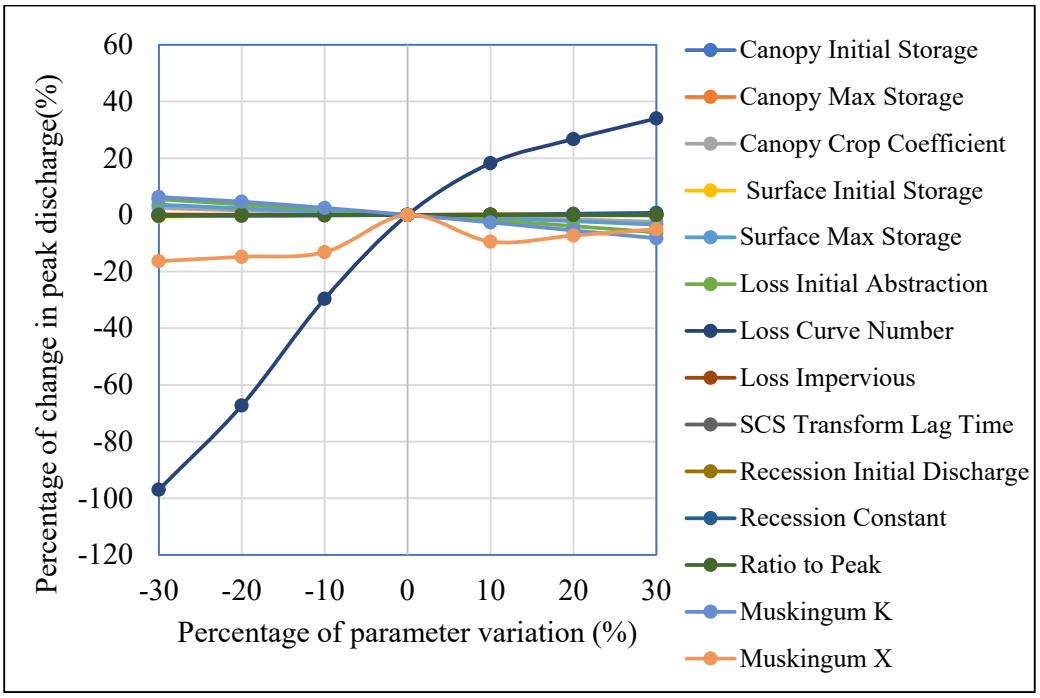

Figure 4-24: Percentage change in simulated peak discharge plotted against the percentage variation in each parameter

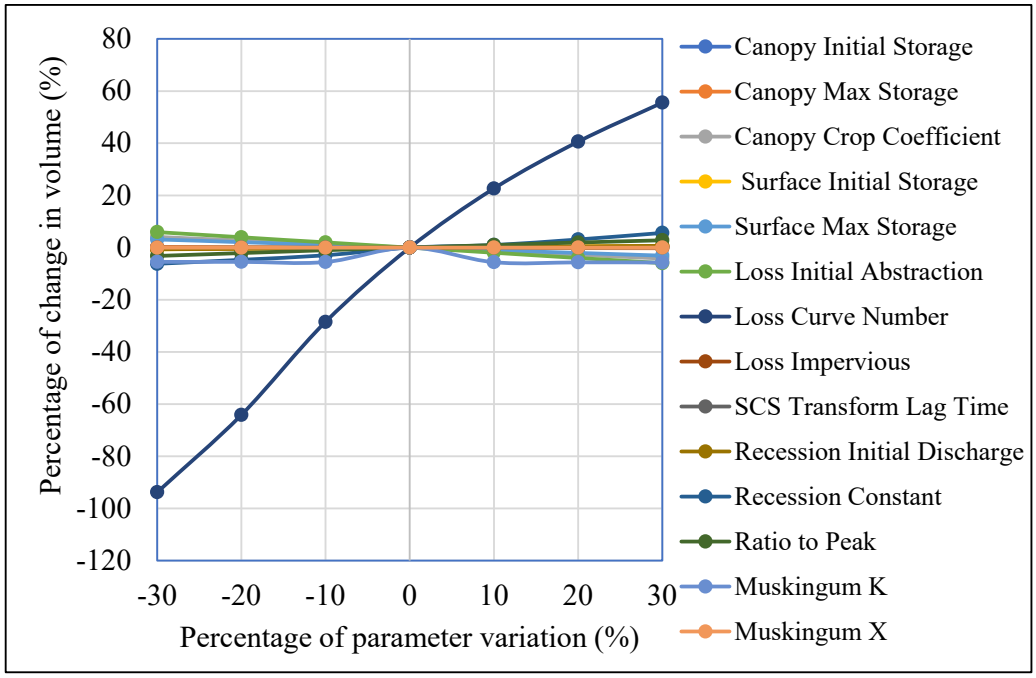

Figure 4-25: Percentage change in simulated discharge volume plotted against the percentage variation in each parameter

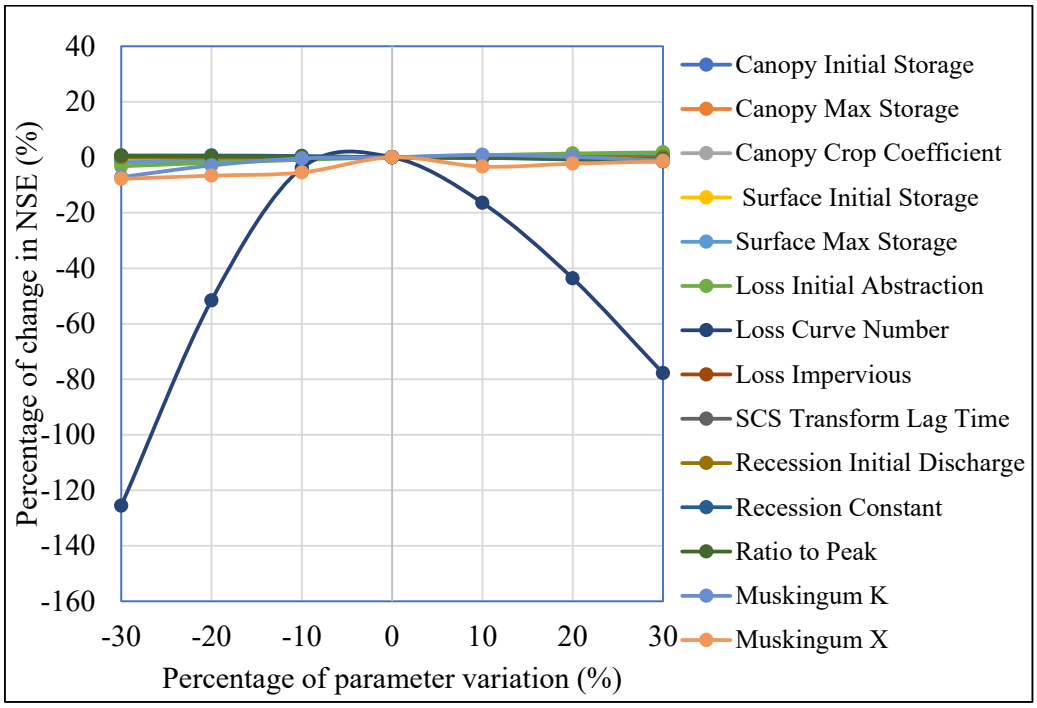

Figure 4-26: Percentage change in simulated NSE plotted against the percentage variation in each parameter

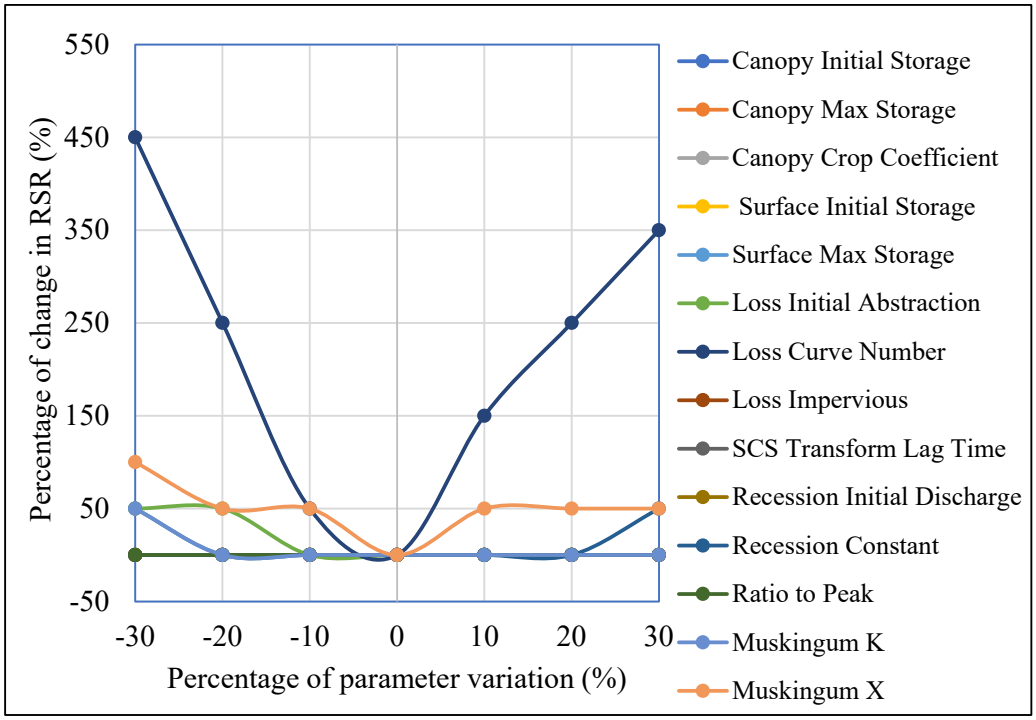

Figure 4-27: Percentage change in simulated RSR plotted against the percentage variation in each parameter

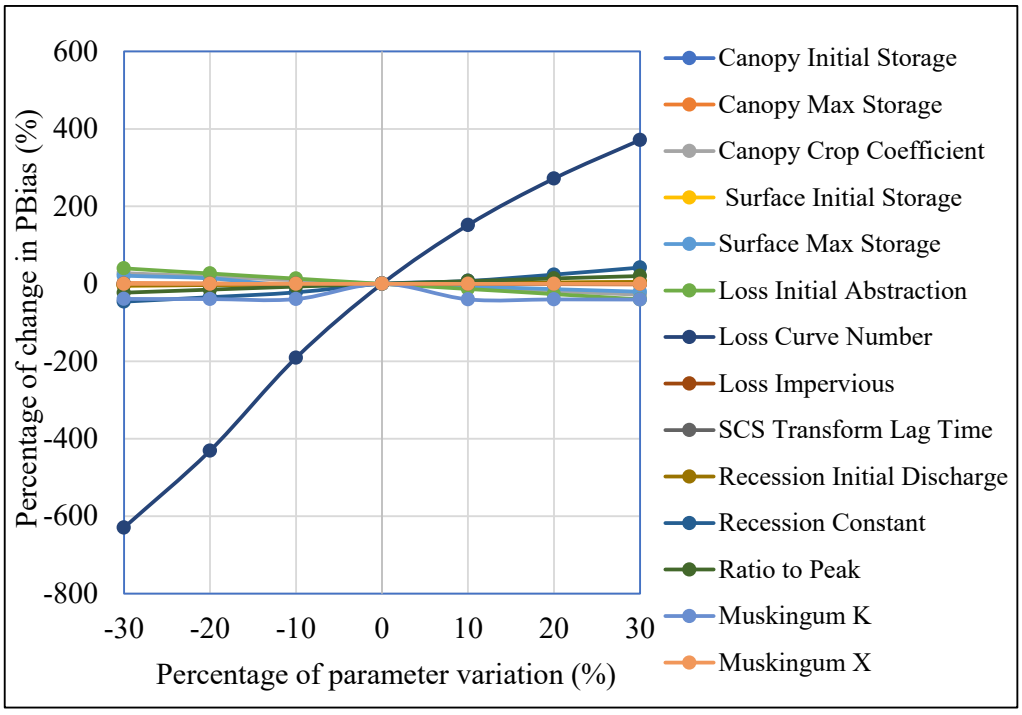

Figure 4-28: Percentage change in simulated PBIAS plotted against the percentage variation in each parameter

To identify the most sensitive parameters, slopes are calculated based on the percentage of change in peak discharge and volume and percentage of parameter variation. Then the parameters are ranked accordingly which is shown in Table 4-12.

Table 4-12: HEC-HMS parameters ranking in respective to peak discharge and volume

Model	Parameter	Ranking Based on Peak Discharge	Ranking Based on Discharge Volume
Loss	Curve Number	1	1
Routing	Muskingum X	2	12
Routing	Muskingum K	3	4
Loss	Initial Abstraction	4	2
Surface	Max Storage	5	6
Canopy	Crop Coefficient	6	5
Surface	Initial Storage	7	8
Baseflow	Recession Constant	8	3
Canopy	Max Storage	9	11
Loss	Impervious	10	10
Baseflow	Initial Discharge	11	9
Canopy	Initial Storage	12	13
Transform	Lag Time	13	14
Baseflow	Ratio to Peak	14	7

4.5 NDVI and Peak Discharge Relationship

The relationship between NDVI and peak discharge is inversely proportional to each other. A high NDVI value indicates dense vegetation which lowers the peak while a lower NDVI results in higher discharges and peaks. In this study, the relationship between NDVI and peak discharge is quietly matching considering the changes in NDVI and flood peak discharge variations in different scenarios. The higher NDVI (0.81) in the 1976 scenario is followed by a lower peak discharge of 842.1 m^3/s. When the NDVI value is decreasing in 1994 (0.50), the peak discharge increases to 1,003.7

m^3/s. In 2009 that the NDVI value is again increasing (0.65), the peak discharge declines to 995.9 m^3/s while a decline of NDVI value in 2021 (0.61) again resulted in an increase in peak discharge to 1,030.3 m^3/s.

4.6 Assessment of Landuse Change Impacts on Flood Peak Discharge

After model calibration and validation, each landuse scenario is applied by changing the SCS curve number, initial abstraction, and impervious area percentage then the model is simulated to produce results for each scenario while keeping all other parameters constant.

- The observed peak discharge was 820 m^3/s in the event 1961 and the simulated peak was estimated 842.1 m^3/s considering the 1976 landuse scenario. By applying the 1994 landuse scenario, the simulated peak discharge is found 1,003.7 m^3/s which shows a 161.6 m^3/s increase in peak discharge while applying the 2009 landuse scenario shows a peak discharge of 995.9 m^3/s which accounts for a 7.8 m^3/s decrease. The simulated peak discharge is 1,030.3 m^3/s for the 2021 landuse scenario which shows a 34.4 m^3/s increase compared to the 2009 scenario and shown in Figure 4-29.

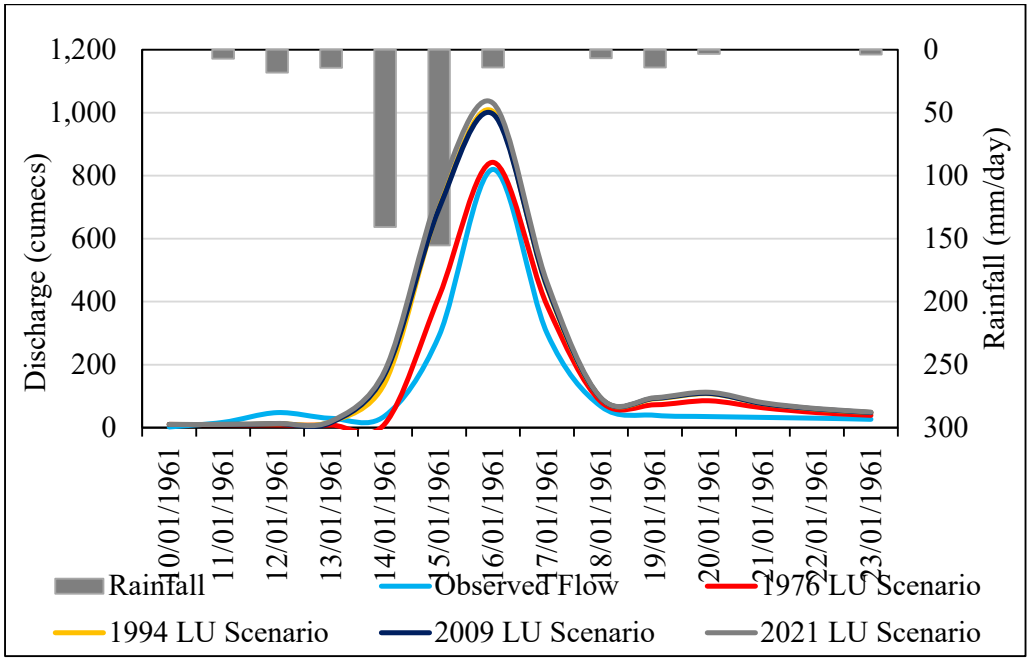

Figure 4-29: Hydrograph variations due to different landuse scenarios simulation

- The observed volume of water for event 1961 was 152.23 MCM and simulated was 178.16 MCM while it increased to 240.83 MCM, 242.50 MCM, and 253.52 MCM after applying 1994, 2009, and 2021 landuse scenarios, respectively. From the results, a significant increment of 75, 36 MCM is found from 1976 to 2021 due to deforestation and landuse change in the basin.

  The results of changes in the volume of water are presented in Table 4-13, Figure 4-30, and Figure 4-31.

Table 4-13: Water volume increment due to deforestation and landuse change

Scenario	Observed Volume	1976 LU Scenario	1994 LU Scenario	2009 LU Scenario	2021 LU Scenario
Simulated Volume	147.87	173.06	233.85	235.55	246.3

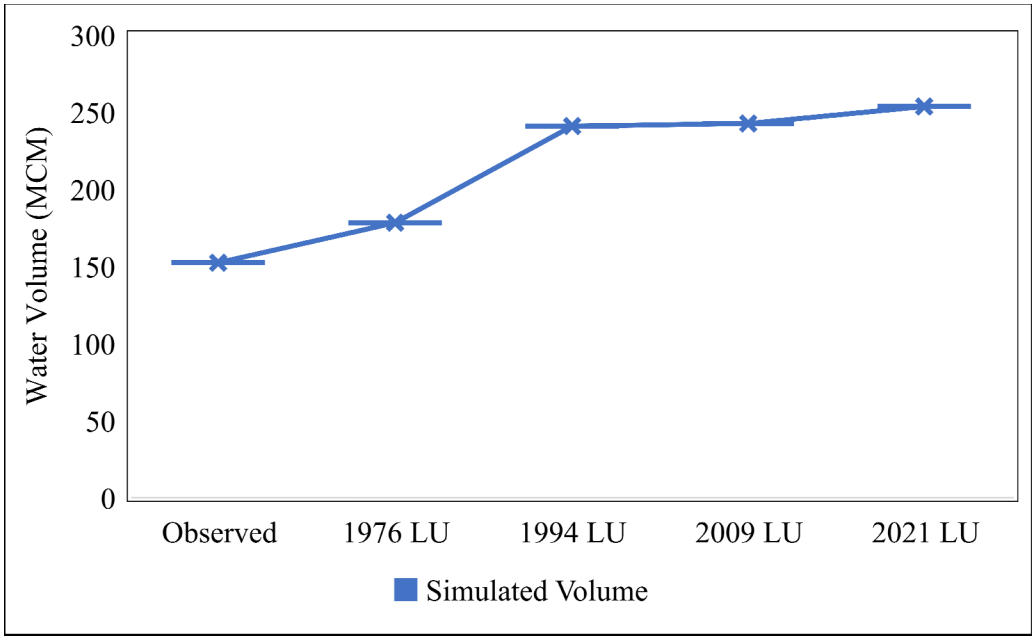

Figure 4-30: Water volume increase due to landuse change

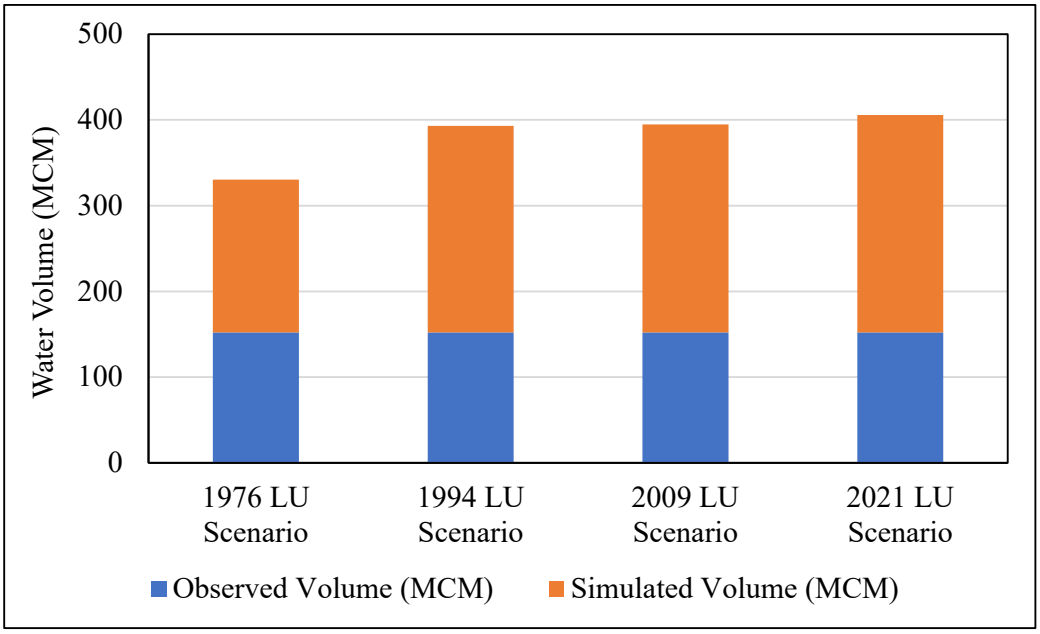

Figure 4-31: Water volume increase from 1976 – 2021

CHAPTER 5

5 DISCUSSION

The deforestation and landuse change impact assessment on flood peak discharge in the Maduru Oya river basin provides useful information for different stakeholders, planners, and policymakers for proper management of forest, land, and water in the basin. Although this research can be considered as a new theme in Sri Lanka that is not previously practiced, certain circumstances restrict the study of landuse change impact on flood peak discharge or regime in Sri Lanka. In the context of the Maduru Oya river basin, these limitations even get increased which will be discussed in the following sections. However, deforestation and landuse change is studied using satellite observations, verified by ground truth data, and used in the process of hydrological modeling. An event-based HEC-HMS model is set up, calibrated, and validated to study the hydrological behavior of the watershed under different landuse scenarios.

5.1 Satellite Data and Observations

The National Aeronautics and Space Administration (NASA) is a governmental organization responsible for the civilian space program, as well as aeronautics and space research in the United States. NASA earth explorer platform provides satellite images in an open-source format which have been widely used in academic projects and research areas. NASA EarthExplorer provides digital images of Landsat 2 covering Maduru Oya from the 1970s.

The literature indicates that satellite observations which are used for LULC studies in Sri Lanka are usually after the 1990s which can be seen in the studies conducted by Ranagalage et al. (2020); Rathnayake et al. (2020), and the reason might be because of the lower resolution of images in the earlier period. Since AMP has resulted in the construction of Maduru Oya reservoir and some other minor tanks in the river basin,

taking the study period after the 1990s would mean ignoring an important landuse change component. Therefore, an effort was made to select the earliest image available based on the predefined criteria.

To select appropriate satellite images for this study, some criteria like extent, cloud cover, time period, or season of image acquisition were considered. The criterion for extent was to select the images which cover the Maduru Oya river basin in terms of space and time. Space extent means to cover the entire river basin while time extent means to cover the study area during the desired period.

The criteria for cloud cover were to select the images with equal or less than 10% cloud cover. It filtered out most of the scenes and restricted the study to a limited number of scenes. Sometimes it is possible that scene cloud cover is showing higher than 10% but does not cover the desired study area. Therefore, an effort was made to check the images with more than 10% of clouds as well. Still, the existence of haze in the scene should be noted and may be optimized by atmospheric corrections.

Time period is important in landuse change studies using satellite observations because minor changes would not be easily detectable in shorter time periods considering data resolution. Initially, the methodology of this study was designed to study decadal deforestation and landuse change impact on flood peak discharge but considering the limitations such as temporal resolution and scene cloudiness of satellite images, it was found impossible. Another factor that is important in the selection of time period is the changes in the seasonal reflection of the vegetation in dry and wet periods. In wet periods, the vegetation and trees look healthier and greener while in the dry periods, it is the opposite. The variation in the extent of the water body due to seasonal climatological variations is also a major concern. During the wet period, the water body extent would be greater than that in the dry period and it may cause misinterpretation of the results. The criteria were to select the satellite images with the same time period, but in some cases, it varied one to two months and that is one of the reasons why the water bodies show small variation between 1994 – 2021.

5.2 Landuse Change Assessment

The images acquired in 1976, 1994, 2009, and 2021 were based on the predefined criteria and then classified using the maximum likelihood algorithm of supervised classification. To perform a supervised image classification and accuracy assessment, reference or ground truth data are needed. Therefore, a literature survey was conducted to collect any available previous maps of the Maduru Oya river basin. The district landuse maps of Sri Lanka are accessible in the 1980s (Panagos et al., 2011) in the European Digital Archive of Soil Maps (EDASM) which is used in this study for classification and accuracy assessment of the satellite image in 1976.

The image in 1994 is classified and accuracy assessment is performed using the 1999 landuse shapefile of Sri Lanka obtained from the Survey department of Sri Lanka assuming that there would not be major changes between 1994 – 1999 and then checked with GoogleEarth Pro. GoogleEarth Pro provides continuous historical imagery available from 1985 to the present. The image in 2009 and 2021 are classified and their accuracies are checked based on the observation in GoogleEarth Pro.

The results of this study indicate that the major deforestation and landuse change have happened between 1976 to 1994 as a result of the Accelerated Mahaweli Program. Implementation of the AMP which resulted in the construction of the Maduru Oya reservoir enabled irrigation of more lands which an increase of the paddy lands can be noticed in later periods in the study area. Chena cultivation is regularly used in the study area which shows the conversion of each landuse type to another and that is the reason for variation in scrubland areas. The reason for changes in the water body extents might be depending on the date of satellite images acquisition, the seasonal pattern of rainfall, and irrigation demand. Efforts were made to select the satellite images of the same period for different scenarios to precisely assess the landuse changes but the temporal resolution of the satellites, cloudiest of the scenes, and unavailability of the images had restricted this objective. However, the nearest scenes were selected based on the predefined criteria. The overall landuse change assessment of the Maduru Oya basin reveals that deforestation and other landuse changes have happened in the study area.

The Normalized Vegetation Index of the study area is assessed in each scenario which shows good agreement with the landuse classified images. The NDVI is high in 1976 when the forested areas are wider and it decreased with deforestation in later periods. The higher NDVI values reveal the fact that there is dense vegetation in the study area which subsequently lowers the peak discharge while lower NDVI values reveal a higher peak discharge. The relationship between the NDVI and the peak discharge indicates that the peak is lower when there is a high NDVI in earlier periods and the peak discharge is increasing when the NDVI is getting lower in post-AMP periods.

5.3 Hydrological and Meteorological Data

Data availability is the main concern of water engineers and river basin managers. On the other hand, data reliability is the most important component of a research. Reliable and accurate data will not only ease the process of modeling but will also provide accurate results and enable the decision-makers and water managers to design, plan and implement various effective and sustainable water projects.

Although a water engineer can encounter a data-scarce situation most often, in most of the cases it is not about data availability – it is about data accessibility. Especially, when it comes to the earlier periods, it gets harder to access the old datasets as they are forgotten or not included in the online database of the responsible organizations.

Maduru Oya river basin has had three streamflow gauging stations so far which are Padiyatalawa in upstream, Damsite in midstream, and Welikanda in the downstream. There are no streamflow gauging stations nearby the outlet of the river basin. Padiyatalawa gauge station is the automatic gauge station which is operating since 1984 and provides almost continuous records. Damsite and Welikanda gauging stations were operating from 1950 – 1978. According to the data collected from the Irrigation Department of Sri Lanka, there are missing data from 1957 – 1978 in the damsite station which makes any further analysis almost impossible. There is no rainfall station found during this study that provides concurrent rainfall data to that of the Welikanda streamflow gauging station in the Maduru Oya river basin and it might be the reason that Welikanda data is remained isolated in the research studies. Most of the stations located in or in a distance of 10 km to the Maduru Oya river basin

boundary, provide the rainfall data after the 1990s. Data scarcity is the most probable reason that very few research are conducted in the Maduru Oya river basin and in most cases, only the upper catchment at Padiyatalawa is studied.

Since the objective of this study was to study deforestation and landuse change impacts on flood peak discharge of Maduru Oya river basin, the selection of study site for hydrological modeling was a challenging task because studying landuse change impact on flood peak discharge at a small undeveloped area like Padiyatalawa catchment would not be meaningful and give the desired results. Moreover, the Accelerated Mahaweli Program which resulted in the construction of the Maduru Oya reservoir had significantly changed the landuse pattern of the basin, and the catchment at Padiyatalawa would not cover the reservoir and subsequent changes.

The catchment at the damsite could not be chosen because of the smaller area and missing data. During landuse change assessment of the river basin, it was found that deforestation has mostly occurred starting from damsite in midstream toward the outlet in downstream. Therefore, the selection of Damsite catchment for hydrological modeling would not give appropriate results due to the short period of data available and smaller area which was not covering major deforestation happened in the river basin.

As there is no river gauge station further downstream or near to the outlet of the Maduru Oya river basin rather than the Welikanda, it was selected as the study area for hydrological modeling, but the problem was the unavailability of concurrent rainfall data inside or nearby the river basin. Initially, it was aimed to use rainfall data of any gauging stations at a maximum distance of 10 km from the basin perimeter which is suggested by Kabeja et al. (2020) but no rainfall gauging station was providing data between 1950 – 1978 at that distance. Then any possible option nearby was searched and found that Batticaloa rainfall station is the only station, which provides historical and continuous records. Batticaloa station is approximately 38 km far away from the Maduru Oya river basin perimeter which was measured through Google Earth Pro. The response of the watershed to the rainfall was highly concerned and that is why the correlation between rainfall and discharge data was checked.

It is noteworthy that there are secondary datasets also available in online sources which can be used in rainfall-runoff modeling, but biases create uncertainties that should be strictly considered and addressed before any further processing.

5.4 Hydrological Modeling

This study was focused on studying peak flows therefore, an event-based modeling approach was selected. The correlation between Batticaloa rainfall data and Welikanda discharge data was found satisfactory during data checking, but cautions should be taken when addressing low flows. The reason would be the distance of Batticaloa station from the upper catchment of the Maduru Oya river basin. There would be a certain amount of rainfall in upstream of Maduru Oya in some extent of time but not observed in the Batticaloa and vice versa. The efforts made were to select the major storm events, but missing data resulted in the isolation of some of the events.

The HEC-HMS model which was selected for hydrological modeling of landuse scenarios was calibrated using auto-calibration and manual adjusting of the parameters. Then the results are validated using the same parameter values found in calibration and different events. A sensitivity analysis of the model was performed with the optimized parameters found during calibration by changing a parameter at a time in increment of 10% from -30% to +30%.

For hydrological modeling, Welikanda station is considered as the outlet of the basin then the basin is divided into 5 subbasins. Discharge data of Welikanda station is used in calibration and validation of the model. The total area of the Maduru Oya river basin is 1,539 km^2 while the Welikanda catchment is encompassing an area of 1,029 km^2 which is almost two the third of the total area of the river basin. According to results found in landuse change assessment, homeland/garden shows an increase near to the outlet of the river basin from 1976 – 2021, and deforestation has taken place in upstream and downstream. Therefore, it should be considered while interpreting the results that the whole river basin results might be slightly different compared to that of Welikanda.

The finding of this study is in agreement with the previous studies that deforestation has widely happened in the dry zone of Sri Lanka while other LULC changes are

noticed in different parts of the country (Ranagalage et al., 2020; Rathnayake et al., 2020; UN-REDD, 2015) and may cause several adverse environmental impacts (Calder & Aylward, 2006; Houghton, 1994; Meade & Trimble, 1974). Although Sri Lanka is one of the cloudiest parts of the world (Nay et al., 2018; Ranagalage et al., 2020; Sandamali & Welikanna, 2018) which was identified as the major restriction of the LULC assessment in this study, however, deforestation and LULC change were assessed and quantified with good overall accuracy.

A synthesis of LULC change impact studies on runoff, flood, and low flows in 37 catchments of East Africa carried out by Guzha et al. (2017) shows that SWAT and HEC-HMS have been highly attractive softwares for researchers which are used in these studies and have produced reliable results. An event-based HEC-HMS model is set up and used in this study as well which the results are showing good performance with the observed data. However, the agreement between observed and simulated flows are dependent on landuse condition, hydrological components, and the assumptions during modeling (Koneti et al., 2018). Therefore, the assumptions made in this study also should be strictly considered while interpreting the results.

The results of this study indicate that deforestation and LULC change has altered the characteristics of the basin in response to rainfall and has increased the flood magnitude and peak discharge which is in accordance with other studies conducted in different parts of the world (Guzha et al., 2017; Hlásny et al., 2015; Kabeja et al., 2020; Lim et al., 2019; Sun et al., 2005).

CHAPTER 6

6 CONCLUSIONS AND RECOMMENDATIONS

The assessment of deforestation and landuse change impacts on flood peak discharge in the Maduru Oya river basin of Sri Lanka indicates that deforestation has happened widely in the basin and other landuse types also have changed which have resulted an increase in flood peak discharge and water volume.

6.1 Conclusions

- An overview of deforestation and landuse change assessment between 1976 to 2021 indicates that deforestation has occurred widely with a rate of 25.4% while homestead/garden, paddy, scrubland, and water bodies have increased by 6.2%, 12.7%, 2.2%, and 4.4%, respectively.
- The NDVI is ranging from -0.975 to 0.818 in 1976, from -0.088 to 0.509 in 1994, from -0.207 to 0.655 in 2009, and from -0.203 to 0.618 in 2021. The overall results of NDVI from 1976 to 2021 show a decrease of 0.2 in the high NDVI values while an increase of 0.772 in the lowest NDVI values. It reveals that the vegetation density is decreased while vegetations (paddy lands) areas are increased which shows higher NDVI values in the lower ranges. The results of NDVI are in good agreement with landuse scenarios simulations.
- The average NSE, RSR, PBIAS, and R^2 values of 0.92, 0.25, 17.60, and 0.94 were achieved in calibration, respectively which all can be rated as very good performance except for PBIAS which is rated as satisfactory.
- The average NSE, RSR, PBIAS, and R^2 values of 0.73, 0.50, -3.03, and 0.78 are found in the validation, respectively which all can be rated very good performance except for NSE which is rated as good performance.

- The sensitivity analysis results reveal that Cuve Number is the most sensitive parameter in respect to peak discharge followed by Muskingum X and K while it is followed by baseflow initial abstraction and recession constant in respect to discharge volume.
- The assessment of the relationship between the NDVI and peak discharge indicates that the peak is lower when there is a higher NDVI and the peak is higher when there is lower NDVI in the study area.
- The application of different land cover scenarios indicates an increase in peak discharge. The simulated peak discharge considering the 1976 scenario is estimated at 842.1 m^3/s while it is estimated to be 1,030.3 m^3/s for the 2021 landuse scenario which shows 188.2 m^3/s increments between respective years.
- Deforestation and LULC change have not only impacted the flood peak discharge but have also raised the volume. The simulated water volume is estimated to be 178.16 MCM considering the baseline scenario (1976) while it increased to 253.52 MCM in 2021 which indicates 75.36 MCM between the respective years.

6.2 Recommendations

Based on the finding of this study following points are recommended:

- Although, Landsat images provide an almost continuous record of the entire world, but sometimes data availability remains a critical concern in a landuse change study. It is recommended that criteria should be defined and then the satellite observations availability within desired time period should be checked.
- Before any study of landuse change, the major components that may have caused a change in landuse should be identified and time period of study should be decided accordingly.
- Since the focus of this study was to assess the deforestation and landuse change impacts on flood peak discharge, the middle and low flows were not studied.

To understand the overall watershed's behavior to landuse change, it is recommended that a continuous modeling approach should be performed in a basin of Sri Lanka located in the dry zone where concurrent rainfall and discharge data are available or it can be further investigated by a comparative model in the wet zone.

- Due to data-scarce situation of the Maduru Oya river basin, the rainfall and streamflow trend analysis was restricted and not done in this study. Trends in the pattern of floods can be a composite of climate change and anthropogenic activities. A combined study of climate and landuse change impacts on flood regimes is recommended to quantify the impact of each on flood peaks, or regimes.
- There are approaches available that predict the landuse for future scenarios. As assessment of landuse change scenario, prediction for the future along with the climate change scenarios would be an attractive topic that is recommended for future studies.

BIBLIOGRAPHY

ACRES. (1979). Maduru Oya Project Feasibility Study - Interim Report (Issue March).

ACRES. (1980). Maduru Oya Project Feasibility Report Annex C Hydrology and Water Balance (Issue August). https://pdf.usaid.gov/pdf_docs/pdaax058.pdf

Alberti, M., Weeks, R., & Coe, S. (2004). Urban land-cover change analysis in Central Puget Sound. Photogrammetric Engineering and Remote Sensing, 70(9), 1043–1052. https://doi.org/10.14358/PERS.70.9.1043

Andréassian, V. (2004). Waters and forests: From historical controversy to scientific debate. Journal of Hydrology, 291(1–2), 1–27. https://doi.org/10.1016/j.jhydrol.2003.12.015

Betts, A. K., & Ball, J. H. (2003). Evaluation of the ERA-40 Surface Water Budget and Surface Temperature for the Mackenzie River Basin. 4(2000), 1194–1211.

Betts, A. K., & Ball, J. H. (2005). Hydrometeorology of the Amazon in ERA-40. 6(1998), 764–774.

Calder, I. R., & Aylward, B. (2006). Forest and floods: Moving to an evidence-based approach to watershed and integrated flood management. Water International, 31(1), 87–99. https://doi.org/10.1080/02508060608691918

Cohen, W. B., & Goward, S. N. (2004). Landsat's role in ecological applications of remote sensing. BioScience, 54(6), 535–545. https://doi.org/10.1641/0006-3568(2004)054[0535:LRIEAO]2.0.CO;2

Danáčová, M., Földes, G., Labat, M. M., Kohnov, S., & Hlavˇcová, K. (2020). Estimating the E ff ect of Deforestation on Runo ff in Small Mountainous Basins in Slovakia and. Water, 12(3113). https://doi.org/10.3390/w12113113

De Zoysa, M. (2001). A Review of Forest Policy Trends in Sri Lanka. In Policy Trend Report (Vol. 2001).

Decker, M., Brunke, M. A., Wang, Z., Sakaguchi, K., Zeng, X., & Bosilovich, M. G. (2012). Evaluation of the Reanalysis Products from GSFC , NCEP , and ECMWF Using Flux Tower Observations. Journal of Climate, 25, 1916–1944. https://doi.org/10.1175/JCLI-D-11-00004.1

Dembélé, M., Oriani, F., Tumbulto, J., Mariéthoz, G., & Schaefli, B. (2019). Gap-filling of daily streamflow time series using Direct Sampling in various hydroclimatic settings. Journal of Hydrology, 569(December 2018), 573–586. https://doi.org/10.1016/j.jhydrol.2018.11.076

Douinot, A., Roux, H., Garambois, P. A., Larnier, K., Labat, D., & Dartus, D. (2016). Accounting for rainfall systematic spatial variability in flash flood forecasting. Journal of Hydrology, 541, 359–370. https://doi.org/10.1016/j.jhydrol.2015.08.024

Dubey, M., & Hardaha, M. K. (2019). Application of Standard Models and Artificial Neural Network for Missing Rainfall Estimation. International Journal of Current Microbiology and Applied Sciences, 8(01), 1564–1572. https://doi.org/https://doi.org/10.20546/ijcmas.2019.801.164

ECMWF. (2021). ERA5: data documentation. https://confluence.ecmwf.int/display/CKB/ERA5%3A+data+documentation

Fan, H., Xu, L., Tao, H., Feng, W., Cheng, J., & You, H. (2017). Accessing the Difference in the Climate Elasticity of Runoff across the Poyang Lake Basin , China. Water, 1–18. https://doi.org/10.3390/w9020135

Guzha, A. C., Rufino, M. C., Okoth, S., Jacobs, S., & Nobrega, R. L. . (2017). Journal of Hydrology : Regional Studies Impacts of land use and land cover change on surface runo ff , discharge and low fl ows : Evidence from East Africa. Journal of Hydrology, 15(November 2017), 49–67. https://doi.org/10.1016/j.ejrh.2017.11.005

Hlásny, T., Kočický, D., Maretta, M., Sitková, Z., Barka, I., Konôpka, M., & Hlavatá, H. (2015). Effect of deforestation on watershed water balance: Hydrological modelling-based approach. Forestry Journal, 61(2), 89–100. https://doi.org/10.1515/forj-2015-0017

Houghton, R. A. (1994). The Worldwide Extent of Land-Use Change. BioScience, 44(5), 305–313. https://doi.org/10.2307/1312380

Hu, S., & Shrestha, P. (2020). Examine the Impact of Land Use and Land Cover Changes on Peak Discharges of a Watershed in the Midwestern United States Using the HEC-HMS Model Examine the Impact of Land Use and Land Cover Changes on. Papers in Applied Geography, 0(0), 1–18. https://doi.org/10.1080/23754931.2020.1732447

Huang, Y., Yu, M., Tian, H., & Liu, Y. (2020). Decomposition and Attribution Analysis of Runo ff Alteration of the Dongting Lake in China. Water, Dmc. https://doi.org/doi: 10.3390/w12102729

Hussein, K., Alkaabi, K., Ghebreyesus, D., Usman, M., & Sharif, H. O. (2020). Land use / land cover change along the Eastern Coast of the UAE and its impact on flooding risk. Geomatics, Natural Hazards and Risk, 11(1), 112–130. https://doi.org/10.1080/19475705.2019.1707718

Jaspers, F. G. W. (2003). Institutional arrangements for integrated river basin management. Water Policy, 5(1), 77–90. https://doi.org/10.2166/wp.2003.0004

Johann, G., Papadakis, I., & Pfister, A. (1998). Historical precipitation time series for applications in urban hydrology. Water Science and Technology, 37(11), 147–153. https://doi.org/10.1016/S0273-1223(98)00327-8

Kabeja, C., Li, R., Guo, J., Edmond, D., & Rwatangabo, R. (2020). The Impact of Reforestation Induced Land Cover Change (1990 – 2017) on Flood Peak Discharge Using HEC-HMS Hydrological Model and Satellite Observations : A Study in Two Mountain Basins , China. Water, 1–23. https://doi.org/10.3390/w12051347

Kalteh, A. M., & Hjorth, P. (2009). Imputation of missing values in a precipitation – runoff process database Aman Mohammad Kalteh and Peder Hjorth. Mi, 420–432. https://doi.org/10.2166/nh.2009.001

Kaspersen, P. S., Nanna, H. R., Karsten, A.-N., Henrik, M., & Drews, M. (2017). Comparison of the impacts of urban development and climate change on exposing

European cities to pluvial flooding. Hydrology and Earth System Sciences, 21(8), 4131–4147. https://doi.org/10.5194/hess-21-4131-2017

Kennedy, R. E., Yang, Z., Braaten, J., Copass, C., Antonova, N., Jordan, C., & Nelson, P. (2015). Attribution of disturbance change agent from Landsat time-series in support of habitat monitoring in the Puget Sound region, USA. Remote Sensing of Environment, 166, 271–285. https://doi.org/10.1016/j.rse.2015.05.005

Koneti, S., Sunkara, S. L., & Roy, P. S. (2018). Hydrological modeling with respect to impact of land-use and land-cover change on the runoff dynamics in Godavari river basin using the HEC-HMS model. ISPRS International Journal of Geo-Information, 7(6). https://doi.org/10.3390/ijgi7060206

Koukoula, M., Nikolopoulos, E. I., Dokou, Z., & Anagnostou, E. N. (2020). Evaluation of global water resources reanalysis products in the upper blue nile river basin. Journal of Hydrometeorology, 21(5), 935–952. https://doi.org/10.1175/JHM-D-19-0233.1

Li, M. S., Mao, L. J., Shen, W. J., Liu, S. Q., & Wei, A. S. (2013). Change and fragmentation trends of Zhanjiang mangrove forests in southern China using multi-temporal Landsat imagery (1977-2010). Estuarine, Coastal and Shelf Science, 130, 111–120. https://doi.org/10.1016/j.ecss.2013.03.023

Lim, J., Kim, K. M., & Lee, K. S. (2019). Does deforestation trigger severe flood damage at hoeryeong city in North Korea? Forests, 10(9), 1–14. https://doi.org/10.3390/f10090789

Meade, R. H., & Trimble, S. W. (1974). Changes in sediment loads in rivers of the Atlantic drainage of the United States since 1900. International Association of Hydrological Sciences, 113, 99–104.

Moriasi, D. N., Arnold, J. G., Van Liew, M. W., Bingner, R. L., Harmel, R. D., & Veith, T. L. (2007). Model Evaluation Guidelines for Systematic Quantification of Accuracy in Watershed Simulations. American Society of Agricultural and Biological Engineers, 50(3), 885–900. https://doi.org/10.13031/2013.23153

Mourad, M. (2018). A method for automatic validation of long time series of data in

urban hydrology. September, 263–270.

Msaddek, M., Kimbowa, G., & Garouani, A. El. (2020). Hydrological Modeling of Upper OumErRabia Basin (Morocco), Comparative Study of the Event-Based and Continuous-Process HEC-HMS Model Methods. Computational Water, Energy, and Environmental Engineering, 09(04), 159–184. https://doi.org/10.4236/cweee.2020.94011

Nay, J., Burchfield, E., & Gilligan, J. (2018). A machine-learning approach to forecasting remotely sensed vegetation health. International Journal of Remote Sensing, 39(6), 1800–1816. https://doi.org/10.1080/01431161.2017.1410296

Nkuna, T. R., & Odiyo, J. O. (2011). Filling of missing rainfall data in Luvuvhu River Catchment using artificial neural networks. Physics and Chemistry of the Earth, 36(14–15), 830–835. https://doi.org/10.1016/j.pce.2011.07.041

Panagos, P., Jones, A., Bosco, C., & Senthil Kumar, P. . (2011). The Soil Maps of Asia. International Journal of Digital Earth, 4 (5), 434–443. https://doi.org/DOI:10.1080/17538947.2011.596580

Ranagalage, M., Gunarathna, M. H. J. P., Surasinghe, T. D., Dissanayake, D., Simwanda, M., Murayama, Y., & Morimoto, T. (2020). Multi-Decadal Forest-Cover Dynamics in the Tropical Realm : Past Trends and Policy Insights for Forest Conservation in Dry Zone of Sri Lanka. Forests, 1–24. https://doi.org/doi:10.3390/f11080836

Rathnayake, C. W., Jones, S., & Soto-Berelov, M. (2020). Mapping Land Cover Change over a 25-Year Period (1993–2018) in Sri Lanka Using Landsat Time-Series. Land. https://doi.org/doi:10.3390/land9010027

Rawat, J. S., Biswas, V., & Kumar, M. (2013). Changes in land use/cover using geospatial techniques: A case study of Ramnagar town area, district Nainital, Uttarakhand, India. Egyptian Journal of Remote Sensing and Space Science, 16(1), 111–117. https://doi.org/10.1016/j.ejrs.2013.04.002

Reusser, L., Bierman, P., & Rood, D. (2015). Quantifying human impacts on rates of erosion and sediment transport at a landscape scale. Geology, 43(2), 171–174.

https://doi.org/10.1130/G36272.1

Revilla-romero, B., Beck, H. E., Burek, P., Salamon, P., Roo, A. De, & Thielen, J. (2015). Remote Sensing of Environment Filling the gaps : Calibrating a rainfall-runoff model using satellite-derived surface water extent. Remote Sensing of Environment, 171, 118–131. https://doi.org/10.1016/j.rse.2015.10.022

Rogger, M., Agnoletti, M., Alaoui, A., Bathurst, J. C., Bodner, G., Borga, M., Chaplot, V., Gallart, F., Glatzel, G., Hall, J., Holden, J., Holko, L., Horn, R., Kiss, A., Quinton, J. N., Leitinger, G., Lennartz, B., Parajka, J., Peth, S., … Viglione, A. (2017). Land use change impacts on floods at the catchment scale: Challenges and opportunities for future research. Water Resources Research, 5209–5219. https://doi.org/10.1002/2017WR020723.Received

Rwanga, S. S., & Ndambuki, J. M. (2017). Accuracy Assessment of Land Use/Land Cover Classification Using Remote Sensing and GIS. International Journal of Geosciences, 08(04), 611–622. https://doi.org/10.4236/ijg.2017.84033

Sandamali, K. U. ., & Welikanna, D. R. (2018). Deforestation or Reforestation , A Time Series Remote Sensing Perspective of Wilpattu National Park , Sri Lanka. Journal of Applied Mathematics and Computation, 2(10), 473–482. https://doi.org/10.26855/jamc.2018.10.003

Sattari, M.-T., Rezazadeh-Joudi, A., & Kusiak, A. (2017). Assessment of different methods for estimation of missing data in precipitation studies Mohammad-Taghi Sattari , Ali Rezazadeh-Joudi and Andrew Kusiak. 1032–1044. https://doi.org/10.2166/nh.2016.364

Schilling, W. (1991). Rainfall data for urban hydrology: what do we need? Atmospheric Research, 27(1–3), 5–21. https://doi.org/10.1016/0169-8095(91)90003-F

Seneviratne, sonia i., Viterbo, P., Lu¨thi, D., & Scha¨r, C. (2004). Inferring Changes in Terrestrial Water Storage Using ERA-40 Reanalysis Data : The Mississippi River Basin. American Meteorological Society, 17, 2039–2057.

Subramanya, K. (2013). Engineering Hydrology (Fourth). McGraw Hidd Education

(India) Private Limited.

Sun, G., Mcnulty, S. G., Lu, J., Amatya, D. M., Liang, Y., & Kolka, R. K. (2005). Regional annual water yield from forest lands and its response to potential deforestation across the southeastern United States. Journal of Hydrology, 308, 258–268. https://doi.org/10.1016/j.jhydrol.2004.11.021

Tang, Y., Tang, Q., Wang, Z., Chiew, F. H. S., & Zhang, X. (2019). Different precipitation elasticity of runoff for precipitation increase and decrease at watershed scale. American Geophysical Union, 0–2. https://doi.org/10.1029/2018JD030129

Tassew, B. G., Belete, M. A., & Miegel, K. (2019). Application of HEC-HMS Model for Flow Simulation in the Lake Tana Basin: The Case of Gilgel Abay Catchment, Upper Blue Nile Basin, Ethiopia. Hydrology, 6(21). https://doi.org/doi:10.3390/hydrology6010021

UN-REDD. (2015). Drivers of deforestation and forest degradation in sri lanka : identification of key policies and measures. April 2015, 12. https://doi.org/10.13140/RG.2.2.15886.15688

USACE. (2000). Hydrologic Modeling System Technical Reference Manual (Issue March).

USACE. (2018). Hydrologic Modeling System HEC-HMS, User's Manual. Version 4.3. Hydrologic Engineering Centre. In Hydrologic Engineering Centre: Vol. (Issue Version 4.3). https://www.hec.usace.army.mil/software/hec-hms/documentation/HEC-HMS_Users_Manual_4.3.pdf

USACE. (2021). HEC-HMS User ' s Manual. https://www.hec.usace.army.mil/confluence/hmsdocs/hmsum/4.7/release-notes/v-4-7-0-release-notes

USDA. (2009). Hydrologic Soil Groups. In National Engineering Handbook. https://directives.sc.egov.usda.gov/OpenNonWebContent.aspx?content=22526.wba

Verburg, P. H., Kok, K., Robert, Gilmore, Pontius, J., & Veldkamp, A. (2008). Chapter

5 Modeling Land-Use and Land-Cover Change (Issue June 2014). https://doi.org/10.1007/3-540-32202-7

Vermote, E., Justice, C., Claverie, M., & Franch, B. (2016). Preliminary analysis of the performance of the Landsat 8/OLI land surface reflectance product. Remote Sensing of Environment, 185, 46–56. https://doi.org/10.1016/j.rse.2016.04.008

Villazon, M. F., & Willems, P. (2010). Filling gaps and Daily Disaccumulation of Precipitation Data for Rainfall-runoff model. 4th International Scientific Conference on Water Observation and Information Systems for Decision Support, August 2015, 1–9.

Vogels, M. F. A., de Jong, S. M., Sterk, G., & Addink, E. A. (2017). Agricultural cropland mapping using black-and-white aerial photography, Object-Based Image Analysis and Random Forests. International Journal of Applied Earth Observation and Geoinformation, 54, 114–123. https://doi.org/10.1016/j.jag.2016.09.003

Wickramasuriya, S. S., & Fernando, W. C. D. K. (2012). Challenges in Dam Safety and Extreme Rainfall Estimation in Relation to Sri Lanka. Engineer: Journal of the Institution of Engineers, Sri Lanka, 45(1), 39. https://doi.org/10.4038/engineer.v45i1.6948

Wijethunga, L. (2019). Deforestation in Sri Lanka and how the civil society could contribute to address it. Deforestation in Sri Lanka and How the Civil Society Could Contribute to Address It. https://www.academia.edu/34858598/Deforestation_in_Sri_Lanka_and_how_the_civil_society_could_contribute_to_address_it

Withanage, N. S., Dayawansa, D. K., Silva, R. P. D., & Rathnayake, C. W. M. R. (2018). Assessment of Morphological Characteristics of Maduru Oya Assessment of Morphological Characteristics of Maduru Oya. 39th Asian Conference on Remote Sensing: Remote Sensing Enabling Prosperity, ACRS 2018 , Malaysia, November, 10.

Woltemade, C. J., Hawkins, T. W., Jantz, C., & Drzyzga, S. (2020). Impact of Changing Climate and Land Cover on Flood Magnitudes in the Delaware River.

Journal of the American Water Resources Association. https://doi.org/10.1111/1752-1688.12835

Zema, D. A., Labate, A., Martino, D., & Zimbone, S. M. (2016). Comparing Different Infiltration Methods of the HEC-HMS Model: The Case Study of the Mésima Torrent (Southern Italy). Land Degradation and Development, 28(1), 294–308. https://doi.org/10.1002/ldr.2591

Zhang, D., Liu, X., Zhang, Q., Liang, K., & Liu, C. (2016). Investigation of factors affecting intra-annual variability of evapotranspiration and streamflow under different climate conditions. Journal of Hydrology, 543, 759–769. https://doi.org/10.1016/j.jhydrol.2016.10.047

Zhang, T., Zhang, X., Xia, D., & Yangyang, L. (2014). An analysis of land use change dynamics and its impacts on hydrological processes in the Jialing River Basin. Water (Switzerland), 6(12), 3758–3782. https://doi.org/10.3390/w6123758

Zhang, Y., & Post, D. (2018). How good are hydrological models for gap-filling streamflow data ? Hydrology and Earth System Sciences, August, 4593–4604. https://doi.org/https://doi.org/10.5194/hess-22-4593-2018

Zope, P. E., Eldho, T. I., & Jothiprakash, V. (2016). Impacts of land use-land cover change and urbanization on flooding: A case study of Oshiwara River Basin in Mumbai, India. Catena, 145, 142–154. https://doi.org/10.1016/j.catena.2016.06.009

Zope, P. E., Eldho, T. I., & Jothiprakash, V. (2017). Hydrological impacts of land use–land cover change and detention basins on urban flood hazard: a case study of Poisar River basin, Mumbai, India. Natural Hazards, 87(3), 1267–1283. https://doi.org/10.1007/s11069-017-2816-4

Zoran, M., Zoran, L.-F., Dida, A., & Dida, M. R. (2012). Climate changes and their impacts on Romanian mountain forests. Remote Sensing for Agriculture, Ecosystems, and Hydrology XIV, 8531(October 2012), 85311S. https://doi.org/10.1117/12.974389

ANNEXURE 1

7 CURVE NUMBER FOR DIFFERENT LANDUSE SCENARIOS

Table 7-1: Curve number calculations for 1976 landuse scenario

Sub catchment	LU Type	Description	Area (km^2)	Area in Percentage	Soil Group	Curve Number (CN)	CN x A	Impervious Area (km^2)	Impervious Area (%)
Sub catchment 1	FRSUA	Forest	184.73	55.11	C	58.00	10714.36	3.06	0.91
	HOMSA	Homestead/Garden	7.07	2.11	C	90.00	636.34		
	PDDYA	Paddy	0.98	0.29	C	95.00	93.37		
	SCRBA	Scrubland	141.45	42.20	C	64.00	9052.65		
	STRMA	Water Body	0.95	0.28	C	97.00	91.84		
Total			**335.18**	**100.00**	**Weighted Average CN**		61.43		
	FRSUA	Forest	58.99	67.12	C	58.00	3421.19	0.08	0.09
	HOMSA	Homestead/Garden	0.28	0.32	C	90.00	24.95		

Sub catchment	LU Type	Description	Area (km^2)	Area in Percentage	Soil Group	Curve Number (CN)	CN x A	Impervious Area (km^2)	Impervious Area (%)
Sub catchment 2	PDDYA	Paddy	0.09	0.10	C	95.00	8.55		
	SCRBA	Scrubland	28.53	32.47	C	64.00	1826.15		
Total			**87.89**	**100.00**	**Weighted Average CN**		60.09		
Sub catchment 3	FRSUA	Forest	158.64	73.24	C	58.00	9201.19	0.90	0.41
	HOMSA	Homestead/Garden	2.23	1.03	C	90.00	200.56		
	PDDYA	Paddy	3.50	1.62	C	95.00	332.42		
	SCRBA	Scrubland	52.01	24.01	C	64.00	3328.36		
	STRMA	Water Body	0.23	0.11	C	97.00	22.70		
Total			**216.61**	**100.00**	**Weighted Average CN**		60.41		
Sub catchment 4	FRSUA	Forest	57.62	35.62	C	58.00	3341.84	5.64	3.49
	HOMSA	Homestead/Garden	4.80	2.97	C	90.00	432.22		
	PDDYA	Paddy	10.23	6.32	C	95.00	971.62		
	SCRBA	Scrubland	84.88	52.48	C	64.00	5432.37		
	STRMA	Water Body	4.21	2.60	C	97.00	408.21		

Sub catchment	LU Type	Description	Area (km^2)	Area in Percentage	Soil Group	Curve Number (CN)	CN x A	Impervious Area (km^2)	Impervious Area (%)
Total			**161.74**	**100.00**	**Weighted Average CN**		65.45		
Sub catchment 5	FRSUA	Forest	153.78	67.91	C	58.00	8919.52	3.04	1.34
	HOMSA	Homestead/Garden	7.62	3.36	C	90.00	685.58		
	PDDYA	Paddy	13.94	6.16	C	95.00	1324.57		
	SCRBA	Scrubland	50.35	22.23	C	64.00	3222.37		
	STRMA	Water Body	0.76	0.34	C	97.00	74.03		
Total			**226.46**	**100.00**	**Weighted Average CN**		62.82		

Table 7-2: Curve number calculations for 1994 landuse scenario

Sub catchment	LU Type	Description	Area (km^2)	Area in Percentage	Soil Group	Curve Number (CN)	CN x A	Impervious Area (km^2)	Impervious Area (%)
Sub catchment 1	FRSUA	Forest	209.58	62.46	C	58.00	12155.50	26.45	7.88
	HOMSA	Homestead/Garden	3.26	0.97	C	90.00	293.38		
	PDDYA	Paddy	3.62	1.08	C	95.00	343.71		
	SCRBA	Scrubland	93.62	27.90	C	64.00	5991.84		
	STRMA	Water Body	25.48	7.59	C	97.00	2471.20		
Total			**335.55**	**100.00**	**Weighted Average C**		63.34		
Sub catchment 2	FRSUA	Forest	55.76	63.28	C	58.00	3234.00	10.25	11.64
	HOMSA	Homestead/Garden	2.11	2.39	C	90.00	189.46		
	PDDYA	Paddy	3.90	4.43	C	95.00	370.73		
	SCRBA	Scrubland	16.72	18.98	C	64.00	1070.32		
	STRMA	Water Body	9.63	2.87	C	97.00	933.67		
Total			**88.12**	**89.08**	**Weighted Average C**		65.80		
	FRSUA	Forest	26.61	12.30	C	58.00	1543.45	35.76	16.53

Sub catchment	LU Type	Description	Area (km^2)	Area in Percentage	Soil Group	Curve Number (CN)	CN x A	Impervious Area (km^2)	Impervious Area (%)
Sub catchment 3	HOMSA	Homestead/Garden	9.66	4.47	C	90.00	869.54		
	PDDYA	Paddy	20.75	9.59	C	95.00	1971.72		
	SCRBA	Scrubland	126.43	58.44	C	64.00	8091.24		
	STRMA	Water Body	32.87	15.19	C	97.00	3188.20		
Total			**216.32**	**100.00**	**Weighted Average C**		72.41		
Sub catchment 4	FRSUA	Forest	31.44	19.37	C	58.00	1823.66	14.75	9.08
	HOMSA	Homestead/Garden	7.93	4.88	C	90.00	713.77		
	PDDYA	Paddy	33.14	20.41	C	95.00	3148.54		
	SCRBA	Scrubland	77.47	47.72	C	64.00	4958.15		
	STRMA	Water Body	12.37	7.62	C	97.00	1200.20		
Total			**162.36**	**100.00**	**Weighted Average C**		72.95		
Sub catchment 5	FRSUA	Forest	60.97	26.86	C	58.00	3536.50	4.09	1.80
	HOMSA	Homestead/Garden	7.62	3.36	C	90.00	685.83		
	PDDYA	Paddy	61.50	27.09	C	95.00	5842.56		

Sub catchment	LU Type	Description	Area (km^2)	Area in Percentage	Soil Group	Curve Number (CN)	CN x A	Impervious Area (km^2)	Impervious Area (%)
	SCRBA	Scrubland	95.08	41.89	C	64.00	6085.15		
	STRMA	Water Body	1.81	0.80	C	97.00	175.91		
Total			**226.99**	**100.00**	**Weighted Average C**		71.92		

Table 7-3: Curve number calculations for 2009 landuse scenario

Sub catchment	LU Type	Description	Area (km^2)	Area in Percentage	Soil Group	Curve Number (CN)	CN x A	Impervious Area (km^2)	Impervious Area (%)
Sub catchment 1	FRSUA	Forest	158.94	47.36	C	58.00	9218.52	14.30	4.26
	HOMSA	Homestead/Garden	5.36	1.60	C	90.00	482.76		
	PDDYA	Paddy	14.20	4.23	C	95.00	1349.45		
	SCRBA	Scrubland	144.40	43.03	C	64.00	9241.29		
	STRMA	Water Body	12.69	3.78	C	97.00	1231.19		
Total			**335.60**	**100.00**	**Weighted Average C**		64.13		

Sub catchment	LU Type	Description	Area (km^2)	Area in Percentage	Soil Group	Curve Number (CN)	CN x A	Impervious Area (km^2)	Impervious Area (%)
Sub catchment 2	FRSUA	Forest	56.09	63.65	C	58.00	3252.95	3.71	4.21
	HOMSA	Homestead/Garden	1.00	1.13	C	90.00	89.59		
	PDDYA	Paddy	5.05	5.73	C	95.00	479.48		
	SCRBA	Scrubland	22.58	25.62	C	64.00	1444.95		
	STRMA	Water Body	3.41	1.02	C	97.00	331.22		
Total			**88.12**	**96.13**	**Weighted Average C**		63.53		
Sub catchment 3	FRSUA	Forest	20.33	9.40	C	58.00	1178.99	28.41	13.13
	HOMSA	Homestead/Garden	9.66	4.46	C	90.00	869.37		
	PDDYA	Paddy	24.30	11.23	C	95.00	2308.50		
	SCRBA	Scrubland	136.55	63.12	C	64.00	8739.42		
	STRMA	Water Body	25.51	11.79	C	97.00	2474.43		
Total			**216.35**	**100.00**	**Weighted Average C**		71.97		
	FRSUA	Forest	34.03	20.96	C	58.00	1973.79	15.87	9.77
	HOMSA	Homestead/Garden	15.74	9.69	C	90.00	1416.37		

Sub catchment	LU Type	Description	Area (km^2)	Area in Percentage	Soil Group	Curve Number (CN)	CN x A	Impervious Area (km^2)	Impervious Area (%)
Sub catchment 4	PDDYA	Paddy	39.35	24.24	C	95.00	3738.66		
	SCRBA	Scrubland	62.11	38.25	C	64.00	3974.86		
	STRMA	Water Body	11.15	6.86	C	97.00	1081.12		
Total			**162.38**	**100.00**	**Weighted Average C**		75.04		
Sub catchment 5	FRSUA	Forest	54.77	24.13	C	58.00	3176.37	8.55	3.77
	HOMSA	Homestead/Garden	24.11	10.62	C	90.00	2169.91		
	PDDYA	Paddy	67.69	29.82	C	95.00	6430.63		
	SCRBA	Scrubland	79.11	34.85	C	64.00	5063.16		
	STRMA	Water Body	1.32	0.58	C	97.00	127.81		
Total			**227.00**	**100.00**	**Weighted Average C**		74.75		

Table 7-4: Curve number calculations for 2021 landuse scenario

Sub catchment	LU Type	Description	Area (km^2)	Area in Percentage	Soil Group	Curve Number (CN)	CN x A	Impervious Area (km^2)	Impervious Area (%)
Sub catchment 1	FRSUA	Forest	162.53	48.43	C	58.00	9426.95	28.38	8.46
	HOMSA	Homestead/Garden	21.15	6.30	C	90.00	1903.42		
	PDDYA	Paddy	9.16	2.73	C	95.00	870.30		
	SCRBA	Scrubland	120.71	35.97	C	64.00	7725.66		
	STRMA	Water Body	22.04	6.57	C	97.00	2137.89		
Total			**335.60**	**100.00**	**Weighted Average C**		65.75		
Sub catchment 2	FRSUA	Forest	55.19	62.63	C	58.00	3201.06	8.50	9.65
	HOMSA	Homestead/Garden	1.46	1.66	C	90.00	131.46		
	PDDYA	Paddy	1.32	1.50	C	95.00	125.17		
	SCRBA	Scrubland	22.09	25.07	C	64.00	1413.68		
	STRMA	Water Body	8.06	2.40	C	97.00	782.21		
Total			**88.12**	**90.85**	**Weighted Average C**		64.16		
	FRSUA	Forest	32.39	14.97	C	58.00	1878.73	36.18	16.73

Sub catchment	LU Type	Description	Area (km^2)	Area in Percentage	Soil Group	Curve Number (CN)	CN x A	Impervious Area (km^2)	Impervious Area (%)
Sub catchment 3	HOMSA	Homestead/Garden	14.60	6.75	C	90.00	1313.90		
	PDDYA	Paddy	23.87	11.03	C	95.00	2267.20		
	SCRBA	Scrubland	113.69	52.55	C	64.00	7276.15		
	STRMA	Water Body	31.81	14.70	C	97.00	3085.09		
Total			**216.35**	**100.00**	**Weighted Average C**		73.13		
Sub catchment 4	FRSUA	Forest	41.00	25.25	C	58.00	2377.97	18.85	11.61
	HOMSA	Homestead/Garden	25.69	15.82	C	90.00	2312.23		
	PDDYA	Paddy	36.86	22.70	C	95.00	3502.17		
	SCRBA	Scrubland	47.68	29.37	C	64.00	3051.76		
	STRMA	Water Body	11.14	6.86	C	97.00	1080.42		
Total			**162.38**	**100.00**	**Weighted Average C**		75.90		
Sub catchment 5	FRSUA	Forest	69.78	30.74	C	58.00	4047.43	9.60	4.23
	HOMSA	Homestead/Garden	23.61	10.40	C	90.00	2125.20		
	PDDYA	Paddy	69.04	30.42	C	95.00	6559.05		

Sub catchment	LU Type	Description	Area (km^2)	Area in Percentage	Soil Group	Curve Number (CN)	CN x A	Impervious Area (km^2)	Impervious Area (%)
	SCRBA	Scrubland	62.04	27.33	C	64.00	3970.66		
	STRMA	Water Body	2.52	1.11	C	97.00	244.09		
Total			**227.00**	**100.00**	**Weighted Average C**		74.65		

The findings, interpretations and conclusions expressed in this thesis are entirely based on the results of the individual research study and should not be attributed in any manner to or do neither necessarily reflect the views of UNESCO Madanjeet Singh Centre for South Asia Water Management (UMCSAWM), nor of the individual members of the MSc panel, nor of their respective organizations.